

**ARTIFICIAL PHOTOSYNTHESIS:
TOWARDS THE DEVELOPMENT OF
MOLECULAR PHOTODIODES**

Promotor: Dr. T.J. Schaafsma, hoogleraar in de Moleculaire Fysica

11103201, 2012

Tom J. Savenije

**ARTIFICIAL PHOTOSYNTHESIS:
TOWARDS THE DEVELOPMENT OF
MOLECULAR PHOTODIODES**

Proefschrift

ter verkrijging van de graad van doctor

op gezag van de rector magnificus

van de Landbouwwuniversiteit Wageningen

Dr. C.M. Karssen,

in het openbaar te verdedigen

op dinsdag 28 januari 1997

des namiddags te een uur dertig in de aula.

15-931506

ISBN: 90-5485-646-7

**BIBLIOTHEEK
LANDBOUWUNIVERSITEIT
WAGENINGEN**

This investigation was supported by the Netherlands Foundation for Chemical Research (SON) with financial aid from the Netherlands Organisation for Scientific Research (NWO).

Stellingen behorende bij het proefschrift "Artificial photosynthesis: towards the development of molecular photodiodes" van Tom J. Savenije.

1. Het gebruik van het verband tussen de fotostroom van een organische heterojunctie én de absorptiecoëfficiënten en diktes van de depletielagen en bulklagen, is alleen toegestaan als de weerstand in de bulklaag verwaarloosd mag worden.
S. Günster *et al. Mol. Liq. & Liq. Cryst. A* **1993**, 229, 111; S. Günster *et al. Mol. Liq. & Liq. Cryst. A* **1993**, 218, 117.
2. Het niet uitvoeren van analyses aan dispersiecurves voor het bepalen van capaciteiten van junctions, maakt voltage-afhankelijke capaciteitsmetingen niet bruikbaar voor de verwerking tot Mott Schottky grafieken.
T. Taleb *et al. J. Appl. Phys.* **1996**, 79, 1701; Y. Harima, *et al. J. Phys. Chem. Solids* **1995** 56, 1223.
3. Het niet kunnen aantonen van een voltage-afhankelijke capaciteit betekent niet dat bandbuiging afwezig is in de betreffende cel.
B. Gregg *J. Phys. Chem.* **1994**, 98, 2412.
4. De voor de hand liggende interpretatie van de tijdsopgeloste fotostroom profielen, namelijk het leeglopen van de door de cel bepaalde capaciteit, wordt door Fox *et al.* ten onrechte niet in beschouwing genomen.
M. A. Fox *et al. , J. Phys. Chem.* **1995**, 99, 11523.
5. Verzadigde vetzuren met verschillende ketenlengte in voedingsmiddelen hebben in verschillende mate effect op het serum LDL cholesterol gehalte. In dat verband valt het gebruik van cacaoboter te prefereren boven dat van kokos- of palmpitolie.

6. Het mag verwacht worden dat toediening van kooiverrijkingsmateriaal (b.v. nestmateriaal) de spreiding in de resultaten van experimenten op een groep proefdieren vermindert.
7. De conclusies van M. Carl *et al.* dat het S-protein van Rickettsia Prowazekii geen signaal peptide bevat en dat Rickettsia Typhi een truncated silent S-layer gen bevat berusten op fouten in de experimentele uitvoering.
M. Carl *et al.* *Proc. Nat. Acad. Sci. US.* **1990**, 87, 8237; M.-J. Hahn *et al.* *Gene*, **1993**, 133, 129.
8. Elementair onderzoek word vooral uitgevoerd door mensen in de leeftijdscategorie tot 3 jaar.
9. De door de oude Romeinen aangehangen gedachte dat het niet hebben van hoofdhaar gepaard gaat met een hogere ontwikkeling blijkt achteraf waar.
10. Reductie van het aantal wetenschappelijke tijdschriften leidt tot een betere verspreiding van wetenschappelijke vooruitgang.
11. Gezien de huidige ontwikkelingen in de distributie van medicijnen moet verwacht worden dat de functie-inhoud van het beroep van apotheker drastisch zal veranderen.
12. De rol van uitstekende blokcopolymeren bij een watergedragenverf is oppervlakkig

Contents

1 Introduction

2 Experimental methods

3 Deposition of watersoluble porphyrins on solid substrates

(Thin solid films, 1995, 265, 84-88)

4 Spectroelectrochemical measurement of charge transport properties of electropolymerised tetra(hydroxyphenyl) porphyrins

(J. Phys. Chem. in press)

5 Photo-induced unidirectional electron transfer in a porphyrin heterojunction

(Chem. Phys. Lett. 1995, 244, 363-370)

Control of photo-current direction by spatial arrangement of porphyrin layers

(submitted to Appl. Phys. Lett.)

6 Photo-generation and transport properties of charge carriers in a porphyrin p/n- heterojunction

(submitted to Phys. Rev. B)

Transient photo-current measurements

Summary

Samenvatting

Introduction

1.1 Introduction

Over the past two decades much effort has been devoted to the development and understanding of photo-induced charge separation as a means of making use of solar energy for energy production. Many approaches to this problem involve chemical systems designed to mimic the primary step of natural photosynthesis. The intact natural photosynthetic process involves the transport of excitation energy from the antenna to the photosynthetic reaction centre, all embedded in a membrane protein. Subsequent to photon absorption and excitation transfer to the reaction centre a number of electron transfer steps from the photo-excited electron donor to suitable acceptors results in a physical separation of the electron and hole across 40-50 Å wide membrane. Following this primary process, potential-driven enzymatic reactions produce high-energy redox intermediates [1-3].

The primary step, in for e.g. bacterial photosynthetic reaction centres, consists of the photo-induced charge separation of an electron from the primary donor, i.e. a chemically identical pair of bacterio-chlorophylls to the primary acceptor pheophytin, in a few pico seconds [3]. However, preceding to this charge transfer step, the initially excited neutral primary donor is proposed to relax to an intradimer charge transfer state at the sub-pico second time scale presumably due to a polarising protein environment [4,5].

To mimic this primary relaxation event non-covalently bound heterodimers in solution consisting of two different porphyrin monomers are attractive models for the special pair of the primary donor [6-8]. The spatial configuration of these porphyrin dimers, a slipped face-to-face structure with a plane-to-plane distance of 3.5 Å, as has been concluded from NMR studies [9], is similar to that of the primary donor [10,11]. The sub-nano second events in these heterodimer models are explained by an intradimer photo-induced electron transfer [7,11,12]. However, until now, there is no straightforward theoretical model to interpret the results from transient optical measurements since existing electron transfer theories, such as the Marcus theory [13], do not seem to apply. Paragraph 1.4 contains a short overview of different electron transfer mechanisms which one may expect to apply for these kind of dimer models.

The organisation of the individual components of these heterodimers as two thin layers on top of each other equipped with electrical contacts, may lead to an opto-electronic device with Giga hertz optical switching characteristics, since the heterodimers of water-soluble porphyrin compounds exhibit sub-nanosecond electron transfer [7,12,14]. Such a device belongs to the field of molecular electronics, to be discussed in Paragraph 1.2. The change, however, of the environment, in particular of the dielectric constant of the condensed phase as compared to that of a solution, may have considerable effect on the kinetics and energetics of the photo-induced electron transfer process at the interface of the two above mentioned thin layers. In general, models developed for describing photo-induced charge separation in solution may not be adequate for solid films. So far there are only a few (theoretical) models which adequately describe photo-induced charge separation in the solid state [15-19].

The phenomena treated in this Thesis can also be frequently observed in semiconductor devices, e.g. photo-diodes, photo-transistors and solar cells. Optical excitation of these devices consisting of two different (semi) conducting materials on top of each other (a heterojunction), also generates charge carriers. A description of the formation and properties of such a heterojunction is given in Paragraph 1.4. Since in solid state physics and photo-electrochemistry a different reference point for energy and potentials is used, a common energy scheme is presented in Paragraph 1.3.

1.2 Molecular electronics

Molecular electronics is an area of rapidly growing interest for information transduction and -storage. Processes, such as charge separation and - recombination , trapping and charge carrier transport in molecular electronic devices are closely related to those in photovoltaic solar cells in particular organic solar cells. Although this is a field involving several disciplines, there is a common challenge, to understand how the electronic properties of a molecular assembly are related to and controlled by the molecular organisation and electronic characteristics of the individual molecular components [20-24].

It has been suggested that the current miniaturisation in semiconductor technology will reach the end in one or two decades, because the limits for this miniaturisation find their origin in diffusion and clustering of doping centers, tunnelling phenomena and power dissipation [20,24]. To increase the density of electronic circuit elements in

integrated circuits, molecular electronics seems a promising approach, because in principle the circuit elements themselves are embodied in the structure and electronic configuration of a limited number of molecules. Consequently, a molecular device need not to be built from individual layers, but molecules with specific electronic functions are prepared as bulk chemicals and subsequently interconnected into an electronic circuit using appropriate techniques. Molecular electronics is expected to offer the highest possible density of circuit elements and an exceptionally high speed of operation, associated with electron transfer events in molecules, theoretically as fast as $1 \cdot 10^{13} \text{ s}^{-1}$. This has motivated feasibility studies of using molecular materials for producing nanometer scale circuits.

Sensors and biosensors form a specific research field in molecular electronics [25] These devices focus on the response of molecular assemblies (containing for example enzymes) on target molecules, i.e. ions or sugars. Further research areas in molecular electronics involve rectifiers, shift registers and information storage [26-28].

A new active field in molecular electronics is based on the response of molecular devices, containing dye molecules, upon optical or electrical inputs. From the application point of view, these devices are important for signal processing, photodiodes, optical computing, energy conversion, non-linear optics and light emitting diodes.

1.3 Energy levels in (organic) solids

Considering a redox system with redox potential E° , dissolved in an electrolyte, the absolute energy w.r.t. the vacuum level ($E=0$) of an electron of this system (E_{abs}) is shifted against the conventional potential scale vs. NHE by ,

$$E_{abs} = -4.5 - eE^\circ \quad (1)$$

with e the electronic charge.

The chemical potential of electrons in a redox couple is determined by the Nernst equation as given by

$$\mu_{e,redox} = \mu^\circ + k_B T \ln \left(\frac{C_{ox}}{C_{red}} \right) \quad (2)$$

where C_{ox} en C_{red} are the concentrations of the oxidised and reduced species of the redox system, respectively and μ° the standard chemical potential.

For a semiconductor the energy levels are characterised by the energies of the conduction band (CB) and that of the valence band (VB). The energy level of the bottom of the CB w.r.t. the vacuum level (E_c) is given by the electron affinity (E_a) as shown in Figure 1. The ionisation energy (I) determines the position of the top of the VB (E_v). For a molecular semiconductor the values of E_a and I can be estimated from the redoxpotentials of the monomeric species in solution [16, 29] by $E_a \approx E^{red} + 4.5$ and $I \approx E^{ox} + 4.5$, where E^{red} and E^{ox} denote the first reduction and oxidation potentials vs. NHE, respectively. Improved theoretical models have been developed for adsorbed species at a solid/liquid interface [30,31] and for solid organic systems [15]. Both models take into account the difference of the reorganisation energy of the surrounding medium w.r.t. that in solution. Experimentally energy levels can be obtained using UV photoelectron spectroscopy (UPS) [32] or Kelvin Probe techniques [33]. In combination with optical spectra, yielding the ΔE_{0-0} gap, the energy levels of the bottom of the CB and top of the VB can be determined. [17, 34]

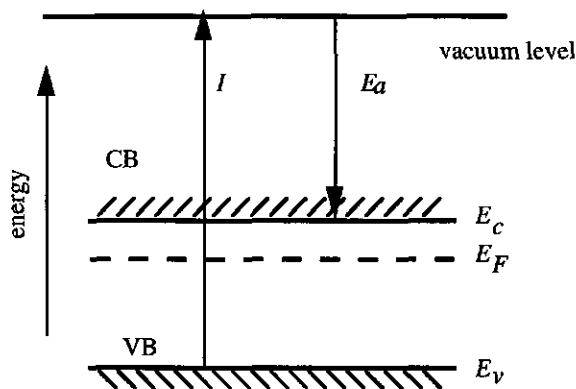


Figure 1. Positions of the energy bands (with respect to the vacuum level) of an n-type semi-conductor.

For an intrinsic semiconductor the Fermi level, defined as the energy level at which the probability to be occupied by an electron is 1/2 at a particular temperature, is located near the middle of the energy gap [35]. If donor impurities are present, resulting in free electrons in the conduction band, the Fermi level shifts upwards, and the semiconductor is denoted as n-type as in Figure 1. In addition to the free electrons in the CB (the so called majority carriers in an n-type semiconductor), a relatively much smaller number

of free holes (the minority carriers) are present in the VB induced by thermal excitation of electrons into the CB. Acceptor impurities result in free holes in the VB, shifting the Fermi level towards to VB, yielding a p-type semiconductor.

The Fermi level of a semiconductor is equivalent to the chemical potential (μ_E) of the electrons and is given by

$$\mu_e \approx E_C + k_B T \ln \left(\frac{n}{N_C} \right) \quad (3)$$

where k_B is the Boltzmann constant, T the absolute temperature, n the electron density N_C is the effective density of states at the bottom of the conduction band.

The Fermi level E_F of the redox couple defined in Equation 2, using the absolute scale (with vacuum as $E = 0$ reference) for the standard chemical potential equals the chemical potential of the electrons in a semiconductor as defined in Equation 3, thus $E_{F,redox} = \mu_{e,redox}$ [30].

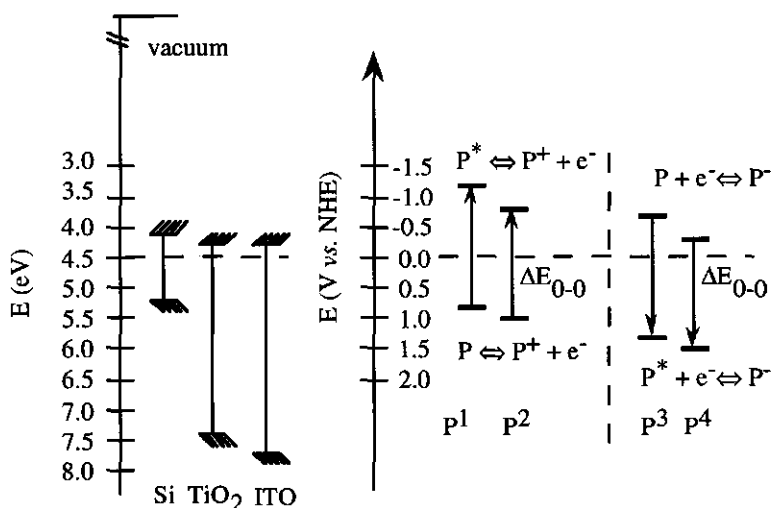


Figure 2. Comparison of band positions of semiconductors after [30] with the redoxpotentials of dye molecules in solution [7]. P¹ and P² mark the oxidation potentials of Zn - and free base tetra carboxy phenyl porphyrin, respectively; P³ and P⁴ mark the reduction potentials for Zn - and free base tetra methylpyridinium porphyrin, respectively. The dashed line represents 0 V (vs. NHE). Note that upon excitation the oxidation potentials for P¹ and P² decreases and the reduction potentials for P³ and P⁴ increases.

An excited dye molecule can more easily be oxidised or reduced. The oxidation potential of a molecule in the excited state can be estimated by subtracting the stored energy ΔE_{0-0} , corresponding to the S_1-S_0 transition, from the Fermi level, as illustrated in Figure 2 (for reduction the transition energy has to be added to the reduction potential).

Oxidation of a dye molecule occurs by removing an electron from the highest occupied molecular orbital (HOMO). On the other hand reduction of a dye molecule occurs by an electron transfer to the lowest unoccupied orbital (LUMO). These two reactions are characterised by two different redox potentials. Dye molecules often have several oxidation and reduction states. Figure 2 only refers to the first oxidation and reduction states.

1.4 Formation of heterojunctions

One type of photovoltaic device, already reported in 1986, is based on phthalocyanine and substituted perylene dyes deposited by vapour deposition on top of each other [17, 36-40]. The mechanism of the photophysical processes in this kind of cells is commonly assumed to be based on the presence of a space charge region, analogously to the contact which is formed between an n- and a p- type inorganic semiconductor. In this Paragraph the formation and the properties of heterojunctions is treated. When combined with the theory described in the different Chapters the observed phenomena can at least qualitatively be understood. The origin of the above mentioned space charge region stems from the difference between the Fermi levels of both types of semiconductors. Band diagrams for this so called p/n junction are shown, before (Figure 3a) and after (Figure 3b) electrical contact between both types of semiconductors is made.

Upon contact electrons flow from the n-type to the p-type semiconductor as indicated by the arrow, until thermal equilibrium is reached and the Fermi levels are equal (Figure 3b). In equilibrium the asymmetric charge distribution gives rise to an internal electric field gradient opposing further diffusion of electrons into the p-type material. Since the majority charge carriers, i.e. electrons of the n-type combine, with holes of the p-type semiconductor, a region depleted of charge carriers is formed, the depletion region. From the charge distribution the potential profile within and outside the depletion region can be determined. The energy band diagram for electrons (Figure 3) is then obtained by multiplying the potential distribution with the electronic charge.

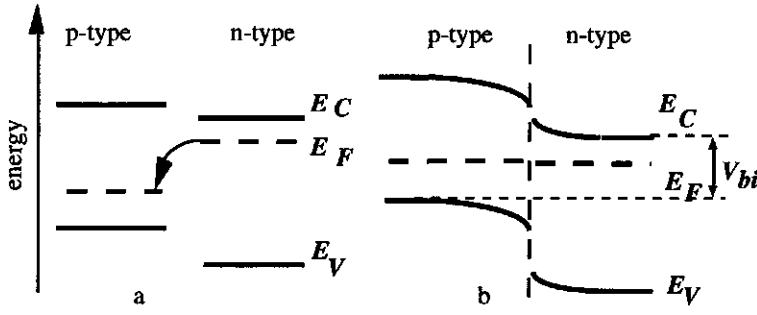


Figure 3. Energy band diagram for two isolated semiconductors (a) and a heterojunction at thermal equilibrium (b).

The built-in potential (V_{bi}) is related to the difference of the Fermi levels of both semiconductors by: $eV_{bi} = E_{nF} - E_{pF}$. The width of the depletion region (ω) and the internal electric field gradient at each side of the p/n interface are related to the amount of doping (N_A) and (N_D) and the dielectric permittivities ϵ_p and ϵ_n of the p-type and n-type material, respectively. E.g. in the p-type material ω_p can be derived as follows:

$$\omega_p = \sqrt{\frac{2\epsilon_p\epsilon_n N_n (V_{bi} - V_a)}{eN_p(\epsilon_p N_p + \epsilon_n N_n)}} \quad (4)$$

where V_a is the applied potential. A similar expression holds for the n-type material with n and p interchanged.

Upon applying a forward potential (V_a) the width of the depletion region decreases and the dark current (i) increases according to [35]:

$$i = i_o \left[\exp\left(\frac{eV_a}{k_B T}\right) - 1 \right] \quad (5)$$

where i_o is the saturation current. For the ideal case the potential-dependent dark current of this rectifying contact is as depicted in Figure 4.

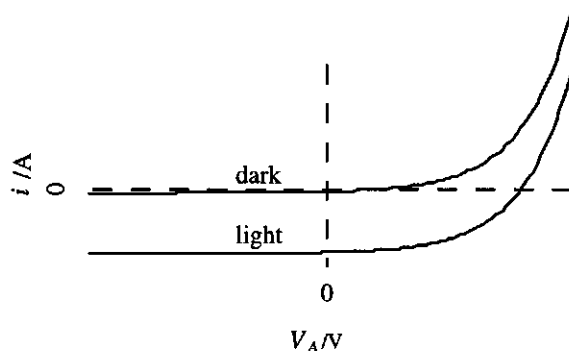


Figure 4. The effect of the applied potential on the dark and photo current in an ideal p/n junction.

Upon optical excitation of semiconducting material in this depletion region (Figure 3b) charge carriers are generated by the internal electric field. The same field causes the charge carriers to drift to the separate electrodes, which eventually leads to a photocurrent. Figure 4 shows the effect of illumination on the i/V curves.

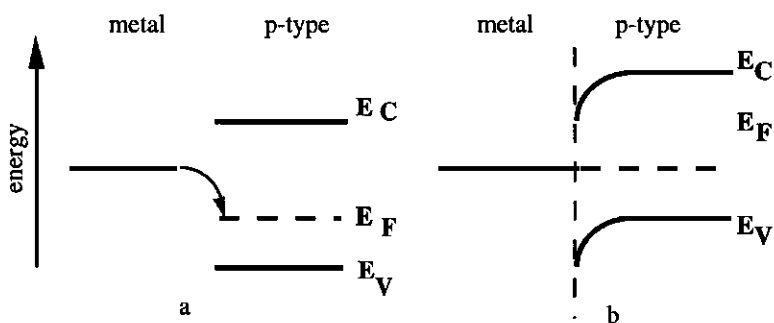


Figure 5. Formation of an ideal Schottky barrier between a metal and p-type semiconductor before (a) and after (b) electrical contact.

Another type of organic photovoltaic cells has been described at the end of the '70's' making use of a molecular semiconductor in combination with a metal [16, 19, 41-43]. Upon electrical contact of the metal with the molecular semiconductor, electrons flow in a direction and to an amount depending on the Fermi level of the semiconductor and the work function of the metal (ϕ_M), resulting in the formation of a Schottky barrier. The work function of a metal is defined as the energy required to remove an electron from the top of the Fermi distribution of the metal to the vacuum level. Band diagrams

of a metal with a low work function i.e. aluminium ($\phi_M = 4.2$ eV) and a p-type semiconductor before and after electrical contact are presented in Figure 5. Upon excitation of the semiconductor a process as described for the heterojunctions occurs, explaining the photovoltaic effect in these cells. If the workfunction of the metal is positioned below the Fermi level of a p-type material an Ohmic contact is formed. For an n-type material the Fermi level should be at a position lower than the workfunction of the metal to obtain a Schottky barrier and higher to obtain an Ohmic contact. When attaching metal electrodes to a p/n heterojunction one therefore should be aware that a Schottky barrier may be formed. A more in-depth treatment of semiconductors is found in [35, 44] and of molecular semiconductors in [29, 45].

1.5 Photo-induced electron transfer

During the past decades much effort has been devoted to study photo-induced charge separation of model systems in solution, resulting in different theoretical models, in particular the well known Marcus theory [46-48], predicting the effects of physical and chemical parameters of a donor acceptor couple and of the medium on the rate of the photo-induced electron transfer process [49-52]. In this Paragraph a short overview is given of the main theories for the photo-induced charge separation and recombination processes.

Classical Marcus theory for electron transfer

The reactions considered here are all so-called outer sphere bimolecular electron transfer reactions i.e. both reactants do not share a common group or atom and thus the interaction between donor and acceptor is weak. Normally, reactants and products have a potential energy surface which is a function of many nuclear co-ordinates. For simplicity a single reaction co-ordinate is introduced so that the energy surface can be reduced to a one-dimensional profile as shown in Figure 6. Since the transfer process only involves an electron the Franck-Condon principle can be applied. This means that the nuclei do not have time to change their position or their momentum. Therefore, electron transfer will only take place at or near a nuclear conformation for which the total potential energy of the reactants and the surrounding medium is equal to that of the products and the surrounding medium. For electron transfer to occur the reactant must distort from its equilibrium state by thermal fluctuation (a in Figure 6A) to a

situation where it has the same nuclear configuration as the resulting product (b). At this stage electron transfer occurs followed by relaxation to the product equilibrium state (c).

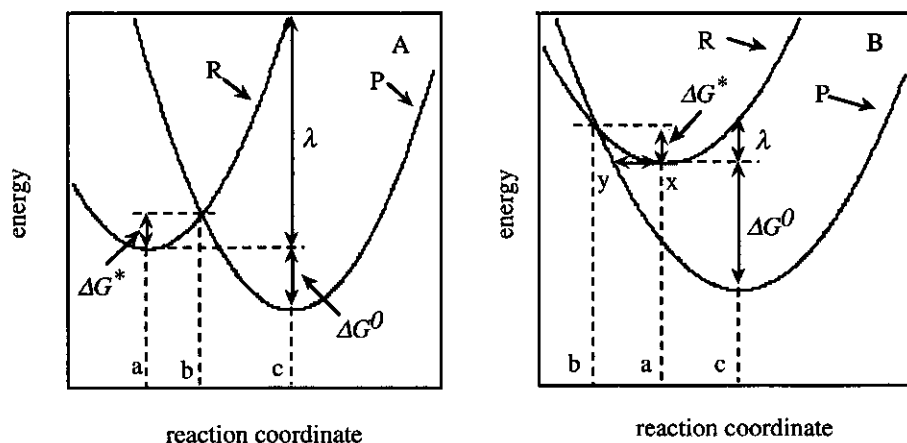


Figure 6. Gibbs free energy diagrams for one reaction co-ordinate showing the intersection of reactant (R) and product (P) potentials. a en c denote nuclear equilibrium configurations for the reactant and the product, respectively; b denotes the configuration at the transition state. In A, $0 < -\Delta G^0 < \lambda$ and this reaction is an example of the "normal region". When $-\Delta G^0 > \lambda$ as in B the reaction is highly exothermic and the reaction takes place in the "inverted region".

Assuming a harmonic potential energy surfaces for reactant and product as in Figure 6, in this classical model it can algebraically be derived, that the free energy of activation has a quadratic dependence on the change of free energy (ΔG^0) involved with the electron transfer reaction resulting in

$$\Delta G^* = \frac{(\lambda + \Delta G^0)^2}{4\lambda} \quad (6)$$

where λ is the total reorganisation energy, consisting of two contribution i.e. λ_i , the internal reorganisation in bond lengths and bond angles of the donor/acceptor system and λ_s , the reorganisation effect of the surrounding medium.

According to the Marcus theory [46-48] the rate constant for electron transfer (k) is

$$k = \kappa Z \exp\left(\frac{-\Delta G^*}{K_B T}\right) = \kappa Z \exp\left(-\frac{(\lambda + \Delta G^0)^2}{4\lambda K_B T}\right) \quad (7)$$

where κ is the probability for the electron transfer normalised to the number of times the system acquires the correct nuclear configuration for electron transfer, Z is the average molecular vibrational frequency ($\approx 10^{13} \text{ s}^{-1}$) and ΔG^* is the Gibbs free energy of activation. κ is dependent on the distance between the two reactants, yielding unity for substantial electronic overlap. Equation 7 expresses the classical nature of this model by using the Boltzmann population at the transition state as the weighting factor. The density of vibrational states of reactants and the product is assumed to be infinite in this model.

Equation 7 implies a maximum for the rate of electron transfer for $\lambda = -\Delta G^0$. For the "normal region" (as illustrated in Figure 6 A) $0 < -\Delta G^0 < \lambda$. If $-\Delta G^0 < \lambda$, ("inverted region") the electron transfer is exothermic, but the transfer rate is slowed down w.r.t. that for $\lambda = -\Delta G^0$ (Figure 6B). The existence of such a region was experimentally shown for the first time by the group of Miller [53] for certain donor/acceptor combinations.

Semi classical Marcus theory for electron transfer

In the preceding Paragraph the motion of the nuclei was treated classically. However, there may be some tunneling through the barrier, depicted schematically by a horizontal motion from x to y in Figure 6B. For a highly exothermic reaction as depicted in this Figure nuclear tunnelling may significantly contribute to the rate constant for electron transfer, especially when the electronic coupling is very small, i.e. $\kappa \ll 1$.

A quantum mechanical treatment for the nuclear co-ordinates for electron transfer starts with Fermi's Golden Rule for the transition probability between two states. The first order rate of electron transfer at fixed distance between the two reactants contains the strength of electronic coupling H_{DA} between donor and acceptor and the Franck-Condon factor (FC), i.e. the sum of the products of overlap integrals of the vibrational and solvent wave functions with those of the product each weighted by a Boltzmann factor.

$$k = \frac{2\pi}{\hbar} H_{DA}^2 \text{FC} \quad (8)$$

The H_{DA} is largely dependent on the distance, and the medium or link between donor and acceptor. The Franck-Condon factor for the nuclear motions of the inner shell coordinates can be calculated quantum mechanically. The contribution of the solvent to the Franck-Condon factor can be converted to a classical expression. In the high temperature limit this treatment yields the following expression [48]:

$$k = \frac{2\pi}{\hbar} H_{DA}^2 \sqrt{\left(\frac{1}{4\pi\lambda k_B T}\right)} \exp\left[\frac{-(\Delta G^o + \lambda)^2}{4\lambda k_B T}\right] \quad (9)$$

which has the same exponent as Equation 7, but the pre-exponential factor is different. In the normal region the classical expression for the rate constant (Equation 7) and the semiclassical expression (Equation 9) give similar results. In the "inverted region" the semi-classical treatment shows a clear deviation from the classical treatment.

In a full quantum analysis of the rate constants for electron transfer all internal and solvent vibrational modes must be taken into account, due to a contribution of tunneling.

The expression for the change in free energy (ΔG^o) in the overall electron transfer reaction in Equations 7 and 9, the so called Weller equation, includes the oxidation potential of the donor, (E_{ox}), the reduction potential of the acceptor, (E_{red}), the energy of the lowest excited state, from which electron transfer occurs (ΔE_{0-0}), and the Coulombic attraction between the donor radical cation and acceptor radical anion [54]:

$$\Delta G^o = E_{ox} - E_{red} - \Delta E_{0-0} - \frac{e^2}{\epsilon_s r} - \left(\frac{e^2}{2}\right) \left(\frac{1}{r_D} + \frac{1}{r_A}\right) \left(\frac{1}{\epsilon_r} - \frac{1}{\epsilon_s}\right) \quad (10)$$

where ϵ_r is the dielectric constant of the medium, in which the redox potentials of donor and acceptor are determined and ϵ_s the dielectric constant of the medium in which the electron transfer process actually takes place. The parameters r_D and r_A represent the ionic radii of the donor radical cation and the acceptor radical anion. Equation 10 holds, if the produced radical ions are surrounded by a medium with the given relative dielectric constant ϵ_s and may therefore not be applicable describing the

rate constants for photo-induced electron transfer reactions, where the donor and the acceptor molecule are at close distance from each other, such as in porphyrin dimers. Furthermore, the solvent reorganisation energy (λ_s) is also a function of the polarity of the surrounding medium and can be estimated using the dielectric continuum model, which in the Born approximation yields [32]:

$$\lambda_s = \frac{e^2}{4\pi\epsilon_0} \left(\frac{1}{2r_D} + \frac{1}{2r_A} - \frac{1}{r_{DA}} \right) \left(\frac{1}{n^2} - \frac{1}{\epsilon_s} \right) \quad (11)$$

where n is the refractive index.

Changing the polarity of the surrounding medium of a particular donor/acceptor system affects both ΔG^0 (Equation 10) and λ (Equation 11). Therefore it is evident that application of the classical and semi-classical photo-induced electron transfer theory on donor/acceptor couples organised as two films on top of each other must be carried out with caution. However, Gaines *et al.* [55] confirmed the applicability of the Marcus theory by determining the rate constants (k_{ET}) of photo-induced electron transfer reactions for a set of donor/acceptor couples in a solid glass. These authors concluded that the reduction of ΔG^0 due to a reduction of ϵ_s in the solid w.r.t. a polar solvent was compensated by a change of λ . The dependence of the rate constant for electron transfer in the solid state on ΔG^0 where donor and acceptor are organised as two thin layers on top of each other has not yet convincingly been demonstrated, however [56, 57].

Other mechanisms:

Electron tunnelling

An alternative theory for photo-induced electron transfer in a donor/acceptor couple is electron tunnelling from the reactant equilibrium state to the product equilibrium state. At short distances this activationless process can result in rate constants close to the vibrational frequencies of the reactants and products.

Electron transfer via super exchange

Electrons do not have to transfer directly from the donor to the acceptor via direct overlap of their wave functions. Molecules with low lying excited states in between

may affect the rate of electron transfer by mixing their electronic states with those of the donor and acceptor.

1.6 Scope and Outline

This Thesis describes the controlled formation of and the photo-physical processes in two ultra thin porphyrin layers, sandwiched between two electrodes. At the interface of these porphyrin layers formation of donor/acceptor couples can be expected, resembling previously investigated water-soluble donor/acceptor complexes[7, 9, 58-60]. Transient absorption measurements on these water-soluble donor/acceptor couples revealed sub-nano second photo-induced electron transfer [7, 12, 14]. Although these experiments were carried out in solution with a high dielectric constant, photo-induced electron transfer still occurs for certain donor/acceptor combinations upon reducing the dielectric constant by freezing the samples, as was demonstrated by fluorescence spectroscopy [59]. In a solid state device containing donor - and acceptor porphyrins organised as two thin layers on top of each other, one may expect photo-induced electron transfer to take place from the donor - to the acceptor layer. However, for the photo-physical description of such a system both approaches as depicted in Paragraphs 1.4 and 1.5 seem important.

The molecular devices described in this Thesis are attractive for utilisation in molecular electronics in view of (i) the broad and chemically variable spectral and electric response, (ii) the in principle short electric response time following light input and (iii) the low cost and relatively simple preparation. For application of charge generation layers in organic solar cells an antenna layer must be added to the cell to increase light absorption. The construction and interfacing of this antenna with the charge generation layer as described in this work is currently carried out within an interdisciplinary consortium of research groups at the Universities of Wageningen, Utrecht and Delft with financial support of the organisation NOVEM.

In Chapter 2 various experimental techniques used in this Thesis are treated. An important aspect is the organisation of dye molecules on solid substrates. Chapter 3 describes the spontaneous adsorption processes of positively charged porphyrins on solid substrates. Chapter 4 deals with a different deposition technique i.e. electro-

polymerisation of porphyrins on transparent conducting substrates i.e. indium tin oxide (ITO). Upon oxidation of porphyrins equipped with at least two hydroxyphenyl groups a covalently bound polymer layer is formed on ITO. Different optical and electrochemical techniques have been applied to these layers, yielding important physical parameters i.e. the diffusion coefficient of charge carriers in the dye matrix. Paragraph 5.1 describes the photo-electric properties of a cell consisting of two thin porphyrin layers. An attempt has been made to demonstrate the dependence of the change of free energy on the rate for photo-induced charge separation. In addition in Paragraph 5.2 evidence is presented that the photo-induced electron transfer i.e. the photo-active part of the cell is located at the interface of the donor and acceptor porphyrin layers. By changing the order of the films the direction of the photo-induced electron transfer can be controlled. Chapter 6 deals with the space charge region which is formed in cells described in Chapter 5. The mechanism for the photovoltaic effect is treated in more detail, showing that next to photo-induced electron transfer process also the formation of a space charge region is important to explain the photo-physical processes in these cells.

References

1. Mathis, P. *Photosynthesis From light to biosphere (Vol. 1)* Kluwer Academic Press: Dordrecht, 1995.
2. Baltscheffsky *Current Research in Photosynthesis (Vol. 1)* Kluwer Academic Press: Dordrecht, 1990.
3. Breton, J.; Vermeglio, A. *The Photosynthetic bacterial reaction centre* Plenum Press: New York, 1988.
4. Breton, J.; Martin, J. L.; Migus, A.; Antonetti, A. and Orszag, A. *Proc. Natl. Acad. Sci. USA* **1986**, *83*, 5121.
5. Meech, S. R.; Hoff, A. J. and Wiersma, D. A. *Proc. Natl. Acad. Sci. US* **1986**, *83*, 9464-9468.
6. Hugerat, M.; Est, A.; Ojadi, E.; Biczok, L.; Linschitz, H.; Levanon, H. and Stehlik, D. *J. Phys. Chem.* **1996**, *100*, 495.
7. Vergeldt, F. J.; Koehorst, R. B. M.; Schaafsma, T. J.; Lambry, J. C.; Martin, J. L.; Johnson, D. G. and Wasielewski, M. R. *Chem. Phys. Lett.* **1991**, *182*, 107.
8. Tran-Thi, T. H.; Lipskier, J. F.; Maillard, P.; Momenteau, M.; Lopezcastillo, J. M. and Jaygerin, J. P. *J. Phys. Chem.* **1992**, *96*, 1073.
9. Hofstra, U.; Koehorst, R. B. M. and Schaafsma, T. J. *Magn. Reson. Chem.* **1987**, *25*, 1069.
10. Deisenhofer, J.; Epp, O.; Mikki, K.; Huber, R. and Michel, H. *J. Mol. Biol.* **1984**, *180*, 385.

11. Allen, J. P.; Feher, G.; Yeates, T. O.; Komiya, H. and Rees, D. C. *Proc. Nat. Acad. Sci. US* **1987**, *84*, 5730.
12. Tran-Thi, T. H.; Dormond, A. and Guillard, R. *J. Phys. Chem.* **1992**, *96*, 3139.
13. Marcus R.A. *Rev. Mod. Phys.* **1993**, *65*, 599.
14. Segawa, H.; Takehara, C.; Honda, K.; Shimidzu, T.; Asahi, T. and Mataga, N. *J. Phys. Chem.* **1992**, *96*, 503.
15. Zakhidov, A. A. and Yoshino, K. *Synth. Met.* **1995**, *71*, 2113.
16. Loutfy, R. and Cheng, Y. C. *J. Chem. Phys.* **1980**, *6*, 2902.
17. Wöhrle, D.; Kreienhoop, L.; Schnurpfeil, G.; Elbe, J.; Tennigkeit, B.; Hiller, S. and Schlettwein, D. *J. Mat. Chem.* **1995**, *5*, 1819.
18. Popovic Z.D. *J. Chem. Phys.* **1982**, *77*, 498.
19. Halls, J. J. M.; Walsh, C. A.; Greenham, N. C.; Marseglia, E. A.; Friend, R. H.; Moratti, S. C. and Holmes, A. B. *Nature* **1995**, *376*, 498.
20. Aviram, A. *Mol. Cryst. & Liq. Cryst. A* **1993**, *234*, 13.
21. Mirkin, C. A. and Ratner, M. A. *Ann. Rev. Phys. Chem.* **1992**, *43*, 719.
22. Shimidzu, T. *Mol. Cryst. & Liq. Cryst. A* **1994**, *252*, 485.
23. Nalwa, H. S. and Kakuta, A. *Appl. Organometal. Chem.* **1992**, *6*, 645.
24. Sigmund, E.; Gribi, P. and Isenmann, G. *Appl. Surf. Sci.* **1993**, *65-6*, 342.
25. Bartlett, P. N. and Cooper, J. M. *J. Electroanal. Chem.* **1993**, *362*, 1.
26. Martin A.S.; Sables J.R. and Ashwell *Phys. Rev. Lett.* **1993**, *70*, 218.
27. Zhao, W. Y.; Marfurt, J. and Walder, L. *Helv. Chim. Acta* **1994**, *77*, 351.
28. Metzger, R. and Panetta, C. *J. Mol. Elec.* **1989**, *5*, 1.
29. Simon J.; André, J.J. *Molecular Semiconductors* ; Springer-Verlag: Berlin, 1985.
30. Gleria, M. and Memming, R. *J. Electroanal. Chem.* **1975**, *65*, 163.
31. Memming, R. *Proc. Ind. Acad. Sci.* **1993**, *105*, 463.
32. Pireaux, J.J.; Sporken, R. in *Analysis of Microelectronic materials and devices*; Garsserbauer, M. and Werner, H. W. (eds) Wiley, J. Wiley& Sons: Chichester, 1991 p111.
33. Lueth, H. *Surfaces and interfaces of solid materials*; Springer-Verlag: Berlin ,1995.
34. Schlettwein, D. and Armstrong, N. R. *J. Phys. Chem.* **1994**, *98*, 11771.
35. Sze, S.M. *Physics of semiconductor devices* ; J. Wiley & Sons: Chichester, 1981
36. Tang, C. W. *Appl. Phys. Lett.* **1986**, *48*, 183.
37. Günster, S.; Siebentritt, S. and Meissner, D. *Mol. Cryst. & Liq. Cryst. A* **1993**, *230*, 351.
38. Karl, N.; Bauer, A.; Holzapfel, J.; Marktanner, J.; Mobus, M. and Stolzle, F. *Mol. Cryst. & Liq. Cryst. A* **1994**, *252*, 243.
39. Gong, J. P.; Ohnishi, S. and Osada, Y. *Pol. J.* **1994**, *26*, 754.

40. Hiramoto, M.; Fukusumi, H. and Yokoyama, M. *Appl. Phys. Lett.* **1992**, *61*, 2580.
41. Morel, D. L.; Feng, T.; Stoggryn, E. L.; Purwin, P. E.; Shaw, R. F. and Fishman, C. *Appl. Phys. Lett.* **1978**, *32*, 495.
42. Nasr, C.; Hotchandani, S.; Kassi, H.; Nsengiyumva, S. and Leblanc, R. M. *Mol. Cryst. & Liq. Cryst. A* **1995**, *36*, 261.
43. Yamashita, K.; Harima, Y. and Iwashima, H. *J. Phys. Chem.* **1987**, *91*, 3055.
44. Rhoderick, E.H. and Williams, R.H. *Metal-semiconductor contacts*; Clarendon Press: Oxford, **1988**.
45. Meier, H. *Organic semiconductors*; Verlag Chemie: Weinheim, 1974.
46. Marcus, R. A. *J. Chem. Phys.* **1956**, *24*, 966.
47. Marcus, R. A. *J. Chem. Phys.* **1965**, *43*, 679.
48. Marcus, R. A. and Sutin, N. *Biochim. & Biophys. Acta* **1985**, *811*, 265.
49. Kakitani, T.; Matsuda, N.; Yoshimori, A. and Mataga, N. *Prog. Reaction Kinetics* **1995**, *20*, 347.
50. Wasielewski, M. R. *Chem. Rev.* **1992**, *92*, 435.
51. Fox, M. A.; Hawley M.D. and Chanon, M. in *Photoinduced electron transfer part A*; Fox, M. A. and Chanon, M. (eds.) Elsevier: Amsterdam, 1988.
52. Gust, D.; Moore, T. A. and Moore, A. L. *Acc. Chem. Res.* **1993**, *26*, 198.
53. Closs, J.R.; Callaterra, L.T.; Green, N.J.; Penfield, K.W. and Miller J.R. *J. Phys. Chem.* **1986**, *90*, 3673.
54. Weller, A. Z. *Phys. Chem.* **1982**, *133*, 93.
55. Gaines, G.L.; O'Neil, M.P.; Svec, W.A.; Niemczyk, M. P. and Wasielewski, M. R. *J. Am. Chem. Soc.* **1991**, *113*, 719.
56. Umeda, M.; Shimada, T.; Aruga, T.; Niimi, T. and Sasaki, M. *J. Phys. Chem.* **1993**, *97*, 8531.
57. Saito, T.; Sisk, W.; Kobayashi, T.; Suzuki, S. and Iwayanagi, T. *J. Phys. Chem.* **1993**, *97*, 8026.
58. Vergeldt, F. J.; Koehorst, R. B. M.; Vanhoek, A. and Schaafsma, T. J. *J. Phys. Chem.* **1995**, *99*, 4397.
59. Hofstra, U.; Koehorst, R. B. M. and Schaafsma, T. J. *Chem. Phys. Lett.* **1986**, *130*, 555.
60. Koehorst, R. B. M.; Hofstra, U. and Schaafsma, T. J. *Magn. Reson. Chem.* **1988**, *26*, 167.

Experimental methods

This Chapter discusses the techniques used in the experiments described in this Thesis. The preparation and characterisation of the compounds and samples is described in the separate Chapters.

2.1 Kelvin-probe measurements

The Fermi level of an (organic) semi-conductor is a valuable tool to describe and predict the energy band diagrams of a p/n heterojunction or a Schottky barrier (Chapter 6). This energy level can be obtained by photo-emission spectroscopy or by Kelvin-probe measurements [1-2]. For Kelvin-probe measurements a probing electrode is used which is positioned at ≈ 1 mm in front of the surface being studied. The distance between the electrode and the surface is electro-mechanically modulated using a piezo-ceramic element (Figure 1). To understand the functioning of a Kelvin-probe, consider a work function ϕ_s for the sample and ϕ_p for the probe, where a work function (ϕ) of a material is defined as:

$$e\phi = E_{vac} - E_f \quad (1)$$

where e denotes the electronic charge, E_{vac} the energy level of a free electron in vacuum and E_f the Fermi energy level. Thus, $e\phi$ is the work needed to remove an electron from the material to the vacuum at infinite distance from the material. If the work function of sample and probe are different, a potential V_{sp}

$$V_{sp} = -(\phi_s - \phi_p) \quad (2)$$

is formed. The capacitor (C) formed by sample and probe carries a charge Q which can be changed by introducing a variable potential (V_a) in the external circuit as in Figure 1:

$$Q = C[V_{sp} + V_a] \quad (3)$$

As long as $Q \neq 0$, vibration of the probe electrode produces an oscillating current. By adjusting V_a , until the oscillating current is fully compensated, $-V_a = V_{sp}$, which equals the difference in work functions of sample and probe. Since the workfunction of the probe under conditions of the experiment is known i.e. $\phi(\text{Ag}) = 5.0$ V, ϕ_s can be calculated using Equation 2.

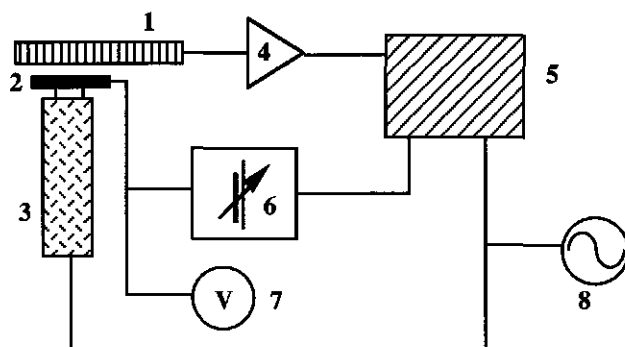


Figure 1. Circuit for the Kelvin-probe measurements, 1: sample; 2: silver probe; 3: piezo electric element; 4: preamplifier; 5: lock-in amplifier; 6: variable voltage supply; 7: voltmeter; 8: frequency controller.

A standard instrument contains an automatic compensating circuit as shown in Figure 1. The oscillating current is amplified and detected by a phase sensitive lock-in detector and amplifier. The reference signal for the lock-in detector is also used to control the frequency of the piezo-ceramic element. The lock-in DC output is fed into a variable voltage source. The compensating voltage is monitored by a voltmeter [3].

For the measurements we used an electrostatic voltmeter (Trek 320B) with a high sensitivity probe (model 3250). The main problem interpreting data obtained with the Kelvin-probe technique is the presence of an electric barrier which may appear at the film/air interface [2]. These barriers may cause deviations of the measured value of hundreds of mili Volts.

2.2 Absorption measurements

For a number of experiments the relation of the amount of absorbed light by a thin dye film on a solid substrate to, the photocurrent (see Chapter 5) [4-8], is a valuable tool to quantify photo-physical processes of interest in the film. An organic layer covering a solid substrate may, however, have a large effect on the reflection coefficient of the substrate. Therefore it is necessary to correct the optical density of thin dye films for reflection. To determine the wavelength dependent reflection for a solid sample a diffuse reflectance sphere has been used as an accessory to a CARY 5e spectrophotometer (Varian Associates). For a dye covered substrate in the centre of the sphere (Figure 2) the corrected optical density ($O.D.$) of a sample is given by the

expression

$$O.D. = -\log\left(\frac{I_{tr} + I_r}{I_0}\right) \quad (4)$$

where I_0 , I_{tr} and I_r are the intensities of the incident, the transmitted and the reflected light, respectively. To compensate for the absorption of the substrate, an uncovered substrate is used as a reference. Separate reflection components for the various interfaces of a sample can also be determined using this set-up. This is achieved by placing the substrate at different positions within the diffuse reflectance sphere and using various algorithms [9-11].

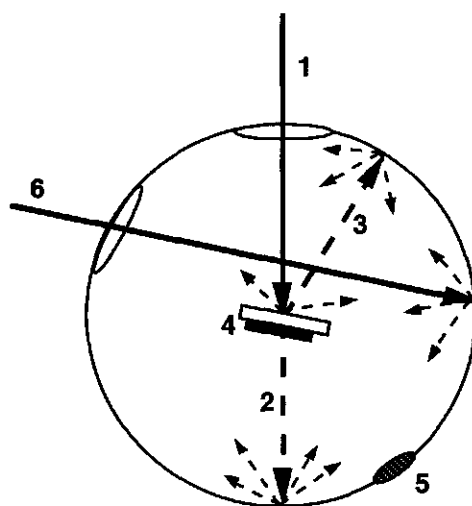


Figure 2. Schematic diagram of the diffuse reflectance sphere accessory, 1: optical excitation beam (I_0); 2: transmitted light (I_{tr}); 3: reflected light (I_r); 4: sample; 5: detector; 6: reference beam.

2.3 Electrochemical measurements

To characterise and prepare thin organic films electrochemical techniques such as cyclic voltammetry and potential controlled electrochemistry have been employed (Chapter 4) [12-16]. Such experiments make use of a conventional three electrode system, consisting of an ITO working electrode ($30\Omega/\phi$) (Glastron), a rectangular platinum

counter electrode and an Ag/AgCl ($[KCl] = 3\text{ M}$) reference electrode. Electrochemical currents were recorded using a potentiostat (Autolab Pstat10, Ecochemie) controlled by GPES3 software (Ecochemie) in combination with a Metrohm 5 or 20 ml vessel. Prior to measurements a flow of dry argon gas was passed through the magnetically stirred electro-chemical solution for 10 min. During cyclic voltammetry, argon was led over the solution and stirring was off.

For transient spectro-electrochemical measurements samples were placed in a 2*2*5 cm. cuvette (Hellma) containing freshly deoxygenated electrolyte, a Pt counter electrode and an Ag/AgCl ($[KCl] = 3\text{ M}$) reference electrode. The electro chromic changes were detected using light from a 150 Watt Xenon lamp (Spectral Energy), passing through a monochromator GM 252 (Spectral Energy) before entering the cuvette, and a negatively biased photo diode Bpw 34 for detection.

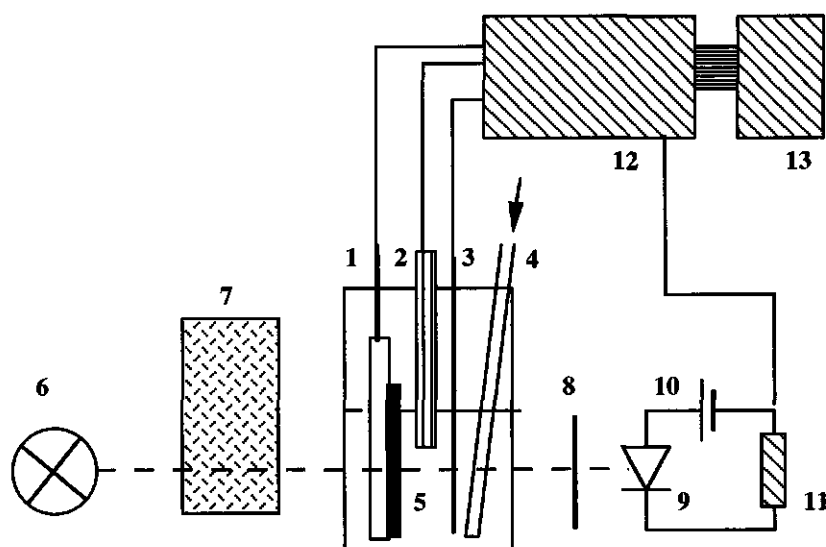


Figure 3. Instrumental details for the transient spectro-electrochemical measurements, 1: sample; 2: Ag/AgCl reference electrode; 3: platinum counter electrode; 4: argon inlet; 5: electrolyte; 6: light source; 7: monochromator; 8: lens (+5 cm); 9: photodiode; 10: power supply; 11: shunt resistance; 12: potentiostat; 13: PC.

Photodiode signals were converted to a voltage over a high-precision 1 k Ω shunt resistor, amplified by a differential amplifier (NF electronic Instruments, type 5305) and recorded by the potentiostat, concurrently with the electrochemical current (Figure 3) Data were processed by a PC (Macintosh LC III) and analysed using Igor (Wavemetrics).

For the spectro-electrochemical measurements the same instrumentation was used as described above, but now spectra were recorded by a CARY 5e spectrophotometer (Varian Associates). Prior to recording an absorption spectrum at a particular potential, the cell was equilibrated for >100 s.

2.4 D.C. and A.C. (photo)-electrical measurements

The most straightforward technique to characterise the behaviour of organic semiconductors junctions consists of measuring the current through a cell as a function of the applied potential (V_a); for photo-electric measurements the samples are illuminated using a 150 Watt Xenon lamp (Spectral Energy) as a light source (Chapters 5 and 6). Varying the externally applied voltage (V_a) linearly in time results in a i/V plot, yielding interesting information, e.g. whether electric barriers are present at the various interfaces and the efficiency of the photon the current conversion efficiency (IPCE). Adding a small sinusoidally varying voltage to V_a yields additional electric parameters e.g. capacities and impurity densities for the cell. This technique is called (electric) impedance spectroscopy. Its essentials can be described as follows:

Applying a sinusoidal potential $V(t)$ over a sample with a finite resistance causes a current $i(t)$ to flow through the sample. For impedance spectroscopy to work the sample has to be in a stable situation and upon removing the perturbation signal, it should return to its original situation. $V(t)$ can be represented in the complex plane with a vector \vec{V} with length V_m and rotating with an angular velocity ω . The current $i(t)$ can be described in the same way in the complex plane, a vector \vec{i} having an angular velocity ω and length I_m . The electric complex impedance (Z) is defined as

$$Z(\omega) = \frac{V_m e^{i\omega\tau}}{i_m e^{i\omega\tau + \theta}} \quad (5)$$

In the complex plane $Z(\omega)$ can be represented by a vector \vec{Z} , with length (V_m/i_m) and making an angle θ with the real axis. The length of \vec{Z} and the angle θ are both a function of the applied frequency ω .

A typical impedance spectrum results by plotting $Z(\omega)$ in the complex plane at different frequencies. The spectrum can be fitted with an equivalent circuit, consisting of a number of electric components like resistances and capacitors, with the same electric properties as the physical processes (e.g. junction capacities, recombination, trapping etc.).

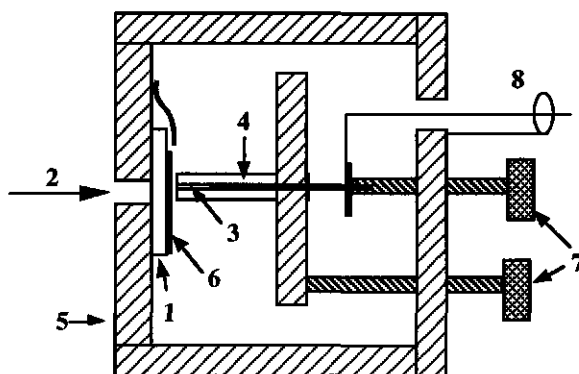


Figure 4. Details of cell for electrical measurements.

1: ITO substrate; 2: optical excitation window; 3: glass capillary with mercury; 4: stainless steel plunger; 5: metal housing; 6: organic layer(s); 7: micrometer screw; 8: BNC connector.

For all electrical measurements the samples were mounted in a sample holder as shown in Figure 4, where a metal clamp makes the electric contact with the ITO substrate. The sensing contact is formed by a mercury droplet with an effective area of 0.78 mm^2 , allowing (photo)electrical measurements of very thin organic layers (5 nm). The metal housing suppresses noise. (Photo)currents were recorded using a potentiostat (Autolab PGstat10, Ecochemie) controlled by GPES3 software (Ecochemie). For illumination of the cells we used the same light source as for the transient electrochemical measurements, described above. The complex impedances were recorded using a frequency response analyser (Solartron Model 1255) combined with an electrochemical interface (Solartron Model 1286). Impedances as a function of applied frequency were fitted using a software program "Equivalent Circuit" developed by Dr. B.A. Boukamp (University of Twente). For a more in-depth treatment of impedance spectroscopy we refer to [17]. Problems arising from impedance measurements stem mostly from impedance spectra, if these can only be fitted with a large number of equivalent components. Often a meaningful relation between these components and physics cannot be made.

2.5 Rutherford back scattering measurements

Ion scattering techniques, like Rutherford Back Scattering measurements (RBS) and Elastic Recoil Detection (ERD) are widely used, non-destructive techniques to determinate the stoichiometry and profile of the vertical cross section of very thin films (even monolayer coverage) [18-20]. In both techniques, ions impinge on the surface of a sample resulting in different impact phenomena. By analysing the number and energy of the ejected particles (back scattered ions for RBS, recoiled for ERD) detailed information is obtained about the chemical composition and the spatial distribution of the chemical species in the substrate.

In a typical RBS experiment (Figure 5a) He^+ ions, with energies ranging from 0.5 - 3 MeV, impinge on a target at an angle of 90° with respect to the surface in a high vacuum chamber (10^{-6} Torr). After elastic collision with a target atom, scattered He^+ ions are recorded by the detector, mounted at a scattering angle of 170° with respect to the surface.

The energy of the back scattered He^+ ions (E_I) depends on the masses (M_1 and M_2) of the particles involved with the collision process, the angles of scattering (α) and recoiling (β) and the energy of the incoming particle (E_0) and can be calculated from the principles of conservation of energy and momentum (Figure 5b). The probability of back scattering of a He^+ ion in the direction of a detector in a solid angle Ω centred around an angle α depends on the scattering *cross section*, which is an analytical function of the energy of the He^+ ions, the mass and atomic number of the target atoms and the scattering angle.

Upon penetrating the sample, the He^+ ions lose energy. This loss is proportional to the thickness of the material traversed and is characterised by the *stopping* efficiency of the sample. This phenomenon is the origin of the depth resolving power of the RBS technique. The loss of energy is due to small angle nuclear collisions of the He^+ ions with target atoms and to inelastic collisions with electrons in the sample. Furthermore, *stopping* is dependent on the energy and mass of the incoming particle and on the electron density of the traversed medium.

An RBS spectrum consists of the fractional number of scattered He^+ ions (yield) vs. their energy. Analysis of RBS spectra yielding elemental analysis as well as depth profiles of the film is routinely performed using the simulation program Rump [21]. One must bear in mind that the spectra give the average over an particular area. Therefore its essential to confirm the homogeneity of the substrate with an independent technique. For a more detailed treatment of the RBS technique and its applications we

refer to literature [22-24]

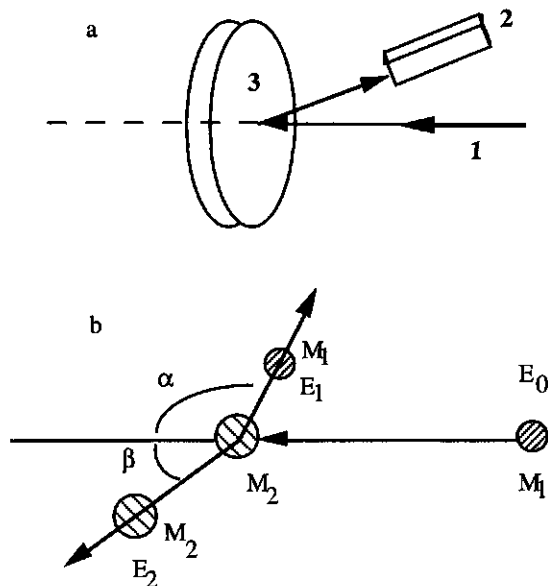


Figure 5 Schematic representation of (a) an RBS-set-up with 1: MeV He⁺ ion beam; 2: particle detector; 3: sample and (b) a scheme of elastic collision pathways of a He⁺ ion with mass M_1 and energy E_0 with a surface nucleus with mass M_2 . Following collision, the He⁺ ion is back scattered at an angle α with an energy E_1 and the surface atom M_2 moves at an angle β with an energy E_2 . The angles α and β are determined by momentum conservation.

References

1. Jones, R.; Tredgold, R. H. and Hoorfar, A. *Thin Solid Films* **1985**, 123, 307.
2. Bruening M.; Moons E.; Yaron-Marcovich D.; Cahen D.; Libman J. and Shanzer A. *J. Am. Chem. Soc.* **1994**, 116, 2972.
3. Lueth, H. *Surfaces and interfaces of solid materials*; Springer-Verlag: Berlin, 1995.
4. Wöhrle, D.; Kreienhoop, L.; Schnurpfeil, G.; Elbe J.; Tennigkeit, B.; Hiller S. and Schlettwein, D. *J. Mat. Chem.* **1995**, 5, 1819.
5. Gregg, B. A. and Kim, Y. I. *J. Phys. Chem.* **1994**, 98, 2412.
6. Karl, N.; Bauer, A.; Holzapfel, J.; Marktanner, J.; Mobus, M. and Stolzle, F. *Mol. Cryst. & Liq. Cryst. A* **1994**, 252, 243.
7. Günster, S.; Siebentritt, S. and Meissner, D. *Mol. Cryst. & Liq. Cryst. A* **1993**, 230, 351.
8. Savenije T.J.; Koehorst R.B.M. and Schaafsma T.J. *Chem. Phys. Lett.* **1995**, 244, 363.

9. Hogue R. *Fres. J. Anal. Chem.* **1991**, 339, 68.
10. Rönnow, D. and Vedszelei, E. *Rev. Sci. Instrum.* **1994**, 65, 327.
11. Grandin, K. and Roos, A. *Appl. Optics* **1994**, 33, 6098.
12. Bard A.J. *Electroanalytical chemistry; Vol 13*; Marcel Dekker: New York, 1984
13. Bard A.J. *Electroanalytical Chemistry; Vol 18*; Marcel Dekker: New York, 1994
14. Bedioui, F.; Devynck, J. and Biedcharreton, C. *Acc. Chem. Res.* **1995**, 28, 30.
15. Malinski, T.; Kubaszewski, E.; Bennett, J.; Fish, J.; Niedbala, H.; Wheeler, D. E. and Czuchajowski, L. *J. Mol. Struc.* **1992**, 270, 125.
16. Schlottwein, D.; Jaeger, N. I. and Wöhrle, D. *Ber. Bunsen-Ges. Phys. Chem.* **1991**, 95, 1526.
17. MacDonald, J.R. *Impedance spectroscopy*; John Wiley & Sons: New York, 1987.
18. Arnold, G. W.; Westrich, H. R. and Casey, W. H. *Nucl. Instrum. Meth B* **1984**, 229, 516.
19. Marée, C. H. M.; Savenije, T. J.; Schaafsma, T. J. and Habraken, F. H. P.M. *Appl. Surf. Sci. in press*.
20. Savenije, T. J.; Marée, C. H. M.; Habraken, F. H. P.M.; Koehorst, R. B. M. and Schaafsma, T. J. *Thin Solid Films* **1995**, 265, 84.
21. Doolittle, L. R. *Nucl. Instr. Meth. B* **1986**, B15, 227.
22. Chu, W.K.; Mayer, J.W; Nicolet and M.A. *Backscattering spectrometry*; Academic: New York, 1978.
23. Feldman, L.C. and Mayer, J.W. *Fundamentals of surface and thin film analysis*; North-Holland: New York, 1986.
24. Marée, C. H. M.; Kleinpenning, A.; Vredenberg, A. M. and Habraken, F. P. H.M. *Nucl. Instr. Meth. B in press*.

Deposition of watersoluble porphyrins on solid substrates

(*Thin solid films*, 1995, 265, 84-88)

Abstract

The deposition of a fourfold positively charged tetrakis(4 - methyl pyridinium) porphyrin (H_2TMPyP) and its metal derivatives on glass surfaces from basic aqueous solutions has been studied by optical and ion beam techniques. Upon exposure to a buffered porphyrin solution, the glass surface is initially almost completely coated with a monomolecular porphyrin layer ($5 \cdot 10^{13}$ molecules \cdot cm $^{-2}$). Subsequently the area of the glass surface available for deposition of porphyrins increases due to leaching by the buffer solution, resulting in an almost linear increase of the amount of adsorbed organic material. Adsorption is limited to a monolayer in the presence of trace amounts of zinc ions.

3.1 Introduction

Ruthenium complexes, phthalocyanines and porphyrin-like compounds have been extensively used as building blocks for molecular devices such as molecular photo diodes and solar cells [1,2]. Devices based on these compounds are gaining interest due to their optical and electrical properties and possible economical advantages as compared to inorganic semiconductors.

During the last decade a number of techniques have been reported to sensitise (semi)conductors with these organic dyes, using various methods, including Langmuir-Blodgett monolayer deposition, spin coating and vacuum deposition. These methods involve the deposition of the dyes on substrates resulting in films with different physical properties, such as the orientation of the dye molecules with respect to the substrate surface, the electrical conductance and the arrangement of the dye molecules in the film. A straightforward technique for applying dye molecules to solid substrates has been developed by Grätzel *et al.* [1]. In the present study hydrophobic as well as Coulombic forces cause a spontaneous, irreversible adsorption from the solution of the dye onto the substrate.

Porphyrins equipped with four positively charged pyridinium groups (Figure1) are attractive dyes because of their relatively low reduction potential [3,4] and high affinity for negatively charged solid surfaces. Although in the solid state the porphyrin redoxpotentials may be somewhat different from those in solution [5-7] , these two properties make these compounds suitable as sensitizers for wide gap semiconductors, either as a single type of porphyrin or as the acceptor in a donor/acceptor complex, deposited on the (semi)conducting substrates.

Close physical contact of the molecule with the substrate favours effective electron injection into the substrate [8,9] which is an important requirement for a molecular device having a high efficiency and a relatively low dark resistance.

Despite the large amount of information about porphyrins, so far only a few papers have dealt with the characteristics of the adsorption of porphyrins and their analogues on solid substrates. [9-14] For a better understanding of the adsorption behaviour of these porphyrins we studied the factors affecting this adsorption on a model substrate, a soda lime glass, using optical spectroscopy and ion beam techniques.

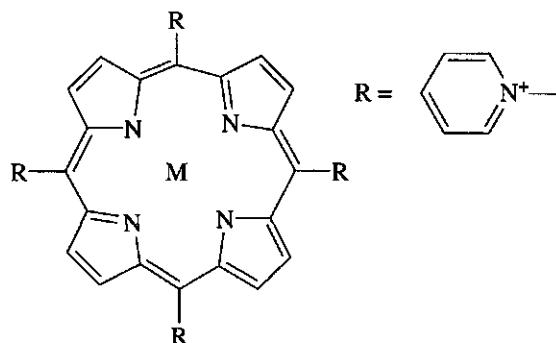


Figure 1. Chemical structures of used porphyrins; M=2H, tetra(4-methyl pyridinium)porphyrin: H₂TMPyP, M=Zn, zinc tetra(4-methyl pyridinium)porphyrin: ZnTMPyP, M=Pd, palladium tetra(4-methyl pyridinium)porphyrin: PdTMPyP.

3.2 Experimental

Microscope slides (Rofa Mavi), consisting of a soda lime like glass, quartz substrates (Westdeutsche Quarzschmelze) and Corning glass were ultrasonically cleaned in a detergent solution (Decon 90), rinsed with demi water, methanol (PA, Merck), acetone (PA, Merck) and dried with nitrogen gas. Porphyrins (Porphyrin Products Inc., USA.) were obtained in crystalline form by dissolving in acetic acid and precipitation using a NaHCO₃ solution. This procedure was repeated twice and the purity of the porphyrins was checked by their spectra in the visible region (380-700 nm). Various types of porphyrins were adsorbed on both sides of the glass slides in plastic vessels from an aqueous carbonate buffer (Merck) at room temperature. After withdrawal from the solution, the slides were subsequently rinsed with p.a. methanol and acetone and then dried with nitrogen gas. This method yields double-sided coated, homogeneously coloured and highly reproducible samples.

The number of adsorbed molecules is determined by desorption of the coated slides in 10% w/v detergent (SDS) solution and measuring the optical absorption of the resulting solution.

Absorption spectra were recorded using a Uvikon 810 spectrophotometer; for fluorescence spectra we used a Perkin-Elmer LS-5 fluorimeter with a front surface accessory. Spectra were processed with a Macintosh LC personal computer and analysed with Igor (Wavemetrics). Rutherford Back Scattering (RBS) measurements

were applied to the adsorbed porphyrin films using a 2.0 MeV He^+ ion beam from a 3 MeV Van de Graaff accelerator. The incident beam made an angle of 70° to the surface normal, and the scattering angle was 170° . The normalized yield is calculated from the raw counts divided by the detector solid angle, the total current collected at the sample and the energy resolution of the detector [15].

3.3 Results and discussion

H_2TMPyP is monomeric ($<10^{-3}$ M) in aqueous solution as follows from optical spectroscopy [16]. During adsorption of H_2TMPyP the increase of the amount Γ (molecules.cm^{-2}) of adsorbed porphyrins can be divided in two parts, a fast non-linear growth followed by a much slower one which is almost linear in time. At a short time scale the first part reaches a quasi-reversible equilibrium and the adsorption kinetics can only be followed at concentrations of $\leq 10^{-7}$ M using reflectometry [17]. The amount of adsorbed material in this quasi equilibrium state is affected by pH (Figure 2) and the porphyrin concentration (Figure 3).

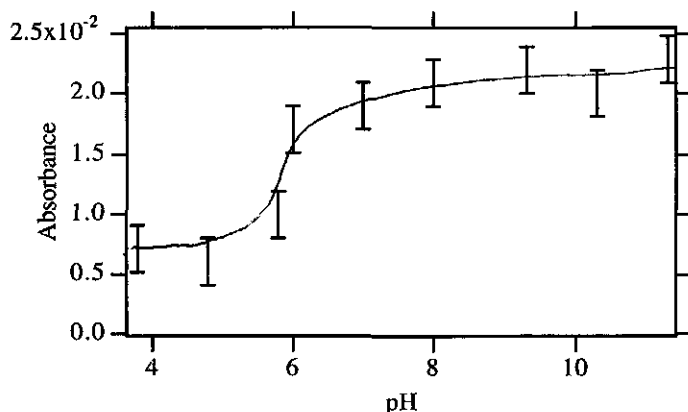


Figure 2 pH dependence of the equilibrium amount of adsorbed H_2TMPyP on glass substrates determined by the optical absorbance of double sided coated slides. $[\text{H}_2\text{TMPyP}] = 1 \times 10^{-4}$ M. Adsorption occurred from an aqueous 10 mM phosphate buffer during 1 hour. Error bars represent estimated errors, due to differences between various substrate samples and instrumental accuracy. Spectra are uncorrected for reflection.

Using desorption techniques, we found $\Gamma = 5 \cdot 10^{13}$ molecules.cm⁻² at pH > 8, [P] > 5.10⁻⁵ M for H₂TMPyP, corresponding to a completely covered surface, assuming that the adsorbed layer consists of porphyrin molecules with molecular dimensions of 1.5 * 1.5 nm and a parallel orientation of the porphyrin molecular plane with respect to the substrate. This assumption is based on the results of total internal reflection fluorescence measurements. From these measurements it follows that the orientational distribution of H₂TMPyP on microscope glasses is rather narrow around $\Theta = 0^\circ$, where Θ is the angle between the normals to the molecular plane and the substrate, respectively. Reducing the number of charged pyridinium substituents causes the orientational distribution to become broader. Obviously the binding of the porphyrin to the glass substrate is at least partially due to electrostatic interaction between positive charged pyridinium groups and negative surface charges of the glass substrate[18]. For H₂TMPyP the second part of the adsorption kinetics exhibits a slow, almost linear growth of Γ , independent of the porphyrin concentration (Figure 4). Γ obtained from desorption agrees with the amount of carbon atoms in the adsorbed film as follows from RBS measurements.

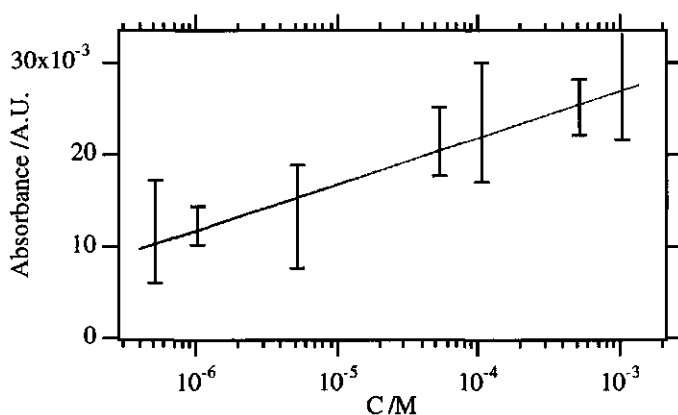


Figure 3. Absorbance of H₂TMPyP on glass slides vs. porphyrin concentration of an aqueous sodium bicarbonate buffer, pH = 9.3. (1 hour adsorption period).

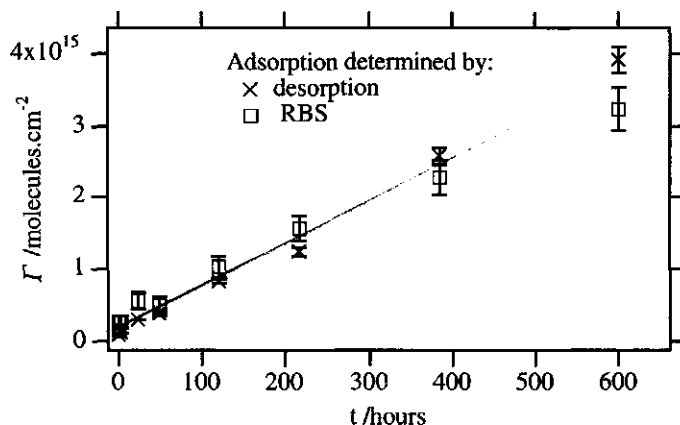


Figure 4. Determination of the amount of adsorbed H₂TMPyP using optical and RBS (amount based on carbon counts) respectively. Error bars of both deposition methods are estimated experimental errors.

The amount of carbon atoms is calculated from the area of the carbon peak in the RBS spectra, (see carbon peak between channels 60 and 80 in fig 5b) the total incident current and from the known absolute Rutherford cross section for scattering of He⁺. The assumption is made that all detected carbon atoms originate from H₂TMPyP. The agreement between the amount of adsorbed material determined by optical spectroscopy and RBS, enables us to relate the optical density at the maximum of the Soret band of a double sided coated sample and Γ . For H₂TMPyP this conversion factor c is $3.7 \cdot 10^{-16}$ (molecules⁻¹.cm²). For monolayer adsorption the correction for reflection is negligibly small.

For a series of RBS measurements on samples with different Γ a double step for the most abundant atoms present in lime glass (O, Ca, Na and Si) is found which is absent for bare glass (cf. Figure 5b with Figure 5a). Each step (expressed as the number of channels) can be converted to a depth by assuming a density of 2.3 gram/cm³ for soda-lime glass. It appears that an increasing amount of carbon due to adsorbed porphyrin, does not correspond to an increasing thickness of the layer covering the glass substrate, but rather to an incorporation of porphyrins into the surface layer of the glass. This surprisingly result is based on our observation that this layer is depleted from Si, O and Ca, giving way to porphyrin incorporation. The RBS ratio of porphyrin atoms and glass atoms remains the same for this surface layer for all glass samples and was found to be independent of the value of Γ .

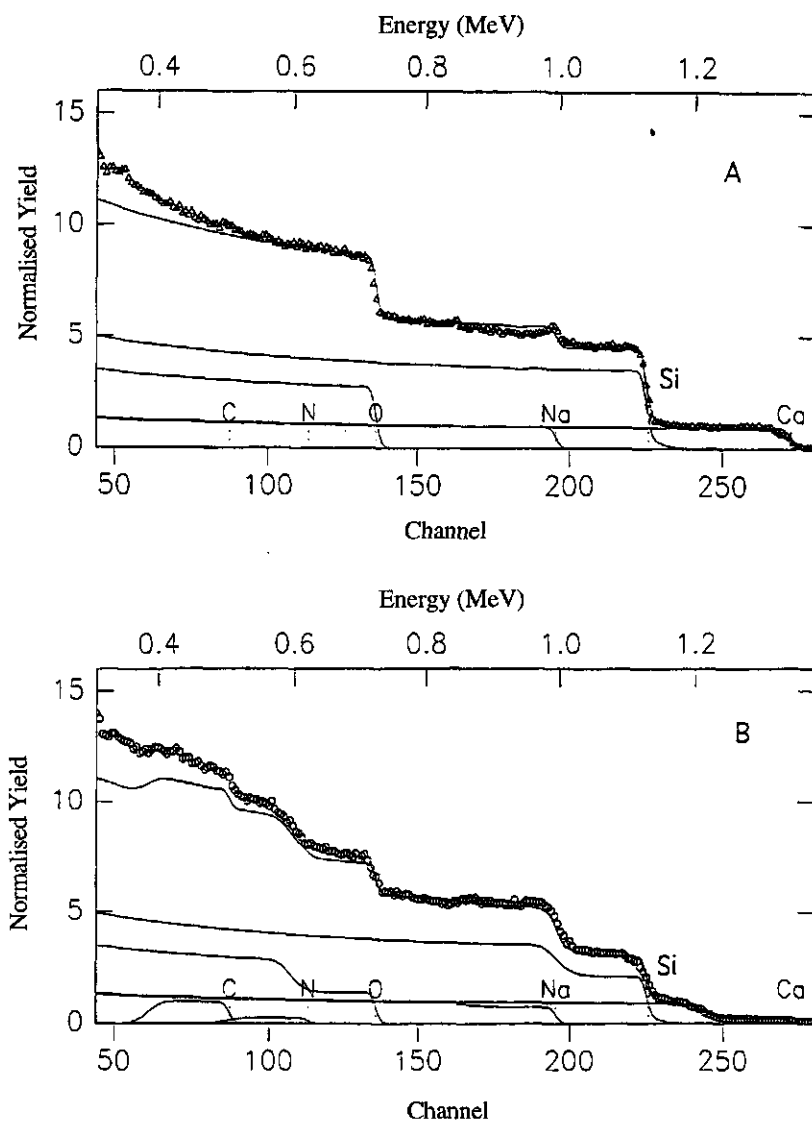


Figure 5. RBS spectra of A: bare soda lime glass and B: soda lime glass with adsorbed H_2TMPyP . Note the depletion of Ca, and to a less extent of Si and O, replaced by carbon and nitrogen from the porphyrins. Full lines represent a computer simulation with the separate contributions of the different atoms, their sum simulating the experimental RBS curve. Δ : experimental bare soda lime glass, \circ : experimental soda lime glass with adsorbed H_2TMPyP , —: computer simulation.

RBS measurements show that after desorption of the adsorbed porphyrins, the Ca/Si ratio is different from that before adsorption of the porphyrin. This indicates that as a result of the experimental conditions, the chemical structure of the glass has changed. Enclosed metal ions present in the surface layer of the glass, e.g. Ca^{2+} and Mg^{2+} are released during the experiment. This release is confirmed by studying the porphyrin solution after adsorption has taken place, revealing a chemical modification of a part of the porphyrins. Subtracting the absorption spectrum of H_2TMPyP from this solution spectrum yields a spectrum with two maxima at 580 and 630 nm, corresponding to those reported for magnesium tetra(4-methyl pyridinium) porphyrin [19]. This means that during porphyrin adsorption Mg^{2+} is also depleted in the substrate and that Mg^{2+} ions are incorporated into the free base porphyrin present in the solution. In the absorption spectra of H_2TMPyP on glass the Soret band is 14 nm red shifted and broadened with respect to that in solution. The Q-band absorption spectrum contains four broadened bands, characteristic for a free base porphyrin spectrum, indicating the absence of chemical modification of the absorbed porphyrin moiety (Figure 6).

Placing a glass substrate in a 1 mM sodium hydroxide solution the amount of adsorbed H_2TMPyP as judged from the optical absorption increases until a plateau is reached and the pH of the solution has changed to ≈ 7 . Adding a fresh amount of sodium hydroxide up to pH=10 to the this solution and replacing the sample in this solution results in an additional increase of Γ and a neutralisation of the solution. Tetra (3-methyl pyridinium)porphyrin, tetra (2-methyl pyridinium)porphyrin, tetra (trimethyl 4-anilinium) porphyrin and PdTMPyP show very similar characteristics for adsorption on glass slides as H_2TMPyP .

The above mentioned leaching process of the glass surface is caused by the attack of OH^- on -O-Si-O- chains at the surface, resulting in -O-Si-OH and $-\text{O}^-$ surface groups. The negative surface charge is neutralised in our experiments by the positively charged porphyrin. By breaking -O-Si-O- chains Ca and other metals ions present in the glass are released into the solution. The amount of released material from the top layers of the glass substrate is linear in time [20], and corresponds to a linear decrease of the calcium content measured with RBS and the linear growth of the optical density of the absorbed porphyrin film. A similar Ca depletion caused by leaching has been found by Arnold *et al.* [21]

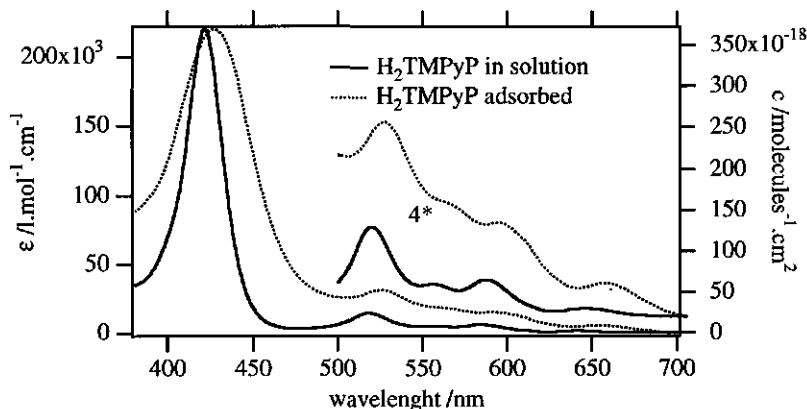


Figure 6. Absorption spectra of H_2TMPyP in solution and adsorbed on glass expressed as extinction coefficient and conversion factor, respectively. Note the red shift of the adsorbed porphyrin spectrum. Spectra of adsorbed porphyrins are uncorrected for reflection. Inset: enlarged Q-band region.

As follows from RBS results (Figs. 5a, b), the resulting porous structure of the glass surface layer thus consists of a decreased amount of constituent glass elements (Si, O, Ca, Na) and a concomitant increase of the amount of the porphyrins elements (C, N) both per unit volume. Using other substrates like quartz or Corning glass, which resist this leaching process, results in samples with a maximum O.D. $\approx 2.5 \cdot 10^{-2}$. The restricted adsorption on inert materials together with the depletion of the top layers of the glass surface are strong evidence that, the growth of the amount of adsorbed material is not due to stacking or island stacking of the porphyrins onto the surface. Further details of RBS, ERD and XPS measurements will be published elsewhere [22].

Adsorbed porphyrins can be exchanged by other positively charged porphyrins, by exposing the adsorbed film to a solution containing an excess of these porphyrins. This prompted us to further investigate the adsorption of porphyrins on glass from solutions containing a mixture of two different porphyrins.

In contrast with H_2TMPyP , $ZnTMPyP$ does not show an increase of Γ in time, even for prolonged adsorption periods in the presence of a carbonate buffer. Also RBS spectra do not show Ca depletion.

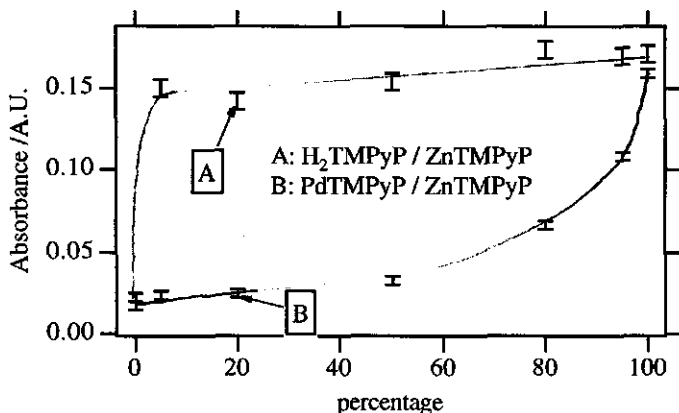


Figure 7. Effect of using different mixtures of porphyrins, as indicated in the figure, on the amount of adsorbed material determined by the O.D. of both porphyrins on the substrate. The horizontal axis represents the percentage H₂TMPyP in the solution containing a mixture of H₂TMPyP/ZnTMPyP (curve A) and the percentage PdTMPyP in the solution containing a mixture of PdTMPyP/ZnTMPyP (curve B), from which adsorption took place. All samples were exposed during 50 hours to a solution with a total porphyrin concentration of $7.5 \cdot 10^{-5}$ M at pH 9.3.

To elucidate the different behaviour of ZnTMPyP and H₂TMPyP we carried out adsorption experiments of H₂TMPyP/ZnTMPyP mixtures in different ratios on microscope glass slides, yielding the Job plots shown in Figure 7. The corresponding Q-band absorption spectra of the porphyrins on the glass slides show an equal ratio of both porphyrins as in the solution, i.e. there is no preferential adsorption of either H₂TMPyP or ZnTMPyP. The kinetics of the above mentioned leaching process of a glass sample in a mixed H₂TMPyP/ZnTMPyP solution remains the same for solutions containing a H₂TMPyP/ZnTMPyP mixture with a percentage H₂TMPyP from 5 up to 100%. In a ZnTMPyP solution without H₂TMPyP, however, the leaching process is found to be fully inhibited. Replacing H₂TMPyP by PdTMPyP in a mixture with ZnTMPyP, the efficiency of the leaching process is again changed. Now, effective leaching occurs only in a solution containing a high percentage of PdTMPyP (Figure 7). These observations suggest that a solution containing only ZnTMPyP protects the glass surface from attack by an alkaline solution. The ratio H₂TMPyP/ZnTMPyP or PdTMPyP/ZnTMPyP does not appear to be the rate determining step for the leaching process.

This prompted us to investigate the presence of other factors in our system affecting this leaching process. Traces of zinc ions adsorbed on the glass are known to strongly inhibit the hydrolysis of the O-Si-O chains by an alkaline solution [20]. Adding a trace of zinc chloride to a PdTMPyP solution was indeed found to fully inhibit the glass surface from being leached by an alkaline solution. On the other hand, eliminating Zn^{2+} ions from the solution, by precipitation with phosphate followed by removal of the zinc phosphate by filtering, was found to restore the leaching of the glass surface.

The Job plots of Figure 7 can now be understood by assuming that ZnTMPyP contains a trace of free zinc ions. In a solution of a $\text{H}_2\text{TMPyP}/\text{ZnTMPyP}$ mixture, free zinc ions are efficiently scavenged by H_2TMPyP , leaving the glass surface unprotected against the leaching process, whereas in a pure ZnTMPyP solution the glass surface is protected by the presence of trace amounts of free Zn^{2+} ions. In a mixture of ZnTMPyP and PdTMPyP the free zinc ions cannot be incorporated as in the free base porphyrin and monolayer adsorption is observed.

A plot of the location of the absorption maximum vs. Γ for H_2TMPyP shows a 10 nm blue shift of the Soret absorption band for relatively thick films after prolonged adsorption. At long adsorption periods leaching is relatively slow, with a concomitant growth of the surface area and a further slow increase of the amount of adsorbed porphyrin, following the first fast phase of monolayer adsorption. Porphyrins adsorbed during this slow secondary phase give rise to the observed blue shift of the absorption maximum of the Soret band. A plot of the normalised luminescence with excitation and emission at the maxima of the absorption- and fluorescence bands exhibits a decreasing relative fluorescence yield per molecule as Γ increases. The fluorescence yield decrease is believed to be due to an increase of radiationless decay channels due to enhanced excitation transport at increasing thickness of the adsorbed film.

The adsorption characteristics of positively charged porphyrins described in this work may constitute a tool for controlled deposition of various organic dyes on suitable substrates. Chemically labile substrates like soda lime glass form a porous structure upon leaching, resulting in very high surface concentrations after adsorption. The finding that porphyrins adsorbed at a glass surface can be partially or completely exchanged by a second type porphyrin suggests that graded porphyrin layers on glass substrates can be produced in a controlled way. Because the structure of the porous surface layer of glass is rough at the molecular level, determination of the orientational distribution is not feasible. Such investigations require flat inert substrates, e.g. quartz [18].

Acknowledgements

This investigation was supported by the Dutch Foundation for Chemical Research (SON) with financial aid of the Dutch Organisation for Scientific Research (NWO) and the Dutch Agency for Energy and Environment (NOVEM) under contract nr. 71.140-0011

References

1. A. Kay and M. Grätzel, *J. Phys. Chem.* **1993**, *97*, 6272.
2. J. B. Whitlock, P. Panayotatos, G. D. Sharma, M. D. Cox, R. R. Sauers and G. R. Bird, *Opti. Eng.* **1993**, *32*, 1921.
3. F. J. Vergeldt, R. B. M. Koehorst, T. J. Schaafsma, J. C. Lambry, J. L. Martin, D. G. Johnson and M. R. Wasielewski, *Chem. Phys. Lett.* **1991**, *182*, 107.
4. M. Neumann-Spallart and K. Kalyanasundaram, *J. Phys. Chem.* **1982**, *86*, 5163.
5. L. Gaillon, F. Bedioui, J. Devynck and P. Battioni, *J. Electroanal. Chem.* **1993**, *347*, 435.
6. A. Bettelheim, D. Ozer, R. Harth and R. W. Murray, *J. Electroanal. Chem.* **1989**, *266*, 93.
7. A. Harriman, V. Heitz, M. Ebersole and H. Vanwilligen, *J. Phys. Chem.* **1994**, *98*, 4982.
8. E. Katz, N. Itzhak and I. Willner, *Langmuir* **1993**, *9*, 1392.
9. K. Kalyanasundaram, N. Vlachopoulos, V. Krishan, and M. Grätzel, *J. Phys. Chem.* **1987**, *91*, 2342.
10. R. Holze, *Electrochim. Acta* **1988**, *33*, 1619.
11. L. A. Khanova and L. F. Lafi, *J. Electroanal. Chem.* **1993**, *345*, 393.
12. K. Itoh, T. Sugii and M. Kim, *J. Phys. Chem.* **1988**, *92*, 1569.
13. C. A. Fierro, M. Mohan and D. A. Scherson, *Langmuir* **1990**, *6*, 1338.
14. S. Kim, I. T. Bae, M. Sandifer, P. N. Ross, R. Carr, J. Woicik, M. R. Antonio and D. A. Scherson, *J. Am. Chem. Soc.* **1991**, *113*, 9063.
15. L. C. Feldman and J.W. Mayer *Fundamentals of Surface and Thin Film Analysis*; New York: Elsevier Science Publishing, 1986.
16. F.J. Vergeldt, R.B.M. Koehorst, A. van Hoek and T.J. Schaafsma *J. Phys. Chem.* **1995**, *99*, 4397.
17. J.C. Dijt, M.A. Cohen Stuart, J.E. Hofman, and G.J. Fleer *Colloids and surfaces* **1990**, *51*, 141.
18. J. Wienke, F. Kleima, R.B.M. Koehorst and T.J. Schaafsma, *Proceedings of the 12th European Photovoltaic Solar Energy Conference*; Bedford: H.S. Stephens & Ass., 1994 p5,64-5,67.
19. J. B. Verlhac and A. Gaudemer, *N. J. de Chemie* **1984**, *8*, 401.
20. M.B. Volf *Technical Glasses*; London: Sir I. Pitman and Sons, LTD, 1961.
21. G. W. Arnold, H. R. Westrich and W. H. Casey *Nucl. Instrum. Methods Phys. Res. B* **1984**, *229*, 516.
22. C.H.M. Marée, T.J. Savenije, T.J. Schaafsma and F.H.P.M. Habraken, *Appl. Surf. Sci.* **1996**, *93*, 291.

Spectroelectrochemical measurement of charge transport properties of electropolymerised tetra(hydroxyphenyl) porphyrins

(J. Phys. Chem. in press)

Abstract

Hydroxy-phenyl substituted metallo-porphyrins have been electro-polymerised as films onto ITO substrates. An ether bond between the phenyl rings of two monomers links the porphyrin units, leaving the porphyrin macrocycles undisturbed. During electrochemical oxidation of the films using a 0.0 - 0.9 V potential window, a single, semi-reversible reaction is observed, with $n \approx 0.5$ electron per porphyrin molecule. The spectro-electrochemical characteristics of these films can be adequately described by assuming that two porphyrin units are involved in the progressive oxidation process, in agreement with the changes in the absorption spectrum of the film.

To characterise charge carrier conduction, diffusion coefficients for chemically different films have been determined. From the optical changes upon oxidation of the film the diffusion coefficients for hole transport were found to be $(1-2) \cdot 10^{-10} \text{ cm}^2 \text{ s}^{-1}$. No correlation was found between the value of the diffusion coefficient and the number of cross links per porphyrin unit. The average distance between vicinal porphyrin macrocycles therefore most likely determines charge carrier diffusion.

4.1 Introduction

Organic dye molecules absorbing visible light have been frequently used as active components in heterojunction photocells [1-5]. Previously, we reported the photoelectric characteristics of a heterojunction, consisting of a spin-coated porphyrin electron-acceptor on top of an electro-polymerised porphyrin electron-donor layer [1]. For applications of such heterojunctions in devices, their charge carrier conductivity must be sufficiently high.

Charge transport in Langmuir-Blodgett- and electro-polymerised films of porphyrins and similar compounds has been extensively studied [6-10]. The conduction mechanism in such films is still incompletely understood, however, due to complications arising from e.g. unintended doping by oxygen or moisture [11,12]. Electrochemical measurement of the charge carrier diffusion coefficient (D) - directly related to the carrier mobility [13] - avoids this problem, since it can be carried out in an inert, moisture-free atmosphere. Theoretical models underlying charge carrier diffusion in redox polymer films have been around for quite some time [14]. (For a recent review, see [15]).

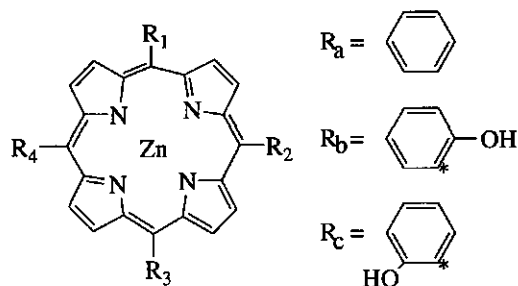


Figure 1. Molecular structures of porphyrins;

R_1 - $R_4 = R_b$: zinc 5,10,15,20,- tetra (4-hydroxyphenyl) porphyrin (1); $R_1 - R_4 = R_c$: zinc 5,10,15,20,- tetra (2-hydroxyphenyl) porphyrin (2); $R_1, R_2 = R_b$ and $R_3, R_4 = R_a$: zinc 5,10,- di (4-hydroxyphenyl) 15,20,- diphenyl porphyrin (3); $R_1, R_3 = R_b$ and $R_2, R_4 = R_a$: zinc 5,15,- di (4-hydroxyphenyl) 10,20,- diphenyl porphyrin (4). Starred atom indicates position for nucleophilic attack during electro-polymerisation.

In the experiments described in this paper an electro-polymerised porphyrin film deposited on an ITO electrode is placed in an electrochemical cell. By applying a sufficiently high potential initially the first (or first few) porphyrin layers directly at the ITO surface are oxidised and subsequently the entire film. Since the electron injection from the first porphyrin layer into the ITO electrode is fast [16], the interaction between vicinal molecules in the film controls the maximum rate for electron transfer from neutral to oxidised layers, and thus the diffusion coefficient (D). Since upon oxidation an electron is withdrawn from the HOMO, D is mainly determined by the HOMO/HOMO (electronic) interaction. Therefore, the charge carriers in the oxidised films are holes.

A number of recent reports discuss the electrochemical characteristics of electropolymerized films of a variety of functionalised porphyrins [8-10], but there is only limited information on the mechanism of film formation and on the charge carrier diffusion coefficients [16, 17]. In this work we have examined (i) the mechanism of film formation and (ii) progressive oxidation of the polymerised films by using spectro-electrochemical techniques. Combining the optical and electrochemical results enabled us to derive the diffusion coefficients for hole transport in the electro-polymerised films. The influence of the film structure on the diffusion coefficients is discussed.

4.2 Experimental

Materials

Zinc-*tetra* (4-hydroxyphenyl) porphyrin (1), zinc-*tetra* (2-hydroxyphenyl) (2) porphyrin (fig. 1) (Mid-century Chemicals) were checked for purity using thin layer chromatography and UV-Vis absorption spectroscopy. Zinc-*di* -5,10, -(4-hydroxyphenyl) *di* -15,20,-phenyl porphyrin (3) and zinc-*di* -5,15-(4-hydroxyphenyl) *di*-10,20,-phenyl (4) porphyrin were prepared according to literature [18]. Analytical grade acetonitrile (MeCN, Merck), electrochemical grade tetra *tert*-butyl ammonium perchlorate (TBAP, Fluka), and p.a. 2,6-*di*(*tert*-butyl)-pyridine (DBUP, Aldrich) were used as received. ITO (30 Ω/\square) (Glastron) substrates were ultrasonically cleaned in demineralised water, washed in p.a. methanol (Merck) and p.a. acetone (Merck) and subsequently dried with nitrogen.

For electro-polymerisation we used a conventional three electrode system, consisting of an ITO working electrode, a platinum counter electrode and an Ag/AgCl ($[KCl] = 3\text{ M}$) reference electrode. For electrochemical measurements we used a potentiostat (Autolab Pstat10, Ecochemie) controlled by GPES3 software (Ecochemie). All potentials are vs. a Ag/AgCl reference electrode unless otherwise stated. UV-Vis absorption spectra of the porphyrin films on ITO were recorded using a Cary 5e spectrophotometer (Varian), equipped with a diffuse reflectance sphere. Absorption spectra were corrected for reflection.

Film formation

The electro-polymerisation was carried out at room temperature using a $\approx 1\text{ mM}$ porphyrin solution in MeCN, containing 0.1 M TBAP as supporting electrolyte and 0.05 M DBUP. All porphyrin solutions were by bubbling argon through for 15 min. prior to measurements. Following polymerisation, the coated substrates were rinsed with MeCN and subsequently washed with ethanol and acetone and dried with nitrogen. The porphyrin-coated substrates were stored in air and kept in the dark.

Characterisation of films

For spectro-electrochemical measurements the coated substrates including counter - and reference electrode were placed in a $2 \times 2 \times 5\text{ cm.}$ cuvette (Hellma) filled with freshly deoxygenated MeCN containing 0.5 M TBAP and used in the Cary spectrophotometer. For transient spectro-electrochemical measurements we used a 150 Watt Xenon lamp (Spectral Energy), passing through a monochromator GM 252 (Spectral Energy) before entering the cuvette, and a negatively biased photo diode Bpw 34 for detection. Photodiode signals were converted to a voltage over a high-precision $1\text{ k}\Omega$ shunt resistor, amplified by a differential amplifier (NF electronic Instruments, type 5305) and recorded by the potentiostat, concurrently with the electrochemical current. Data were processed by a PC (Macintosh LC III) and analysed using Igor (Wavemetrics). Thickness measurements were performed with a step profilometer (Sloan Dektak, 3030 ST). The swelling of the films during prolonged exposure to the electrolyte solution, resulting in an increased thickness, was neglected in the subsequent data-analysis.

4.3 Results

Film formation

Figure 2a shows the evolution of the voltammogram during progressive electro-polymerisation of zinc-*tetra* (4-hydroxy phenyl) porphyrin (**1**) in a sequence of 10 cyclic scans from +0.1 to +1.0 V and a potential scan rate ν of 0.1 V.s⁻¹. Repeated cycling is accompanied by an increase of the amplitude of the oxidation- and reduction waves, which is commonly interpreted [9,16,19] to be due to an increase of the number of porphyrin molecules per cm⁻² area (Γ). The resulting layer thickness (varying from several nm till \approx 100 nm) depends on the potential window, the number of scans and the porphyrin concentration. Following its formation by electro-polymerisation, the film is insoluble in MeCN or any other common solvent. Zinc-*tetra* (2-hydroxyphenyl) porphyrin (**2**) behaves similarly. In the absence of DBUP a semireversible oxidation is visible, but without any significant increase of the oxidation waves upon repetitive cycling in contrast with the cyclic voltammograms in Figure 2. In consequence, no film formation is seen.

Film formation was also observed for porphyrins equipped with 2 hydroxy-phenyl substituents, i.e. zinc-*di* -5,10,-(4-hydroxyphenyl) *di* -15,20,-phenyl porphyrin (**3**) and zinc-*di*-5,15-(4-hydroxyphenyl) *di*-10,20,-phenyl porphyrin (**4**). Electro-oxidation of zinc mono (4-hydroxy phenyl) triphenyl porphyrin in the potential range 0.0 - 1.0 V does not result in a film with thickness continuously increasing with the number of scans. For this compound polymerisation stops at low coverage. Comparison of the optical absorbance of this film with that of a spontaneously adsorbed porphyrin monolayer, indicates the electro-polymerisation for this compound ceases at monolayer or submonolayer coverage [20]. Introduction of methyl or butyl groups at both meta positions of the para hydroxy phenyl substituents of the porphyrins completely prevents film formation.

During electro-polymerisation of **4**, and similarly of **3**, a cyclic voltammogram is observed which is different from that for **1** and **2** (Figure 2b). The first oxidation wave occurs at 0.78 V, close to that for zinc *tetra* phenyl porphyrin [21], though the molecules and the solvent differ. This indicates that also for compound **2**, the macrocycle is oxidised instead of the metal atom. The maximum of the cathodic wave is at 0.64 V, which shifts to 0.82 V after several scans.

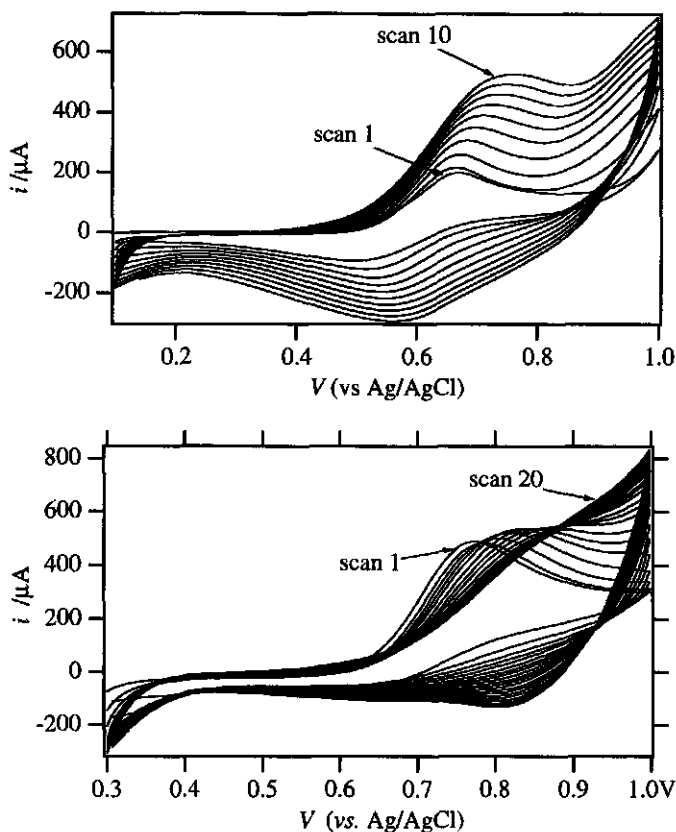


Figure 2. Consecutive cyclic voltammetric scans at ITO electrodes of **1** (a) and **4** (b) in 0.1 M TBAP/MeCN at 100 mV/s. Cell area : 3.4 cm².

Spectroelectrochemical characterisation of the films

UV-Visible spectra of a film of **1**, **3** and **4** on ITO show a Soret band at 442 nm, broadened in comparison with the corresponding band of the monomer in solution. The two Q bands of a film of compound **1** at 563 and 605 nm are also broadened (Figure 3); their positions are close to those of the monomer in solution. The Q₀₀ band of a film of **2** is ≈20 nm red shifted with respect to the corresponding monomer band in solution. The intensities of the Q₀₀ and Q₁₀ bands for this film have reversed as compared to those of the monomer.

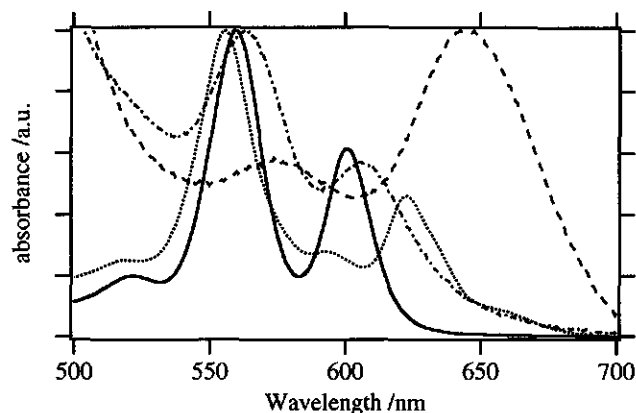


Figure 3. Absorption spectra of Q band region of porphyrin monomers in ethanol of **1** (—), and **2** (····), and of polymerised films of **1** (-·-) and **2** (---).

For a number of samples with different optical densities, the relation between the surface coverage Γ (molec.cm⁻²) and the thickness d (m) was experimentally determined. We used of Rutherford Back Scattering (RBS) [20] to measure Γ , whereas d was determined using a step profilometer. Now the experimentally measured optical density ($O.D.$) can be related to the sample thickness [5], using

$$O.D. = \alpha d \quad (1)$$

where d is the layer thickness (in m) and $\alpha = 3.7 \times 10^6 \text{ m}^{-1}$ at 563 nm.

Figure 4 shows cyclic voltammograms of polymerised films of different porphyrins on ITO in MeCN containing 0.5 M TBAP, at $\nu = 0.1 \text{ V/s}$. The films of both polymerised di-functionalised porphyrins (**3** and **4**) are electro-chemical similar and exhibit well resolved waves with half wave potentials estimated by the mean of anodic and cathodic potential at 0.81 V. The oxidation waves for electro-polymerised films of tetra-functionalised porphyrins are distinctly broader than for the other compounds.

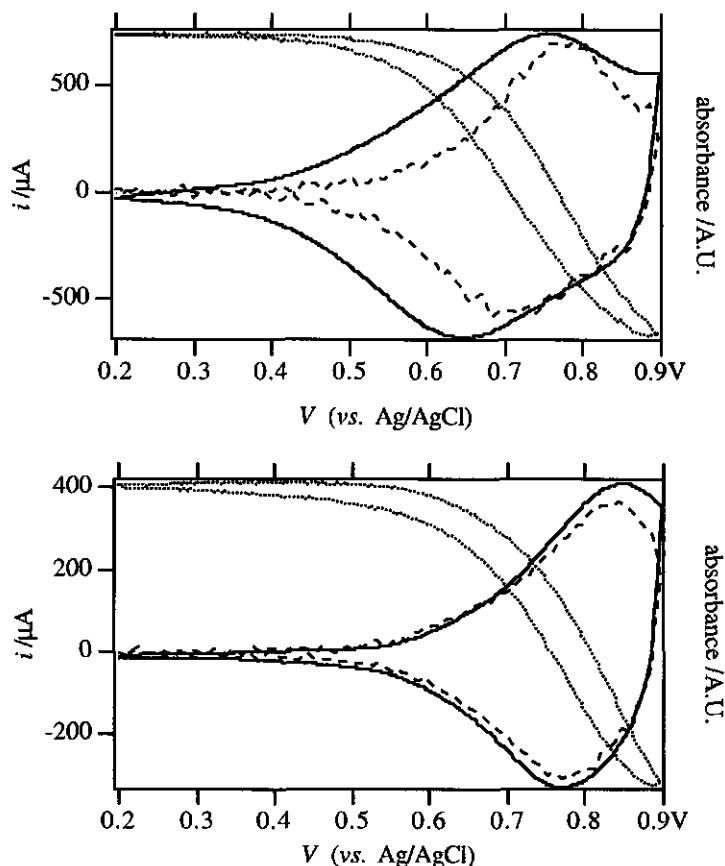


Figure 4. Cyclic voltammograms and absorbance changes at $v = 0.1 \text{ V.s}^{-1}$ in MeCN/ 0.5 M TBAP of different porphyrin films on ITO. Total current: (—), *O.D.* ($\lambda = 440 \text{ nm}$): (···) faradaic currents: (— · —) for a: 1, b:3.

To separate the faradaic from the capacitive contribution to the total current in the voltammogram we combined optical absorbance and electrochemical measurements: the changes in the absorption spectrum of the films during oxidation were monitored simultaneously with the voltammograms. Increasing the oxidation potential to 0.9 V results in a decrease of the Soret band (442 nm) intensity for a film of **1**; the band shifts to slightly lower wavelength and a broad band at 480 nm appears with isosbestic points at 403 and 458 nm (Figure 5). The Q bands broaden and a low structureless absorption appears between 500 and 900 nm. The absorption spectrum of the neutral film is regained by applying the starting potential and is for $\lambda = 440 \text{ nm}$ illustrated in Figure 4. Above 0.9 V the absorbance gradually decreases and the isosbestic points disappear, with concomitant loss of electrochemical activity.

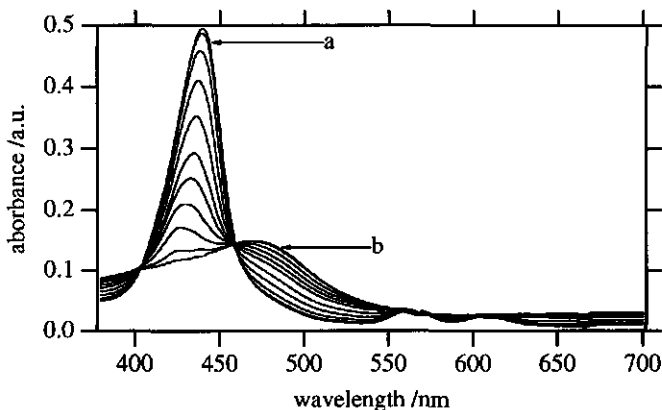


Figure 5. Absorption spectra of a polymerised film of **1** on ITO in MeCN/0.1 M TBAP at different potentials (a through b) $V = \text{O.C.V.}$ (a), stepwise increased to 0.40; 0.50; 0.55; 0.60; 0.65; 0.7; 0.75; 0.80; 0.85; 0.90 V (b). Each spectrum is recorded after a period of 100 s. after the potential step.

The changes in *O.D.* and current vs. applied voltage for films of **1** and **3** on ITO are shown in Figures 4a and 4b, respectively. The results for films of **4** are similar to those of **3**. Figure 6 shows voltammograms at different scan rates for 2 nm thick films of **4**. A striking feature in the cyclic voltammogram is the shift of the position of i_{pc} to higher potentials upon increasing scanrates in agreement with previous reports [22,23]. This phenomenon was interpreted by the formation of an intermediate compound during the reversible neutralisation process. On similar grounds we associate peak I (Figure 6) with the reduction of the oxidised film and peak II the reduction of a transient intermediate, of which the formation can be retarded by increasing the scanrate. For these films the irreversible loss of electrochemical activity and optical absorption is less than 10% in 50 scans. Thanks to this stability the diffusion coefficient for hole transport could be determined.

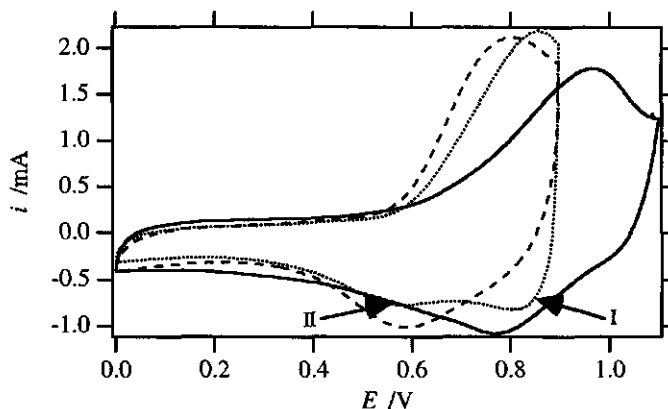


Figure 6. Cyclic voltammograms of a 2 nm thick electro-polymerised layer of 4 on ITO at different scan rates; (---): 0.1 (current amplified 50x), (....): 0.5 (current amplified 10x) and (—): 5 V.s^{-1} . Note that at a scanrate of 0.5 V/s two cathodic waves indicated by I and II are visible.

4.3 Discussion

Film formation

Our results show, that electro-polymerised hydroxyphenyl- substituted zinc porphyrins form electrochemically stable films, with controlled thickness. The maximum position of the anodic current corresponding to the first ring oxidation at 0.65 V of **1** is close to the previously reported value [18]. The oxidation of different tetra hydroxyphenyl porphyrins in basic solution has been systematically investigated by Milgrom [18]. This author reported that in a CH_2Cl_2 solution containing sodium ethoxide, the four hydroxyphenyl groups of compound of the type **1** readily dissociate, resulting in a large decrease of the oxidation potential to $E = 0.16 \text{ V}$ (vs.SCE). From the value of 0.65 V for the film of **1** we conclude that the porphyrin hydroxy groups are not dissociated, even in the presence of the DBUP base. The UV-Vis absorption spectrum of hydroxyphenyl porphyrins in MeCN is not affected by the presence of DPUB. Adding pyridine to the solution results in profound spectral changes, however (data not shown). Whereas pyridine readily ligates to the porphyrin zinc ion, DBUP does not, probably due to sterical hindrance. Its addition to the solution therefore does not affect the porphyrin absorption spectrum. Both bases, pyridine and DBUP are capable to catalyse the polymerisation reaction of all the investigated porphyrins, with or without central

metal atom. From these observations we conclude the hydroxy phenyl protons are transferred to the base in an intermediate step.

There have been numerous studies of solid film formation using electro-polymerisation of functionalised porphyrins (for a review see [9]), but the mechanism(s) of this process are known for only a few polymerisations [24,25]. Although the compounds studied by Malinski *et al.* (i.e. nickel tetra(3-methoxy-4-hydroxyphenyl) porphyrin) are comparable to those in the present study, the evolution of the cyclic voltammograms during the film formation in their experiments is quite different from what we find. Evidently, the mechanism suggested by Malinski *et al.* does not apply to our case, possibly because of the different substrates and/or media in both experiments. This is further supported by the failure of attempts to polymerise our porphyrins on platinum or glassy carbon electrodes.

For porphyrin films to be formed, the porphyrin derivative apparently must contain at least two phenolic groups. Furthermore, the absorption spectra of the polymerised films show that the porphyrin macrocycle is not perturbed at the β -pyrrole- or the meta carbon positions, except for **2**. In view of the similarities with the spectroscopic data of β -pyrrole substituted tetraphenyl porphyrins [26], electro-polymerisation of compound **2**, most likely results in an etherlinkage at the β pyrrole carbon atom. ESR spectra of radical cations of partially deuterated tetra phenyl porphyrins show [21] that the carbon atoms of the hydroxy phenyl ring carry some unpaired electron density, as a result of σ - π interaction.

Introduction of alkyl groups at the meso positions of the phenyl ring was found to prevent film formation. From these results we may conclude that a base-catalysed nucleophilic attack of a porphyrin hydroxy group takes place at a second oxidised porphyrin, more precisely at its phenyl carbon atom at the meta position with respect to the OH group. This attack most likely results in an ether linkage. Ether linkages were also reported for the electrochemical polymerisation of phenol under similar conditions [27,28]. Increasing the number of hydroxy groups is expected to lead to a higher degree of cross linking between adjacent porphyrin units.

Spectro-electrochemical characteristics of films

The oxidation potentials for the porphyrin films **1**, **3**, and **4** are found to be very close to those of the monomers in solution (see Table 1). This indicates that electro-polymerisation leaves the macrocycle of these porphyrins remains intact. On the other hand, the much larger difference for **2** suggests that the porphyrin becomes chemically modified during the polymerisation process.

Figure 6 presents cyclic voltammograms of a thin (2 nm) film of **4**. The peak current of the anodic waves (i_{pa}) is found to be proportional to the scanrate (V). Clearly, the redox reactions for these ultra thin films are not diffusion controlled. Under these conditions, n can be calculated from the slope of a plot of i_{pa} vs. V , using [14]

$$i_{pa} = \frac{\Gamma n^2 F^2 A}{4RT} v \quad (2)$$

where F is the Faraday constant, A is the electrode area, R is the gas constant, and T is the absolute temperature. The charge $\Gamma n FA$ involved with oxidation of the film in the potential window can be determined from the area under the oxidation wave in a voltammogram recorded at low V . The numbers of transferred electrons (n) for the various films have been summarised in Table I. Since now $\Gamma n FA$ and n are known, Γ can be calculated and compared to its value obtained from RBS and O.D. measurements [5]. Both values agree within 20%.

The spectro-electrochemistry characteristics of the porphyrin films do not correspond to those for zinc-(tetra-phenyl)-porphyrin monomers or -dimers in solution, reported previously [21,29,30]. In a closely packed film, the excitonic interactions between adjacent porphyrins results in a red shift of the absorption spectrum [31]: the Soret band is red shifted from 423 nm for the monomer in solution to 442 nm for the polymer film. As expected, the Q bands exhibit a smaller red shift (Figure 3). Oxidation of the film breaks the excitonic interaction between adjacent porphyrins, resulting in a decrease of the red shift of the Soret band, i.e. upon progressive oxidation the Soret band shifts slightly to the blue with respect to that of the neutral film. (Figure 5).

In the same figure it can be seen, that the oxidation-wave of a film of **1** extends over a potential range of 0.5 V. This is to be expected, since the spread in the number of cross links in the film results in a range of oxidation potentials. In addition, the oxidation potential of individual neutral porphyrins gradually increases as the number of oxidised nearest neighbours increases [30]. Evidently, the resulting electric field induced by an oxidised porphyrin at its non-oxidised neighbour is incompletely compensated by a counterion from the electrolyte solution.

The finding that at 0.9 V the number of transferred electrons n is ≈ 0.5 per porphyrin monomer and per oxidation step indicates that the film can be more adequately described as involving transfer of one electron per two neighbouring molecules, instead of one neutral and one oxidised molecule. This is consistent with the spectral changes in the 400 -500 nm region: the neutral "dimer" band at 442 nm (curve a in Figure 5) gradually shifts towards the monomer position at ≈ 430 nm. Concomitantly, a "dimer" cation band appears at ≈ 475 nm. Above 0.9 V the changes in the optical spectra indicate (data not shown) that further oxidation is possible, so there is still hole transport through the film. Under these conditions the original absorption can not be restored, implying that consecutive reactions occur resulting in electrochemically inactive material.

It is interesting to compare the above mentioned results with the finding that for typical electron conducting polymers the conductivity is at maximum for partially oxidised materials [32,33] as has also been suggested from theoretical models [34,35]. It is tempting to speculate that progressive oxidation of the porphyrin results eventually in an insulating part just near the ITO surface and thus preventing complete oxidation. So far, however, we do not have experimental evidence for this.

Charge Transport in films

Ideally, redox polymer films can be represented as a large number of stacked monolayers of redox centres. Charge transport is thought to occur by electron self-exchange reactions between neighbouring redox active molecules, resulting in electron hopping and a diffusion limited current. Under such conditions the faradaic peak current i_{pa} is related to the v by [36]:

$$i_{pa} = 0.4463FnA \frac{\Gamma}{d} \sqrt{\frac{Fn}{RT}} \sqrt{V} \sqrt{D} \quad (3)$$

where D is the diffusion coefficient for charge transport.

In an actual voltammogram, the measured current contains a faradaic and a capacitive contribution. To separate the faradaic current from the total current in the voltammogram the optical transmission (I_{tr}) at 442 nm (corresponding to the neutral dimer) was recorded simultaneously with the total current during a potential scan. $d(I_{tr})/dt$ has been shown to be directly proportional to the faradaic current [37]. Note that the total change in absorption $\Delta I_{tr,tot}$ is related to the charge $nFA\Gamma$ involved in the film oxidation by

$$knFA\Gamma = \Delta I_{tr,tot} \quad (4)$$

with k a constant. Differentiation of (4) with respect to time, and noting that the faradaic current $i_f = d(nFA\Gamma)/dt$, yields:

$$ki_f = \frac{d(\Delta I_{tr,tot})}{dt} \quad (5)$$

Combining (4) and (5) yields:

$$\frac{i_f}{nFA\Gamma} = \frac{\frac{d(I_{tr})}{dt}}{\Delta I_{tr,tot}} \quad (6)$$

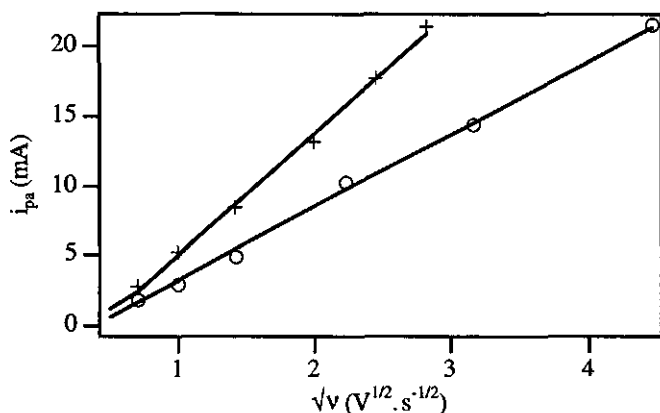


Figure 7. i_{pa} vs. \sqrt{v} (+: 3; o: 1) determined from the calculated faradaic currents, including a linear fit to the data points.

D for the different films has been obtained by plotting the peak faradaic current i_{pa} against V (Figure 7, Table I). Varying the intensity of the 440 nm probing light from $2.5 \mu\text{W}\cdot\text{cm}^{-2}$ to $2.5 \text{ mW}\cdot\text{cm}^{-2}$ did not result in any change of D .

To make sure that the measured diffusion coefficients are those for hopping of charge carriers and not for counterion transport [15] we compared D for different electrolyte anions and different electrolyte concentrations in an optical absorption probed potential step experiment. Replacing chlorate with fluoroborate or varying the TBAP concentration between 0.05 and 0.5 M did not result in a significant change of D , however. At an electrolyte concentration $< 50 \text{ mM}$ D drastically decreases for each of the investigated films. Replacing chlorate by chloride leads to a large reduction of the diffusion coefficient. This is to be expected since Cl^- effectively ligates to the porphyrin central metal atom [38]. Probably, as a result the transport of Cl^- from a particular porphyrin molecule to its neighbour is slowed down. From these results we conclude that for 0.5 M TBAP as the electrolyte, charge transport in the polymer film is controlled by diffusion of holes. Other elaborate techniques e.g. bipotentiostatic electrochemistry have been developed to determine both the counterion- and the hole-transport rates [39]

The values of D for the porphyrin films are in the same range as for various electropolymerised tetra aminophenyl metallo porphyrins [16]. For porphyrin Langmuir Blodgett multilayer films D values are one order of magnitude lower [17]. The difference with the present films probably originates from the presence of alkyl groups in LB films, forming electronic barriers between the layers.

Table I. Electrochemical data for electropolymerised porphyrin films on ITO substrates.

sample	E_{ox} (V) ^a	E_{ox} (V) ^b	n ^c	$D \times 10^{-10}$ ^d ($\text{cm}^2\cdot\text{s}^{-1}$)
1	0.65	0.64	0.49	0.85
2	0.85	0.71	0.46	2.1
3	0.78	0.75	0.44	2.6
4	0.76	0.77	0.42	2.3

^a Position of maximum of first anodic oxidation wave at $V = 0.1 \text{ V}\cdot\text{s}^{-1}$ during polymer formation (See also Figure 2). ^b Position of the maximum of the first anodic oxidation wave at $v = 0.1 \text{ V}\cdot\text{s}^{-1}$ of thin (2-5 nm) polymer film (See also Figure 6). ^c Number of electrons per monomer oxidation step. Accuracy of $\pm 10\%$ estimated by comparison of Γ obtained from electrochemical, O.D. and R.B.S. measurements.

^d Diffusion coefficients for films with 60 - 80 nm thickness. Accuracy: $\pm 40\%$ dependent on the accuracy of n and the thickness d .

Self diffusion of the polymer chain may contribute to the electron transport through a redox-active polymer film [15]. This applies in particular to redox active polymers having linear structures and no extensive cross linking. Although for our films this seems unlikely, polymer self-diffusion cannot *a priori* be excluded, and may contribute to the experimental D values.

If charge transport through the films proceeds *via* cross links between the porphyrin units, we should expect that the magnitude of D is related to the degree of cross linking. The data of Table I show, that there is no such correlation. For example, D for films of **3** and **4** is \approx three times higher than for **1**, even though the film of the latter compound most likely has more cross linking. Therefore, we tentatively conclude that the charge transport proceeds *via* direct electron transfer between the macrocycles of vicinal porphyrins, as a result of intermolecular electronic interaction. Then, it is rather the average plane-to-plane distance and the relative orientation between the porphyrin macrocycles which determine the value of D for the different films, than the number of cross links. Effective charge transport through face-to-face oriented macrocycles has previously been reported for Langmuir Blodgett films [7] and stacks of porphyrins and phthalocyanines [40-43].

Using the Einstein relation Equation (7), the hole mobility for the films can be calculated from [13]:

$$\mu_h = -\frac{e}{k_B T} D_h \quad (7)$$

The calculated mobilities of $\mu \approx 1 \cdot 10^{-8} \text{ cm}^2 \text{V}^{-1} \text{s}^{-1}$ are four orders of magnitude smaller than for thin vacuum deposited phthalocyanine films [13]. Therefore, the major drawback of organic films of the kind described in this work in electronic devices is their low mobility for hole transport of the pure material. Low mobilities were also reported for electro-polymerised films of porphyrins with other functional groups i.e. amino or vinyl substituents [9].

4.5 Conclusions

Porphyrins equipped with at least two hydroxy groups readily polymerise into films onto an ITO substrate at an electrochemical potential which is sufficiently high to produce a porphyrin radical cation. With the exception of **2**, the optical and electrical characteristics of these films closely resemble those of the monomer porphyrins in solution, indicating that the structure of the porphyrin macrocycle is preserved during polymerisation. In a potential window from 0.0 till 0.9 V a single semi-reversible reaction is observed with the transfer of ≈ 0.5 electron/monomer from the porphyrin film to the ITO substrate, indicating that during the oxidative polymerisation process a dimer-like radical-ion species is formed in the film. Spectro-electrochemistry of the completely polymerised film was used to extract the faradaic current if from the total current in a voltammogram.

From the linear relation between if and V , characteristic for diffusive charge transport, the diffusion coefficients for charge transport through the porphyrin polymer film have been determined. Diffusion coefficients are found to be uncorrelated with the number of cross links per porphyrin unit in the film. Probably, charge transport occurs directly between adjacent macrocycles and is not significantly affected by the details of the film structure, as long as the film density is about the same. The electronic interaction between vicinal porphyrin macrocycles in their solid films most likely determines the electric conductivity of solid films of these compounds.

References

1. Savenije, T.J.; Koehorst, R.B.M. and Schaafsma, T.J. *Chem. Phys. Lett.* **1995**, *244*, 363.
2. Wöhrle, D.; *et al. Mat. Chem.* **1995**, *5*, 1819.
3. Yu, G.; Pakbaz, K. and Heeger, A. J. *Appl. Phys. Lett.* **1994**, *64*, 3422.
4. Morita, S.; Lee S. B.; Zakhidov, A. A. and Yoshino, K. *Mol. Cryst. & Liq. Cryst. A* **1994**, *256*, 839.
5. Marée, C.H.M.*et al. J. Appl. Phys.* **1996**, *80*, 3381.
6. Jones, R.; Tredgold, R. H. and Hoorfar, A. *Thin Solid Films* **1985**, *123*, 307.
7. Zhang, X. Q.; Wu, H. M.; Wu, X.J.; Cheng, Z. P. and Wei, Y. *J. Mater. Chem.* **1995**, *5*(3), 401.
8. Hayon, J.; Raveh, A. and Bettelheim, A. *J. Electroanal. Chem.* **1993**, *359*, 209.
9. Bedioui, F.; Devynck, J. and Biedcharreton, C. *Acc. Chem. Res.* **1995**, *28*, 30.
10. Pichler, K.; *et al. Mol. Cryst. & Liq. Cryst. A* **1994**, *256*, 415.
11. Yamashita, K.; Harima, Y. and Matsubayashi, T. *J. Phys. Chem.* **1989**, *93*, 5311.

12. Collins, G. E.; *et al. J. Vac. Sci. & Techn. A* **1993**, *11*, 1383.
13. Simon, J. and André, J.J. *Molecular semiconductors*: Springer-Verlag: Berlin, 1985.
14. Laviron, E. *J. Electroanal. Chem.* **1979**, *101*, 19.
15. Inzelt, G. in *Electroanalytical chemistry*; Vol 18 ed. by Bard A.J.; Marcel Dekker: New York, 1994.
16. White, B. A. and Murray, R. W. *J. Am. Chem. Soc* **1987**, *109*, 2576.
17. Ueyama, S.; Isoda, S. and Maeda, M. *J. Electroanal. Chem. Interfac. Electrochem.* **1990**, *293*, 111.
18. Milgrom, L.R. *J. Chem. Soc. Perkin Trans. I* **1983**, 2535.
19. Balasubramaniam, E.; Ramachandraiah, G.; Natarajan, P.; Biedcharreton, C.; Devynck, J. and Bedioui, F. *J. Mat. Chem.* **1995**, *5*, 625.
20. Savenije, T.J. *et al. Thin Solid Films* **1995**, *265*, 84-88.
21. Fajer, J.; Borg D.C.; Forman, A.; Dolphin, D. and Felton, R.H. *J. Am. Chem. Soc.* **1970**, *92*, 3451.
22. Schlettwein, D.; Wöhrle, D.; Jaeger, N.I. *J. Electrochem. Soc.* **1989**, *136*, 2882-2886.
23. Jaeger, N.I.; Lehmkuhl, R.; Schlettwein, D.; Wöhrle, D. *J. Electrochem. Soc.* **1994**, *141*, 1735-1739.
24. Malinski, T.; Ciszewski, A.; Fish, J. and Czuchajowski, L. *J. Electrochem. Soc.* **1991**, *138*, 2008.
25. Bettelheim, A.; Ozer, D.; Harth, R. and Murray, R. W. *J. Electroanal. Chem.* **1989**, *266*, 93.
26. Giraudeau, A.; Ruhlmann, L.; Kahef, E.; Gross, M. *J. Am. Chem. Soc.* **1996**, *118*, 2969-2979.
27. Goss, C.A.; Brumfield, J.C.; Irene, E.A. and Murray, R.W. *J. Am. Chem. Soc.* **1996**, *118*, 2969.
28. McCarley, R.L. *J. Electrochem. Soc.* **1990**, *4*, 218c.
29. Kadish, K.M. and Rhodes, R.K. *Inorg. Chem.* **1981**, *20*, 2961.
30. Lerner, Y.; L'Her M.; Hendricks, N.H.; Kim, K. and Collman, J.P. *J. Am. Chem. Soc.* **1992**, *31*, 835.
31. Maltzan, B. *Z. Naturforsch.* **1985**, *40a*, 389.
32. Feldberg, S.W. *J. Am. Chem. Soc.* **1984**, *106*, 4671.
33. Milgrom, L.R.; Hill, J.P. and Bone, S. *Adv. Mat. Opt. Elec.* **1993**, *2*, 143.
34. Barbero, C.; Tucceri, R.I.; Posadas, D.; Silber, J.J. and Sereno, L. *Electrochim. Acta* **1995**, *40*, 1037.
35. Chidsey, C.E.D. and Murray, R.W. *J. Phys. Chem.* **1986**, *90*, 1479.
36. Murray, R.W. in *Electroanalytical chemistry*; Vol 13 ed. by Bard, A.J.; Marcel Dekker: New York, 1984.
37. Zhang, C. and Park, S.-M. *Anal. Chem.* **1988**, *60*, 1639.
38. Seely, G. R.; Gust, D.; Moore, T. A. and Moore, A. L. *J. Phys. Chem.* **1994**, *98*, 10659.
39. Surridge *et al. Faraday Disc. Chem. Soc.* **1989**, *88*, 1.
40. Gregg, B. A. *Mol. Cryst. & Liq. Cryst. A* **1994**, *257*, 219.
41. Liu, C. Y.; Pan, H. L.; Tang, H. J.; Fox, M. A. and Bard, A. J. *J. Phys. Chem.* **1995**, *99*, 7632.
42. Shimizu, Y.; *et al. J. Chem. Soc. Chem. Comm.* **1993**, 656.
43. Schouten, P. G.; *et al. Mol. Cryst. & Liq. Cryst. A* **1993**, *234*, 397.

Photo-induced unidirectional electron transfer in a porphyrin heterojunction

(*Chem. Phys. Lett.* **1995**, 244, 363-370)

Abstract

Organic heterojunctions made by deposition of two different types of porphyrins onto an ITO substrate by electro-polymerisation and spin-coating exhibit rectification upon illumination. The thickness of the first, few nanometers thick, layer can be accurately controlled. The redoxpotentials for the various porphyrin D/A combinations can be changed by using different porphyrin metal centres. Varying the exothermicities for photo induced electron-transfer in this way, results in different values of the short circuit current. Depending on layer thickness and type of porphyrins, the open circuit voltage is ≤ -0.4 Volt and the incident photon to current efficiency (IPCE) is 2.5 % at 440 nm. The fill factor is typically ≈ 0.25 . Possible mechanisms for the observed rectification are discussed.

5.1.1 Introduction

Organic dye molecules absorbing visible light have been frequently employed as active components in heterojunction photocells [1-6]. By adjusting the redox potentials of these dyes, donor/acceptor (D/A) heterojunctions have been produced, showing photo-induced electron transfer (ET) in a configuration of dye layers of two different types on top of each other, e.g. vacuum-deposited phthalocyanines or porphyrins and perylene diimides [1-4]. A major drawback of this deposition method is the limited number of dyes with sufficient stability at elevated temperatures. To achieve pinhole free vacuum deposited layers, their thickness must be typically ≥ 50 nm. Organic heterojunctions have also been made using Langmuir-Blodgett films of redox active compounds equipped with alkyl chains [5,6]. Until now, cells made by these methods have low quantum efficiencies, mainly because of their high internal resistance.

D/A complexes of water soluble porphyrins with different substituents exhibit picosecond photo-induced ET in polar solvents [7-9]. For different D/A combinations the decay of the D^+A^- state was found to be approximately three orders of magnitude slower, presumably due to a non-adiabatic charge recombination to the ground state [7,8]. In frozen solutions and solids the D^+A^- energy level is destabilized w.r.t. that in polar solvents, resulting in a reduction of the driving force ΔG^0 for photo-induced ET. For a solid porphyrin D/A system this level is only below the S_1 excited state energy, if E_{ox} (D) and E_{red} (A) in polar solutions are sufficiently low.

In order to use thin films of combinations of dyes with electron-donating and accepting properties on solid substrates in photo-electric devices, these films should be pinhole free, sufficiently conductive and have a high optical absorption. Several (metallo)porphyrin analogues equipped with different reactive groups have been successfully electro-polymerised [10,11] resulting in active electrodes for use in chemical sensors and catalytic devices. We have applied this method to different 5,10,15,20-tetra (4-hydroxy-phenyl) porphyrins (THOPP) in acetonitrile (Figure 1). This paper reports unidirectional photo-induced ET between ultra thin electron-donating and -accepting porphyrin layers in an organic heterojunction of a novel type, i.e. the resulting double layer is rectifying upon illumination. In this heterojunction the electro-polymerised porphyrin layer donates an electron upon optical excitation to a second (spin-coated) electron accepting porphyrin layer on top of the first.

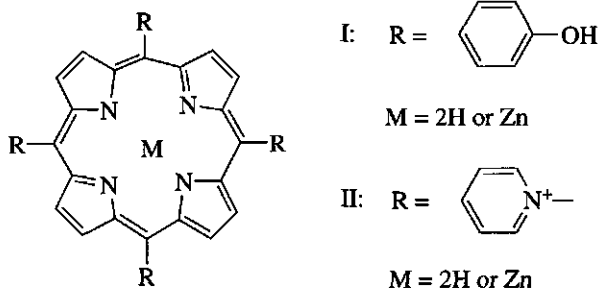


Figure 1. Molecular structures of porphyrins;

- I: M=2H, tetra(4-hydroxyphenyl)porphyrin (H₂THOPP)
M=Zn, zinc tetra(4-hydroxyphenyl)porphyrin (ZnTHOPP)
- II: M=2H, tetra(4-methyl pyridinium)porphyrin (H₂TMPyP)
M=Zn, zinc tetra(4-methyl pyridinium)porphyrin (ZnTMPyP)

5.1.2 Experimental

H₂THOPP, ZnTHOPP, ZnTMPyP and H₂TMPyP (Midcentury Chemicals) (Figure 1) were checked for purity by thin layer chromatography and absorption spectroscopy. Analytical grade acetonitrile (MeCN, Merck), electrochemical grade tetra *tert*-butyl ammonium perchlorate (TBAP, Fluka), and p.a. 1,5-di(*tert*-butyl)-pyridine (DBUP, Aldrich) were used as received.

Electro-polymerisation was carried out using a conventional three electrode system, consisting of an ITO working electrode (Glastron), a platinum counter electrode and an Ag/AgCl ([KCl] = 3 M) reference electrode. The ITO substrates were ultrasonically cleaned in demineralised water, washed in p.a. methanol (Merck) and acetone (Merck) and subsequently dried with nitrogen. Electro-polymerisation was carried out at room temperature using a 1 mM porphyrin solution in MeCN, containing 0.1 M TBAP as supporting electrolyte and 0.05 M DBUP. All porphyrin solutions were deoxygenated by bubbling argon through for 15 min. prior to measurements. Following polymerisation, the coated substrates were rinsed with MeCN and subsequently washed with ethanol and acetone and dried with nitrogen. UV-Vis absorption spectra of the porphyrin films were recorded using a Cary 5e spectrophotometer (Varian), equipped with a diffuse reflectance sphere. For cyclic voltammetry measurements we used a potentiostat Autolab Pstat10 (Ecochemie) controlled by GPES3 software (Ecochemie).

The second organic layer was applied by spin coating at 3000 RPM a 10^{-3} porphyrin solution in methanol on top of the first layer. The cells were dried at 100°C for 30 min. , stored in air and kept in the dark.

The back contact of the cell consists of a mercury drop (figure 2) with an effective area of 0.78 mm^2 for photo electrical measurements of very thin (several nm thick) organic layers. Samples were irradiated with light from a 150 Watt Xenon lamp (Spectral Energy) which passed through a monochromator GM 252 (Spectral Energy). The output spectrum of the light source was determined using a calibrated silicon photo diode (model 400) and an optical energy meter (model 66XLA Photodyne Inc.) The output spectrum of the light source, determined in steps of 5 nm, was used to correct the action spectra and efficiencies in the following way:

Since the efficiency of the cell is non-linearly dependent on the light intensity, the incident photon to current efficiency (IPCE) vs. the incident light intensity was determined at different excitation wavelengths. With these data, the photocurrent action spectra were corrected for the spectral region 380-500 nm. Current-voltage (i/V) plots and photocurrent action spectra of various porphyrin cells were recorded using the potentiostat described before (Hg contact connected with working electrode). Short circuit currents were determined using an HP 3458A multimeter. Since no difference was found between i/V curves with chopped (on/off) optical excitation and separate light and dark i/V curves, all measurements were made using a 0.005 V/s voltage sweep and chopped (0.5 Hz) 440 nm light at $\approx 13\text{ mW cm}^{-2}$ incident power.

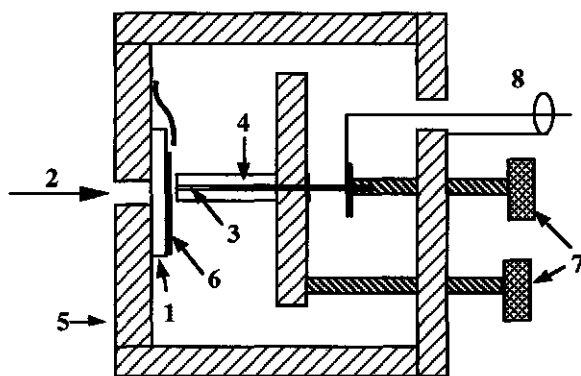


Figure 2. Cell for measuring i/V curves and action spectra. 1: ITO substrate, 2: optical excitation window, 3: glass capillary with mercury, 4: stainless steel plunger, 5: metal housing, 6: organic layer(s), 7: micrometer screw and 8: coaxial connector.

5.1.3 Results

Figure 3 shows the evolution of the electro-oxidation of ZnTHOPP during a sequence of 10 cyclic scans from +0.1 to +1.0 V at a potential scan rate of 0.1 V.s^{-1} . The first ring oxidation at 0.65 V (*Vs* Ag/AgCl) is close to that for similar porphyrins equipped with electron donating substituents e.g. zinc tetra (4-sulfonato-phenyl) porphyrin or zinc (tetra-carboxy-phenyl) porphyrin [7]. Repeated cycling is accompanied with an increase of both the amplitude as well as the potential of the oxidation and reduction waves.

UV-Visible spectra of the film formed on the ITO substrate show a broadened Soret band at 442 nm and two Q bands at 561 and 605 nm for the ZnTHOPP film. By varying the number of scans, films with different thickness can be produced. Most likely due to non-radiative traps in the film, the fluorescence of the porphyrin layers is strongly quenched. Following electro-polymerisation, the polymer film is insoluble in men or any other common solvent. Also porphyrins equipped with electron withdrawing (e.g. pyridinium) substituents, in combination with hydroxyl groups can be electro-polymerised onto the ITO substrate, resulting in an acceptor layer (data not shown).

For electrical characterisation of the double layer structures, both organic layers were tested separately to check whether a Schottky barrier is formed at the interfaces of the porphyrin layers with the electrical contacts. The i/V curves of separate electro-polymerised and spincoated layers exhibit a non-linear, light-independent resistance and do not show a short circuit current in the light (data not shown).

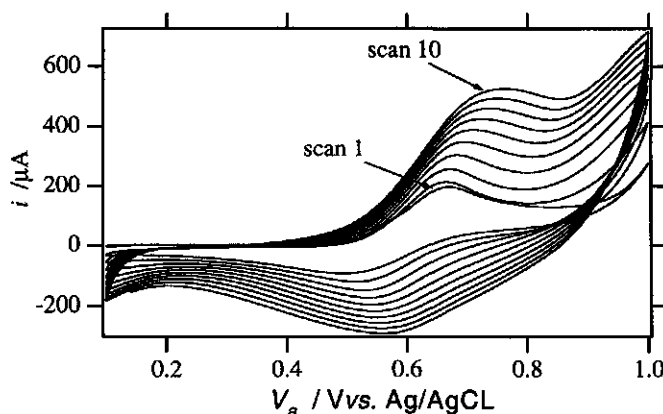


Figure 3. 10 successive cyclic voltammograms of the polymerisation of ZnTHOPP in MeCN. Cell area = 8.7 cm^2 .

Figure 4 shows the i/V curves of two ITO/ ZnTHOPP/ H₂TMPyP/ Hg cells with different thickness of the electropolymerised layer. At zero current (open circuit voltage = V_{oc}) the mercury contact is negative w.r.t. the ITO contact, indicating that the electro-polymerised layer is acting as the electron donor and the spin-coated layer as the acceptor. A thinner electro-polymerised layer results in a higher i_{sc} (Figure 4a), but at the same time a lower V_{oc} , which results from a higher leakage current for these thin cells. At ≈ -0.4 V there is no difference in photo- and dark currents for both cells, however. Fill factors of different samples are typically 0.25, as determined by the internal resistance of the organic layers, and are close to that of vapour deposited organic heterojunctions [1,3]. The values of i_{sc} for different D/A combinations have been collected in Table 1. In comparison with Langmuir-Blodgett cells [5-6] the best IPCE of our cells is higher.

Figure 5 shows short circuit action spectra expressed as IPCE vs. wavelength for a number of cells consisting of polymerised ZnTHOPP with different thickness and a H₂TMPyP layer on top with constant O.D. of 0.2 at 420 nm. Increasing the polymerised layer thickness leads to a decrease of the maximum short circuit photo current (Figure 5 a). In the cell of Figure 2 the incident light enters through the ITO side which results in an increasing filter effect with thicker donor layers, since the bulk of the polymerised layer absorbs most of the incident light. This indicates that there is no efficient energy transfer from the bulk material to the active part of the cell. Cells with < 7 nm thick polymerised layers show decreased i_{sc} values, probably due to pinholes.

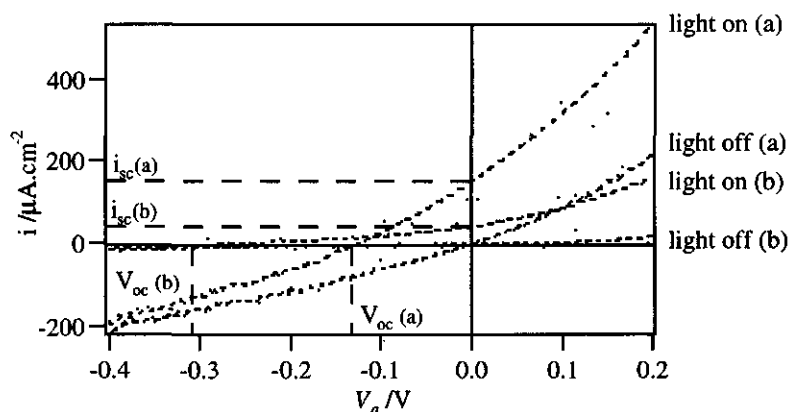


Figure 4. Typical i/V curves for two ITO/ ZnTHOPP/ H₂TMPyP/ Hg cells differing in donor thickness.

a: 5 scans, $V_{oc} = -0.12$ V, $i_{sc} = 130 \mu A.cm^{-2}$; b: 10 scans, $V_{oc} = -0.28$ V, $i_{sc} = 40 \mu A.cm^{-2}$

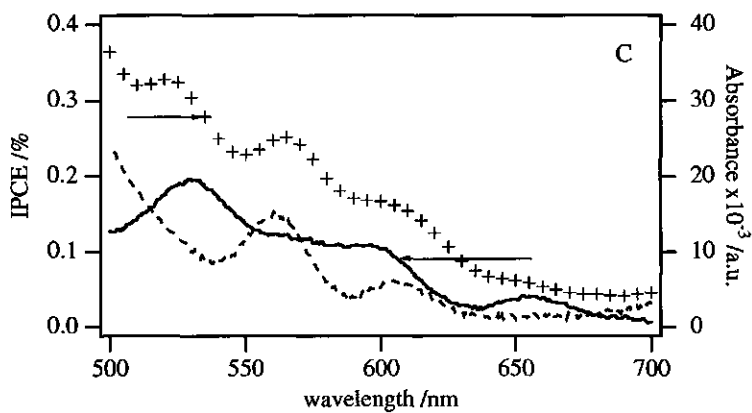
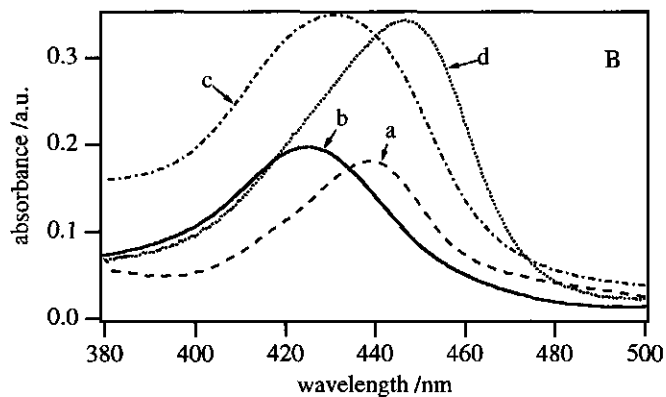
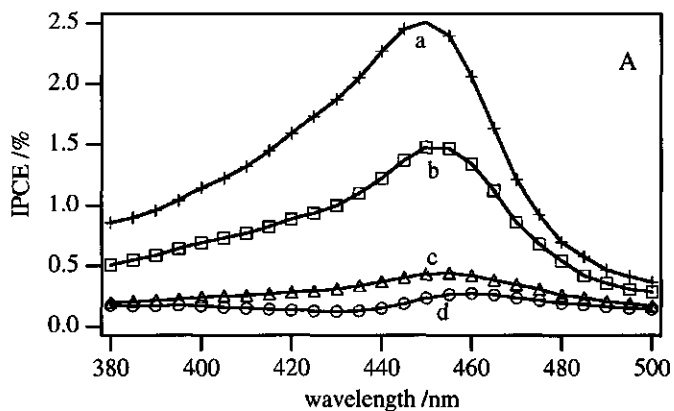


Figure 5. A: Short circuit action spectra of various ITO/ ZnTHOPP/ H₂TMPyP/ Hg cells with different thickness of the electro-polymerised layer (a: 7 nm (-+--+); b: 14 nm (- - -); c: 24 nm (-◊-◊-); d: 50 nm (-o-o-)) expressed in IPCE. At marked positions the incident light intensity has been calibrated.

Figure 5 B: Absorption spectra of a: polymerised layer of 7 nm ZnTHOPP (---), b: spincoated H₂TMPyP layer (___), c: ZnTHOPP/ H₂TMPyP cell with polymerised layer of 7 nm (-.-.-) and d: spincoated 1: 1 mixture of ZnTHOPP/ H₂TMPyP (.....). Figure 5 C: Action spectrum of Q band region of ZnTHOPP/ H₂TMPyP cell with polymerised layer of 7 nm (-+--+)) with absorption spectra of the separate polymerised layer (---) and spincoated H₂TMPyP layer(___)

Note in Figure 5 that the maximum of the action spectrum of the cell does not coincide with the maximum of its absorption spectrum (cf. Figure 5b, curve c with Figure 5a) or with that of either components (cf. Figure 5b, curves a and b with Figure 5a). On the other hand the absorption maximum of a mixed D/A layer on an ITO substrate, made by spincoating a methanol solution of a 1 : 1 ZnTHOPP/ H₂TMPyP mixture is very close to the maximum of the action spectrum. A cell consisting of a spincoated mixed D/A layer has a negligibly low short circuit photocurrent, however, demonstrating that for photocurrent generation separate donor and acceptor layers are required.

Table 1. Short circuit currents of different D/A combinations including the redoxpotentials [12] and the calculated exothermicities for photoinduced ET in water.

D/A combination	i_{sc} ($\mu\text{A.cm}^{-2}$)	E_{ox} (V vs .NHE)	E_{red} (V vs. NHE)	$E_{ox}-E_{red}$ -E ₀ -0
ZnTHOPP/ H ₂ TMePyP	60	0.8	-0.26	-0.78
ZnTHOPP/ ZnTMePyP	2	0.8	-0.55	-0.6
H ₂ THOPP /H ₂ TMePyP	5	1.0	-0.26	-0.58
H ₂ THOPP /ZnTMePyP	<1#	1.0	-0.55	-0.29
ZnTHOPP/ H ₂ TPP*	<1#	0.8	-0.82	-0.22
ZnTHOPP/ H ₂ THOPP	<1#	0.8	-0.85	-0.19

* H₂TPP is spincoated from a chloroform solution

i_{sc} values inaccurate, due to low and unstable currents.

5.1.4 Discussion

Our results show, that electropolymerised tetra(4-hydroxyphenyl) porphyrins can form stable and pinhole free films, which can, combined with a second spincoated or electropolymerised organic layer, be used as photoactive layers in molecular devices. The use of a mercury back contact makes photoelectric measurements of very thin (7 nm thick) organic layers possible. The advantage of such cells is their relatively small internal resistance, allowing photoelectric measurements of cells even if they have a low IPCE.

Only cells consisting of two different porphyrins exhibit unidirectional photo induced ET. This indicates that no active Schottky-barrier is formed at the ITO/porphyrin or at the Hg/porphyrin contact. Both electrical contacts can thus be assumed as ohmic. Furthermore in the i/V plot of Figure 4 does not show a typical p/n heterojunction curve, with a steep increase of light and dark currents at $V > V_{OC}$. (The potential range was restricted from -0.4 to +0.2 due to the risk of a blow out of the cell.) Since our spin coated layer is deposited in air, we do not exclude oxygen in this layer, which would rather yield a p-type layer instead of a n-type, in view of the doping effects of O_2 . [12] The signs of the V_{OC} and i_{SC} of the cell suggest that this spincoated layer has n-type character, however.

Decreasing the thickness of the polymerised layer from 100 nm to 7 nm, results in a non-exponential increase of the i_{SC} . This can be understood by the decrease of the absorption of the bulk material and of the decrease of the internal resistance of the cell with lower layer thickness. This implies, that the photo active region of the polymerised layer is at most 7 nm thick. One may wonder, whether this observation is in accordance with a band structure model.

Since the maxima of the photoaction spectra agrees with the maximum absorption of the D/A complex, this is a strong indication that the active part of the cell is a complex of D and A. In our cell this complex can *only* be present at the interface between both organic layers.

Due to considerable overlap between the spectra of D and A, the porphyrin layers cannot be excited separately. However, from the action spectrum of Figure 5c it can be concluded, that the D/A complex indeed consists of the spincoated acceptor layer and the polymerised donor layer, in view of the presence of pronounced Q bands of both ZnTHOPP and H₂TMPyP at 555 nm and 520 nm, respectively.

Several mechanisms have been proposed for the photo voltaic effect in systems containing organic dyes [1-3,13,14]. One model [1-3] is based on band structures

similar to those in inorganic semi-conductors. The chemical nature of different dyes or additional doping causes the resulting organic layer to have a n or p-type character. In the region near the interface of a n and p-type layer, a depletion region is formed, where the internal electric field results in dissociation of an excited electron/hole pair into free charge carriers.

In an alternative model [13,14] the photo voltaic effect occurs exclusively at the interface of an organic dye with a second dye or with a semi-conductor. The interfacial kinetics for photo induced ET processes mainly control the efficiency of the cell. Since the charge separation takes place at the interface, an extended internal electric field is not required. Very recently [15], a detailed model for selective charge injection at the interface of two different organic layers has been proposed, invoking the difference in polarisation energies of charge carriers in the first few molecular layers at both sides of the interface.

In view of the above mentioned results we tentatively describe the mechanism of the rectifying effect of the porphyrin double layer as a interfacial photo- induced ET from the donor to the acceptor layer, rather than charge separation in a p-n depletion layer.

To verify whether the optical absorption by a D/A bilayer interface is sufficient to produce the observed photocurrent in our cell, we calculated the ratio R between the number of absorbed photons per cm^{-2} and the number of generated charge carriers, corresponding to the observed photocurrent. To determine the number of absorbed photons per cm^{-2} , the O.D. of the D/A bilayer was related to the number of polymerised porphyrin molecules using Rutherford Back Scattering measurements [16]. Assuming an interface consisting of face-to-face oriented D/A complexes with dimensions $1.6 \times 1.6 \text{ nm}$, 100% reflection at the acceptor/mercury interface and a yield for photoinduced ET $\phi_{\text{ET}}=1$, we calculate $R=1.1$. For a deviation from the face-to-face D/A orientation, it can be shown that $R>1.1$. This result means, that an extended (multilayer) region in the D/A layer is not required to generate the observed photocurrent.

A mechanistic model for the observed photoelectric effects based on a p-n junction is also not very acceptable in view of the redoxpotentials of the donor and the acceptor. Based on their respective redoxpotentials a net $D > A$ electron transfer is predicted. The generated internal electrical field however is now directed from the donor to the acceptor, which would yield a photocurrent with an opposite sign, as was found. To establish an internal electrical field in opposite direction however, is not very likely since an electron transfer vice versa is much more endothermic, e.g. for the first couple

of Table 1, $\Delta G > 2.5\text{eV}$ [7]. Similar conclusions are made [4] for photocells consisting a Cu phthalocyanine perylene heterojunction.

To study the effect of a change of ΔG^0 on the interfacial ET and in an attempt to determine the energy of the D^+A^- levels in the solid interface region for the various D/A combinations, we varied the redox potentials of the donor and/or acceptor. To be able to compare the photo-electric effect for various D/A couples we have assumed a similar orientation and distance between the donor- and acceptor molecules in the interface region. This assumption seems reasonable since all donors and acceptors have the same substituents. From the observed i_{sc} we may conclude that the first three D/A couples of Table 1 have a D^+A^- energy level below the S_1 level. If we assume a similar destabilisation energy for all the D/A couples upon changing the dielectric constant of the surrounding medium from 69 (water) to 2-3 (solid film), this indicates that the D^+A^- level of the first couple is located at least 0.20 eV below the S_1 level ($E_{0-0} = 1.84$ eV), i.e. $E_{(D+A^-)} \leq 1.64$ eV. For this D/A couple in a water/methanol solvent the D^+A^- level is at 1.06 eV [7]. These data imply a destabilisation energy of the D^+A^- level of ≤ 0.58 eV, less than that for covalently bound porphyrin-acceptor model systems in frozen solution [17,18]. This difference may be due to the different molecular dimensions of the radical pair in both types of modelsystems. Adding the calculated destabilisation energy of ≈ 0.58 eV to ΔG^0 for the three remaining D/A combinations, one predicts that $E_{(D+A^-)} > ES_1$ and no photocurrent should be observed, in agreement with experiment (Table 1). To understand the exact mechanism of photoinduced ET in solid D/A systems, obviously more data are required. Since the resulting destabilisation energy in solid systems is appreciable, the number of organic D/A couples with a sufficiently high absorption coefficient and with $E_{(D+A^-)} < ES_1$ is rather limited. To overcome the restriction of the absorption of a single D/A interface, which makes these cells unsuitable as solar cells, the photoactive D/A layer should be equipped with a light harvesting and energy transferring antenna [19].

Acknowledgements

This investigation was supported by the Dutch Foundation for Chemical Research (SON) with financial aid of the Dutch Organisation for Scientific Research (NWO). The authors wish to thank A. van Hoek and J. M. Kroon for helpful discussions, C.H.M. Marée for the RBS- and thickness measurements and H. van Beek and colleagues for construction of the measuring cell.

References

1. D. Wöhrle, B. Tennigkeit, J. Elbe, L. Kreienhoop and G. Schnurpfeil, *Mol. Cryst. Liq. Cryst. A* **1993**, 230, 221.
2. S. Günster, S. Siebentritt and D. Meissner, *Mol. Cryst. Liq. Cryst. A* **1993**, 230, 351.
3. K. Takahashi, S. I. Nakatani, T. Matsuda, H. Nanbu, T. Komura and K. Murata, *Chem. Lett.* **1994**, 11, 2001.
4. N. Karl, A. Bauer, J. Holzäpfel, J. Marktanner, M. Möbus, F. Stölzle, *Mol. Cryst. Liq. Cryst. A* **1994**, 252, 243.
5. M. Sakomura and M. Fujihira, *Thin Solid Films* **1994**, 243, 616-619.
6. S. Isoda, S. Nishikawa, S. Ueyama, Y. Hanazato, H. Kawakubo and M. Macda, *Thin Solid Films* **1992**, 210, 290.
7. F. J. Vergeldt, R. B. M. Koehorst, T. J. Schaafsma, J. C. Lambry, J. L. Martin, D. G. Johnson and M. R. Wasielewski, *Chem. Phys. Lett.* **1991**, 182, 107.
8. H. Segawa, C. Takehara, K. Honda, T. Shimidzu, T. Asahi and N. Mataga, *J. Phys. Chem.* **1992**, 96, 503.
9. T.-H. Tran-Thi, J. F. Lipskier, M. Simoes and S. Palacin, *Thin Solid Films* **1992**, 210, 150.
10. B. A. White, S. A. Raybuck, A. Bettelheim, K. Pressprich and R. W. Murray, *ACS Symp. Ser* **1988**, 360, 408.
11. J. R. Fish, E. Kubaszewski, A. Peat, T. Malinski, J. Kaczor, P. Kus and L. Czuchajowski, *Chem. Mat.* **1992**, 4, 795.
12. J. Simon, J.J. André, *Molecular semiconductors*, Springer-Verlag: Berlin/Heidelberg, 1985 p112-116.
13. B. A. Gregg and Y. I. Kim, *J. Phys. Chem.* **1994**, 98, 2412.
14. A. Kay, R. Humphrybaker and M. Grätzel, *J. Phys. Chem.* **1994**, 98, 952.
15. A.A. Zakhidov and K. Yoshino, *Synth. Met.* **1994**, 64, 155.
16. Savenije T.J., Marée C.H.M., Habraken F.H.P.M., Koehorst R.B.M. and Schaafsma T.J., *Thin Solid Films* **1995**, 265, 84.
17. G. L. Gaines, M. P. O'Neil, W. A. Svec, M. P. Niemczyk and M. R. Wasielewski, *J. Am. Chem. Soc.* **1991**, 113, 719.
18. A. Harriman, V. Heitz, M. Ebersole and H. Vanwilligen, *J. Phys. Chem.* **1994**, 98, 4982.
19. J. M. Kroon, P. S. Schenkels, M. van Dijk and E.J.R. Sudhölter *J. Mater. Chem.* **1995**, 5, 1309.

Control of photo-current direction by spatial arrangement of porphyrin layers

(submitted to *Appl. Phys. Lett.*)

Abstract

This work identifies the photo-active region of organic photovoltaic cells based on two different types of porphyrins, of which one, (the electron donor) is characterised by a low ionisation potential and the other, (the electron acceptor) by a high electron affinity. By electro-polymerisation of both types porphyrins onto ITO cells were produced differing in the number and the order of the two types of layers. Cells consisting of a layer of a single type of porphyrin exhibit a negligible photovoltaic effect, in contrast with cells containing both types. The sequence of the layers in the porphyrin heterojunction determines the direction of the photocurrent, confirming that the photo-active part is located at or near the interface of both organic layers. This is consistent with what can be expected in view of the redoxpotentials of the monomeric units constituting the heterojunction.

5.2.1 Introduction

Macrocyclic organic dyes such as porphyrins, phthalocyanines and perylenes have been frequently employed as active components in photovoltaic cells. By a suitable choice of the redox potentials of the dyes and of the workfunctions of the electrodes, organic heterojunctions can be made, showing photovoltaic properties [1-8]. Several mechanisms have been proposed for the photo-generation of charge carriers in these kind of organic heterojunctions. One mechanism is based on the model that charge carriers generation occurs entirely at the interface between both dyes [7,8]. Then, interfacial kinetics for charge separation and - recombination mainly control the efficiency of the cell. In an alternative model the organic dyes are assumed to form band structures similar to those as in inorganic semiconductors. Depending on the nature of the dyes or additional doping, the organic layer has n- or p-type character. Upon contacting of two such layers, a depletion region is formed, where an exciton dissociates into free charge carriers by the internal electric field [1-3].

On the other hand, cells of a single type of organic layer on a particular metal electrode may also exhibit a photovoltaic effect. To explain this, the presence of an electric barrier at the organic/electrode interface (a Schottky barrier) has been proposed, as a result of the different electron affinities of the organic layer and the metal. The internal electric field dissociates an exciton into free charge carriers, resulting in the observed photocurrent [9-10].

Recently, we reported the formation of an organic heterojunction consisting of two types of porphyrin layers of which one is electro-polymerised and one is spin-coated, together sandwiched between an ITO and a Hg electrode [5, 6]. Photo-action spectra of the cell resemble dimer-like species implying that the photo-active part of the cell is located at the interface of both layers.

By comparing cells with opposite order of the organic layers w.r.t. the electrodes it can be decided which interface (ITO/porphyrin, porphyrin/porphyrin, porphyrin/Hg) is responsible for the observed photovoltaic effect.

To produce < 100 nm thick electro-polymerised layers on ITO we used a porphyrin, asymmetrically substituted with an electron-accepting pyridyl group and additional polymerisable hydroxyphenyl substituents, free base tris(4-hydroxyphenyl)-mono(4-pyridyl)-porphyrin (**1**) (Figure 1). By one or two electro-polymerisation steps of (**1**) and/or an electron donating porphyrin i.e. zinc tetra-hydroxyphenyl-porphyrin (**2**) (Figure 1) cells with the configurations ITO/(**1**)/Hg, ITO/(**2**)/Hg, ITO/(**1**)/(**2**)/Hg and

ITO/(2)/(1)/Hg were prepared. The photo-active interface in the composite cell was identified by optical and photo-electrical measurements.

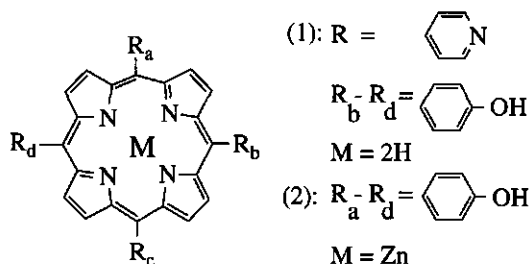


Figure 1. Molecular structures of porphyrins;

- (1): $M=2H$, free base tris(4-hydroxyphenyl)-mono(4-pyridyl) porphyrin
 (2): $M=Zn$, zinc tetra(4-hydroxyphenyl)porphyrin.

5.2.2 Experimental

Compound (1) was prepared by hydrolysis of its methoxy analogue with BBr_3 in dry CH_2Cl_2 . The methoxy substituted porphyrin was synthesised following the mixed aldehyde procedure [11]. The isomeric mixture was separated by column chromatography over silica (Kieselgel 60, Merck) with $CHCl_3$ as the eluent. Compound (2) (Midcentury Chemicals) (Figure 1) was checked for purity by thin layer chromatography and absorption spectroscopy. Analytical grade acetonitrile (MeCN, Merck) and electrochemical grade tetra *tert*-butyl ammonium perchlorate (TBAP, Fluka) were used as received.

Electro-polymerisation of (1) and/or (2) onto ITO ($30\Omega/\square$, Glastron) was carried out as previously described [5]. However, to prevent precipitation instead of polymerisation of (1) during electro-polymerisation, 10% (v/v) pyridine was added to the solution. To produce films, electro-polymerisation of one type of porphyrin was followed by rinsing the film with MeCN and drying in air. A second layer was electro-polymerised on top of the first one, by placing the film in a solution of the other type of porphyrin. Following these steps, the porphyrin heterojunction on ITO was rinsed with MeCN and ethanol, dried at $100^\circ C$ for 30 min., stored in air and kept in the dark. To determine the redoxpotentials of the polymerised films (spectro)-electrochemical techniques were

carried out using previously described methods [12], with tetra-hydrofuran (Aldrich) replacing MeCN.

I/V curves were recorded at a scanning speed of 10 mV/s using a home-built cell [5] and chopped excitation ($\lambda = 440$ nm, 13 mWatt/cm²) with the Hg electrode (area = 0.78 mm²) as the sensing contact.

5.2.3 Results

Figure 2 shows the evolution of the electro-oxidation of (1) during a sequence of 10 cyclic scans from -0.1 to +1.0 V at a potential scan rate of 0.1 V.s⁻¹. The first ring oxidation at 0.88 V (vs. Ag/AgCl) is slightly more positive than for porphyrins with two hydroxyphenyl substituents, i.e. zinc bis-(hydroxy phenyl) bis-phenyl porphyrin [12]. Repeated cycling is accompanied with an increase of both the amplitude as well as the potential of the maximum of the oxidation waves.

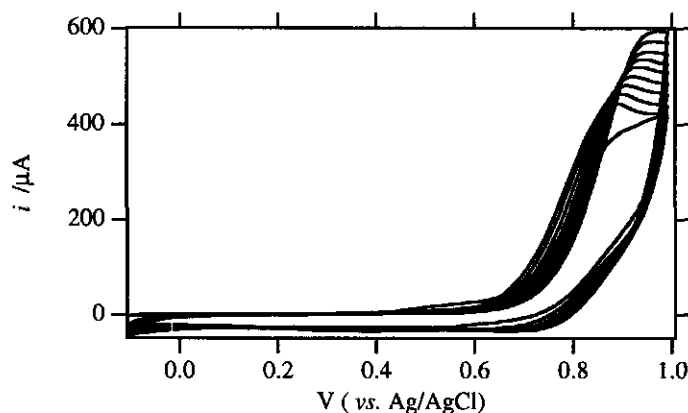


Figure 2. Ten successive cyclic voltammograms of the electro-polymerisation of (1) in MeCN/TBAP (0.1M); cell area = 8.7 cm².

Figure 3 presents the UV-Visible spectrum of an ITO substrate covered with a ≈ 16 nm film of (1). Next to the broadened Soret absorption band at 437 nm, the spectrum contains four Q bands are present, typical for a free base porphyrin. A film of (2) has a broadened Soret band at 442 nm and two Q bands at 561 and 605 nm. Since the films, once formed, do not dissolve in MeCN, different types of porphyrins films can be stacked on top of each other by consecutive electro-polymerisation. Absorption spectra of films containing both types of porphyrins show features of both types of porphyrins i.e. Q bands at 555 nm and 520 nm (Figure 3). The thickness of each layer can be controlled by the number of potential cycles.

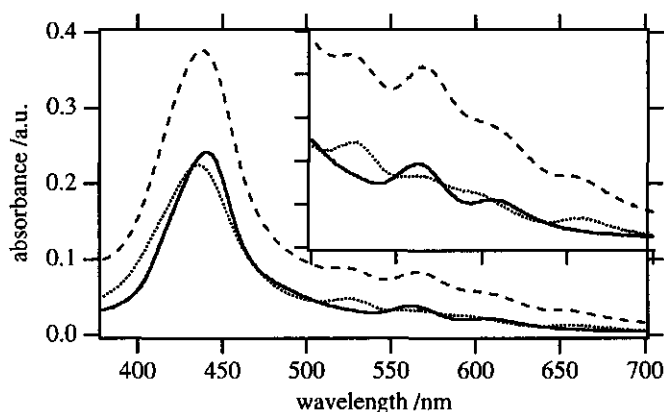


Figure 3. UV/Vis absorption spectra of electro-polymerised (2) (—), (1) (....) on an ITO substrate. Consecutive polymerisation of (2) followed by (1) yields an absorption spectrum (---) with features of both types of porphyrins.

Figure 4 shows the spectral changes upon reduction of an electro-polymerised film of (1) at potentials of 0.0 to -0.9 V, revealing isobestic points at 405 and 452 nm. Decreasing the potential to more negative values results in a decrease of the Soret band with the simultaneous appearance of a broad absorption in the 600-700 nm spectral region, as previously reported for other porphyrins [13, 14]. The electrochemical reduction turns out to be irreversible as indicated by the almost complete loss of the electrochemical material in the applied potential window.

Photo-electric measurements of differently prepared cells were recorded under chopped illumination (Figure 5). The i/V curves of the separate electro-polymerised porphyrin

layers exhibit non-linear resistances and short circuit currents below 0.5 nA, corresponding to an incident photon to current conversion efficiency ($IPCE$) $< 1.10^{-3}$ % (Figures 5a and 5b). Figure 5b shows that the ITO/(2)/Hg cell exhibits some photo-conduction, which is commonly observed for polymerised organic semiconductors [6, 15]. The absence of any photo-conduction in the ITO/(1)/Hg cell has also been observed in spincoated films of free base tetrakis-(methylpyridinium)-porphyrin [5] and films of evaporated pyridyl porphyrins [16] and has been ascribed to the high concentration of free charge carriers in these layers.

Figures 5c and 5d show the i/V curves of an ITO/(1)/(2)/Hg and an ITO/(2)/(1)/Hg cell, respectively. Note that now a short circuit current as well as an open circuit voltage is generated with opposite signs for the two composite layers. Conversion efficiencies are ≈ 0.1 % for both cells.

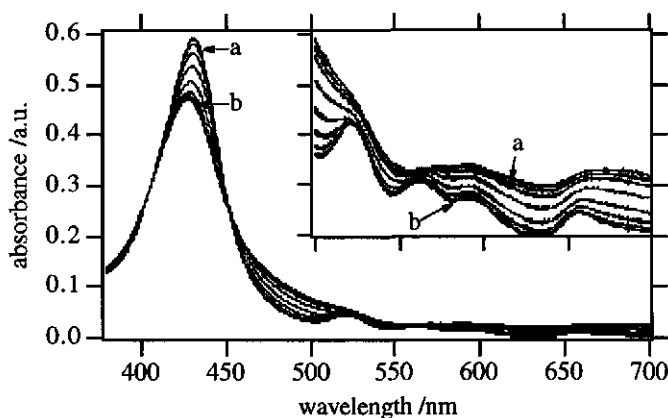


Figure 4. UV/Vis absorption spectra of an electro-polymerised (1) film on ITO at different applied potentials: (a) $V_a = -0.4$ (top), stepwise changed with 0.1 V steps to (b) -1.1 V (bottom). Each spectrum is recorded 100 s. after the potential step. Insert: magnified Q-band region.

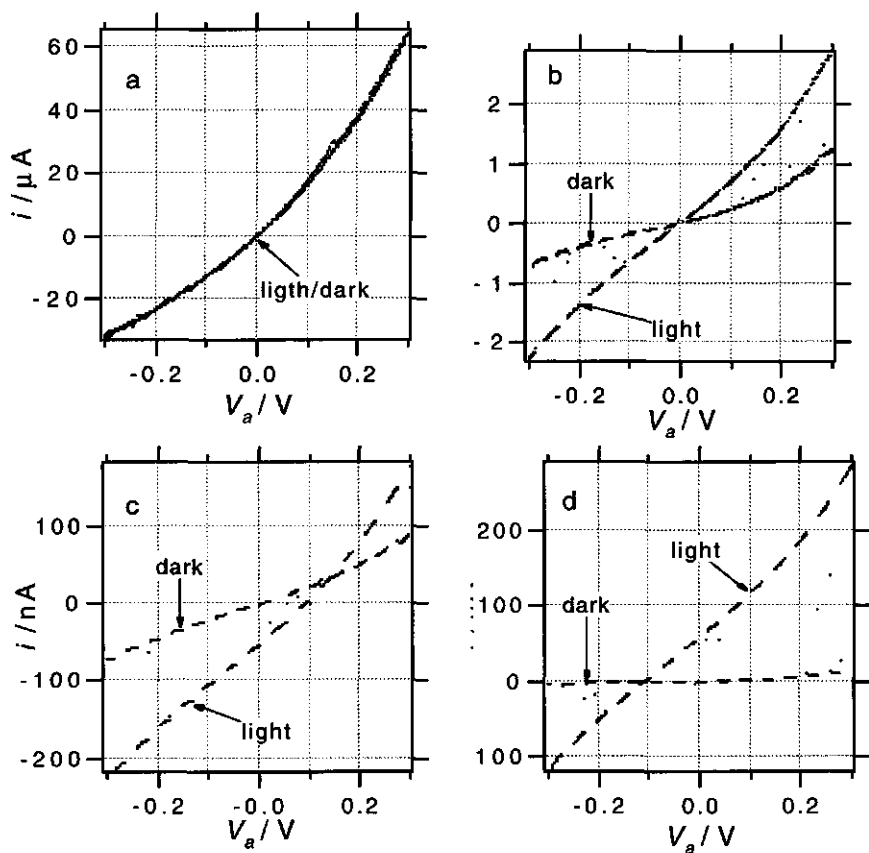


Figure 5. i/V curves under chopped illumination of 13 mWcm^{-2} at 440 nm , for different cells: (a) ITO/(1)/Hg, (b) ITO/(2)/Hg, (c) ITO/(1)/(2)/Hg and (d) ITO/(2)/(1)/Hg, Area = 0.78 mm^2 . Note that cells consisting of only one type of porphyrin layer (A en B) have a short circuit current $\leq 1 \text{ nA}$ and an open circuit voltage $\approx 0 \text{ V}$. Both cells consisting of two different types of layers (C en D) have a short circuit current of $\approx 50 \text{ nA}$ and an open circuit voltage of $\approx 0.1 \text{ V}$.

5.2.4 Discussion

Our results demonstrate, that electro-polymerisation of hydroxy porphyrins equipped with a pyridyl electron-accepting group form stable, non-soluble films. In contrast with the cyclic voltammograms during electro-polymerisation of (2) [5], (1) does not have a reductive wave, indicating that in the potential window (-0.1 to 1.0 V) no (semi)reversible reaction occurs. From the absorption spectrum (Figure 3), however, it is clear that the macrocycle of (1) remains intact. Therefore it may be concluded that upon ring oxidation a consecutive reaction occurs, resulting in a polymer-like film. The positive shift of the position of the maximum peak current is most probably due to the uncompensated potential in the already formed film and/or to the diffusion limited hole transport.

The introduction of the electron-accepting group pyridyl group is expected to result in a film with relatively low reduction potential. A cyclic voltammogram of a polymerised film of (1) in the potential window from 0.0 to -1.2 V turns out to be also irreversible. Fortunately, the reduction potential for this electro-polymerised porphyrin can, however, be estimated from the spectro-electrochemical measurements. The largest optical changes in the absorption spectrum, which are coupled to the reduction current [17] occur in the potential region -0.5 to -0.7 V vs. Ag/AgCl, i.e. comparable to the reduction potential $E^{1/2} \approx -0.6\text{V}$ for free base mono-pyridyl-tris-phenyl-porphyrin in acetonitrile [18]. We conclude therefore that the reduction potential of the porphyrin subunits in the film is not significantly affected by the electro-polymerisation reaction, and the organisation in a solid matrix.

From the very low short circuit photo-current (Figures 5a and 5b), we conclude that (i) there is no photo-active electric barrier at the porphyrin/electrode interfaces leading to efficient photo-induced charge separation or (ii) a photo-active barrier at one interface is quenched by a blocking contact at the opposite interface.

Cells containing films of both (1) and (2) show a photovoltaic effect. The photocurrent action spectrum show features of both porphyrin layers (data not shown). In the presence of a Schottky barrier at a particular interface in combination with a photo-conduction effect, changing the electrode material in contact with one of both types of porphyrins gives rise to a different Schottky barrier in view of the significantly different Fermi levels of ITO (4.35 eV) and the workfunction of Hg (5.1 eV). Since ITO/(1)/(2)/Hg and ITO/(2)/(1)/Hg cells both exhibit a similar photovoltaic effect we

conclude that the porphyrin/porphyrin interface must be the photo-active region, since this is the only interface common to both cells.

For both cells the direction of the electron flow is from (2) to (1) (Figures 5c and 5d). Assuming that the mechanism underlying the photovoltaic effect in these cells is based on photo-induced charge separation at the interface of both porphyrin layers, the direction of the electron transfer agrees with the redoxpotentials of the individual components of both films, i.e. a low oxidation potential of (2) and a low reduction potential of (1). In model studies on porphyrin heterodimers based on analogues of components (1) and (2), it was also found that upon excitation, the analogue of (2) acts as the (electron) donor and the analogue (1) as the (electron) acceptor [19].

The photon to current conversion efficiencies of the porphyrin heterojunctions in the present work are smaller than those previously reported [5]. This is not surprising, since the reduction potential of (1) is lower than that for the compound previously used (≈ -0.6 V in stead of ≈ -0.3 V vs. NHE). This is another indication that the photo-voltaic mechanism is based on interfacial photo-induced charge separation, since the redox potentials of the monomer units used to produce the film have been found to be an important determinant for the conversion efficiency [5, 20]. Control of the photocurrent flow in organic heterojunctions by the ordering of the constituents has also been found in other types of cells. Though the order is changed w.r.t. the electrodes, in both type of cells the electron flow is directed from phthalocyanine to (substituted) perylene.

Summarising, we conclude that the electro-polymerisation technique provides a convenient way to produce a pin-hole free ultrathin film consisting of covalently bound porphyrin units with electron-accepting substituents on an electrically conducting substrate. In addition porphyrin layers of different types can be superimposed, each with thickness in the nanometer range. Since the charge separation is confined to the interface of both organic layers the order of the organic layers controls the direction of the photo-current.

References

1. Wöhrle, D.; Kreienhoop, L.; Schnurpfeil, G.; Elbe, J.; Tennigkeit, B.; Hiller, S. and Schlettwein, D. *J. Mat. Chem.* **1995**, *5*, 1819.
2. Günster, S.; Siebentritt, S. and Meissner, D. *Mol. Cryst. & Liq. Cryst. A* **1993**, *230*, 351.
3. Tang, C. W. *Appl. Phys. Lett* **1986**, *48*, 183.
4. Morita, S.; Lee, S. B.; Zakhidov, A. A. and Yoshino, K. *Mol. Cryst. & Liq. Cryst. A* **1994**, *256*, 839.
5. Savenije, T.J.; Koehorst, R.B.M. and Schaafsma, T.J. *Chem. Phys. Lett.* **1995**, *244*, 363.
6. Marée, C.H.M.; Roosendaal, S.J.; Savenije, T.J.; Schropp, R.E.I. and Schaafsma, T.J. *J. Appl. Phys.* *in press*
7. Kay, A.; Humphrybaker, R. and Grätzel, M. *J. Phys. Chem.* **1994**, *98*, 952.
8. Gregg, B. A. and Kim, Y. I. *J. Phys. Chem.* **1994**, *98*, 2412.
9. Harima, Y.; Kodaka, T.; Okazaki, H.; Kunugi, Y.; Yamashita, K.; Ishii, H. and Seki, K. *Chem. Phys. Lett.* **1995**, *240*, 345.
10. Nasr, C.; Hotchandani, S.; Kassi, H.; Nsengiyumva, S. and Leblanc, R. M. *Sol. Ener. Mat. & Sol Cells* **1995**, *36*, 261.
11. Little, R. G. *J. Heterocyclic Chem.* **1981**, *18*, 129.
12. Savenije T.J.; Koehorst R.B.M. and Schaafsma T.J. *J. Phys. Chem. submitted*
13. Mosseri, S.; Nahor, G. S.; Neta, P. and Hambright, P. *J. Chem. Soc. Faraday Trans.* **1991**, *87*, 2567.
14. Kadish, K. M.; Liu, Y. H.; Sazou, D.; Senglet, N. and Guillard, R. *Anal. Chim. Acta* **1991**, *251*, 47.
15. Bedioui, F.; Devynck, J. and Biedcharreton, C. *Acc. Chem. Res.* **1995**, *28*, 30.
16. Schlettwein, D. and Armstrong, N. R. *J. Phys. Chem.* **10 1994**, *98*, 11771.
17. Hoier, S.N. and Park, S.-M. *J. Phys. Chem.* **1992**, *96*, 5188.
18. Worthington, P.; Hambright, P.; Williams, R. F. X.; Reid, J.; Burnham, C.; Shamim, A.; Turay, J.; Bell, D. M.; Little, R. G.; Datta-Gupta, N. and Eisner, U. *J. Inorg. Biochem.* **1980**, *12*, 281.
19. Vergeldt, F. J.; Koehorst, R. B. M.; Schaafsma, T. J.; Lambry, J. C.; Martin, J. L.; Johnson, D. G. and Wasielewski, M. R. *Chem. Phys. Lett.* **1991**, *182*, 107.
20. Umeda, M.; Shimada, T.; Aruga, T.; Niimi, T. and Sasaki, M. *J. Phys. Chem.* **1993**, *97*, 8531.

Photo-generation and transport of charge carriers in a porphyrin p/n- heterojunction

(submitted to *Phys. Rev. B*)

Abstract

Using impedance spectroscopy the formation of a depletion layer is demonstrated upon contacting two films of different type of porphyrins. This depletion layer can be described in the same way as in a conventional p/n heterojunction of inorganic semiconductors. From Mott-Schottky plots the doping concentration is found to be $\approx 10^{17} \text{ cm}^{-3}$ for electro-polymerised ZnTHOPP films and two orders of magnitude higher for spin-coated H₂TMPyP films. Since the photocurrent action spectra are independent of the thickness of either of the layers, we conclude that charge separation and thus the photo-active part of the cell is confined to the interface of both layers. For charge collection, consecutive dissociation of the electron/hole pair competes with charge recombination. The internal field over the space charge layer causes the photo-induced charge carriers generated at the interface to drift through the bulk layer to the electrodes.

6.1.1 Introduction

Organic dye molecules have recently gained interest as building blocks for optoelectronic devices, due to their chemical and electronic properties and high optical absorption. In this field of application, dyes have been mainly used as sensitizers for oxidic (nanocrystalline) semiconductors [1-7] or as active components in heterojunction photocells [8-19]. Previously, we reported the formation of a heterojunction, consisting of two types of porphyrin layers, of which one, (the electron donor) is characterised by a low ionisation potential and the other, (the electron acceptor) by a high electron affinity. Upon illumination, photo-induced charge separation between both layers, followed by electron transport through the non photo-active bulk layer, results in a unidirectional photo-current and an open circuit voltage (OCV) of ≈ 0.5 V [8].

Several mechanisms have been proposed for the photo-voltaic effect in organic heterojunctions. One model is based on the finding that the photovoltaic effect occurs entirely at the interface between an organic dye and a second dye or a semiconductor. Then, mainly the interfacial kinetics for charge separation and - recombination mainly control the efficiency of the cell. Since the charge separation takes place at the interface, an extended internal electric field as in p-n junctions is not required [1,2].

In an alternative model the organic dyes are assumed to form band structures similar to those in inorganic semi-conductors. Depending on the nature of the dyes or additional doping, the organic layer has a n- or p-type character. Upon contacting of an n and p-type layer, a depletion region is formed, where an exciton dissociates into free charge carriers by the internal electric field [20]. The presence of a depletion region was invoked to explain the relatively large generated photo-current [9 -12, 21]. The photo-active zone in this band model stretches out across the depletion region, in contrast with the interface model where efficient photo-induced charge separation solely takes place at the interface of both organic dyes. Recently, however, the role of the depletion region in organic heterojunctions was reconsidered [13], since the contribution of the exciton diffusion length in the p-n model is not yet clear.

Formation of a depletion layer for molecular semiconductors has been demonstrated using impedance measurements on Schottky barrier systems, consisting of a porphyrin-like compound/metal contact [23-25]. Such experiments have shown that a well-behaved Schottky barrier is formed upon contacting the porphyrin-like material with e.g. aluminium. In this work we demonstrate -to our knowledge for the first time- the

presence of a depletion layer between two types of organic layers, using impedance measurements. A combination of this band model with the interface model based on the photocurrent action measurements can explain the observed photovoltaic properties.

6.1.2 Experimental

Zinc tetra (hydroxyphenyl) porphyrin (ZnTHOPP) (Figure 1) polymer films on ITO substrates were made by electro-polymerisation as previously published [8]. The free base tetra (methyl-pyridinium) porphyrin (H₂TMPyP) layer (Figure 1) was applied by spin coating at 3000 RPM a 10⁻³M solution in methanol onto the ZnTHOPP/ITO substrate. The samples were dried at 100°C for 30 min., stored in sealed vessels and kept in the dark.

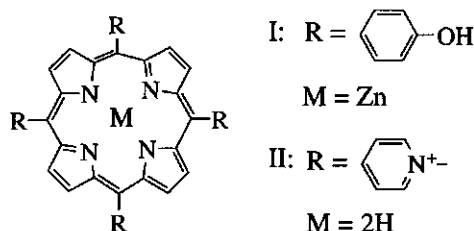


Figure 1. Molecular structures of porphyrins;

I: M=Zn, zinc tetra (4-hydroxyphenyl) porphyrin (ZnTHOPP)

II: M=2H, tetra (4-methyl pyridinium) porphyrin (H₂TMPyP).

The film thickness was measured by step profiling (Dektak 3030) mechanically made grooves in the film. UV-Vis absorption spectra of the porphyrin films were recorded using a Cary 5e spectrophotometer (Varian Associates) and corrected for reflection by using a diffuse reflectance sphere.

The electrical top contact of the cell consists of a mercury drop, connected to the sensing electrode, with an effective area (*A*) of 0.78 mm² integrated in a metal housing [8]. For (photo)current measurements used a potentiostat Autolab PGstat10 (Ecochemie) controlled by GPES3 software (Ecochemie) in combination with a 150 Watt Xenon light source (Spectral Energy) and a monochromator GM 252 (Spectral Energy). The output spectrum of the light source was determined using a calibrated silicon photodiode (Photodyne Inc. model 400) and an optical energy meter (Photodyne

Inc. model 66XLA). This spectrum was used to correct the photocurrent action spectra and quantum efficiencies. The complex impedances were recorded in the dark using a frequency response analyser (Solartron Model 1255) combined with an electrochemical interface (Solartron Model 1286). Impedances as a function of applied frequency were fitted using a software program "Equivalent Circuit" developed by Dr. B.A. Boukamp (Technical University Twente). For analysing the potential dependent capacities we made use of the Schottky equation (1). In the presence of a depletion layer the concentration of ionised impurities in the space charge region (N_d) and the built-in potential (V_{bi}) can be determined from [22]:

$$\frac{1}{C^2} = \left(\frac{2}{e\epsilon_r\epsilon_0 N_d} \right) (V_a + V_{bi}) \quad (1)$$

where C is the capacitance, e the electronic charge, ϵ_r the relative dielectric constant, ϵ_0 the permittivity of free space and V_a the applied potential.

Fermi energy levels were estimated by making use of Kelvin Probe technique. This technique is a non-contact method to determine the potential difference between the Ag reference electrode and the sample. The value of this potential difference is obtained by mechanically vibrating the Ag electrode in close proximity ($\approx 1\text{mm}$) of the sample, thus forming a capacitor. The periodically changing capacity and the difference in potential of both materials causes an alternating current in the external circuit. The potential, which must be applied in this external circuit to minimize the current, is the negative of the potential difference between both materials. For these measurements we used an electrostatic voltmeter (Trek 320B) with a high sensitivity probe (model 3250). Experimental details are presented elsewhere [26].

6.1.3 Results

As previously shown [8] porphyrins equipped with four hydroxy groups i.e. zinc tetra (4-hydroxy) phenyl porphyrin (ZnTHOPP) (Figure 1) can be electro-polymerised efficiently on ITO substrates. By changing the number of cyclic voltage scans the thickness of the porphyrin films can be controlled between several nm and at least 100 nm.

UV-Visible spectra of ZnTHOPP films formed on ITO show characteristically broadened Soret bands at 442 nm and Q bands at 565 and 605 nm. For different samples the optical density (*O.D.*) at the maximum of the Q band were plotted against the thickness (*d*) of the organic layer (Figure 2). For films the *O.D.* is expressed as

$$O.D.=1000\Gamma\epsilon \quad (2)$$

where Γ is the coverage, i.e. the number of molecules cm^{-2} , and ϵ is the extinction coefficient (typically 20×10^3). Since the density for these organic layers is 1.09×10^{21} molecules. cm^{-3} as determined by Rutherford Backscattering [27], (2) can be rewritten to relate the *O.D.* and *d* by,

$$O.D.=\alpha d \quad (3)$$

with $\alpha = 3.7 \times 10^6 \text{ m}^{-1}$ in figure 2 at 561 nm for ZnTHOPP layers, and *d* expressed in m.

First, the photo-electric characteristics of single porphyrin films on ITO substrates were examined to check whether a Schottky barrier was formed at the porphyrin/electrodes interfaces. Details about the different investigated junctions are presented in Table 1.

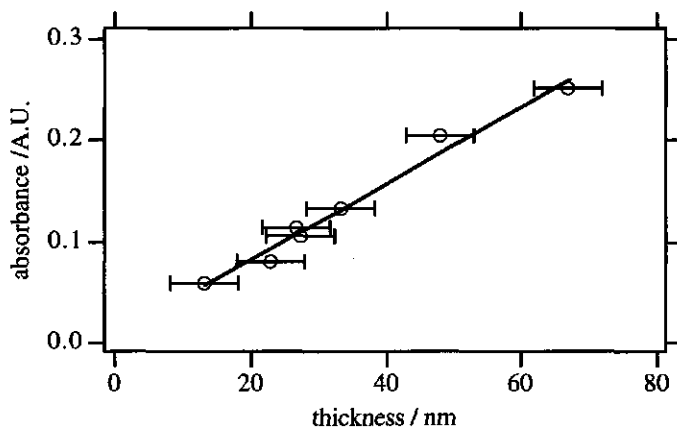


Figure 2. *O.D.* vs. thickness of organic layer for ZnTHOPP at 561 nm.

Figure 3a shows the dark i/V characteristics of an ITO/ZnTHOPP/Hg cell. Upon illumination no significant short circuit photocurrent ($i_{sc} < 1\text{ nA}$) or $V_{oc} (< 10\text{ mV})$ is observed. Figures 3b and 3c show the impedance plots at -1 V and $+1\text{ V}$, which can be fitted with an equivalent circuit consisting of a capacitance (C) parallel to a resistance (R_p) in series with a resistance (R_s). Table 2 collects the fit results to these impedance plots. Since already at an analysing frequency of 10 kHz the current through R_p cannot be neglected (Figures 3b and 3c), the dependence of C on the applied potential (V_a) was calculated using an equivalent circuit, consisting of only R_p and C , from:

$$C = \frac{-Z''}{\omega[(Z')^2 + (Z'')^2]} \quad (4)$$

where Z' and Z'' are the real and imaginary components of the impedance. The Mott-Schottky plot ($1/C^2$ vs. V_a), is shown in Figure 3a.

Table 1. Characteristics of the different cells measured in this work.

Cell	<i>O.D.</i> (λ in nm)	<i>d</i> ^a layer (nm)	<i>E_{pa}</i> ^b vs NHE (V)	<i>E_f</i> (vs. vac.) (eV)	<i>C</i> (nF)	<i>N_d</i> (cm^{-3})	ϵ_r ^c
ITO/or/Hg						10^{18}	
ZnTHOPP	0.084 (564)	18	0.85	5.3	1.6		4.2
H ₂ TMPyP	0.095 (529)	25	≈ 1.5	4.7	32		
ZnTHOPP/ H ₂ TMPyP		18	-	-	1.4	0.31	3.8

^a thickness of p-type layer. ^b anodic peak potential from [44]. ^c calculated using Equation (6) for ZnTHOPP layer

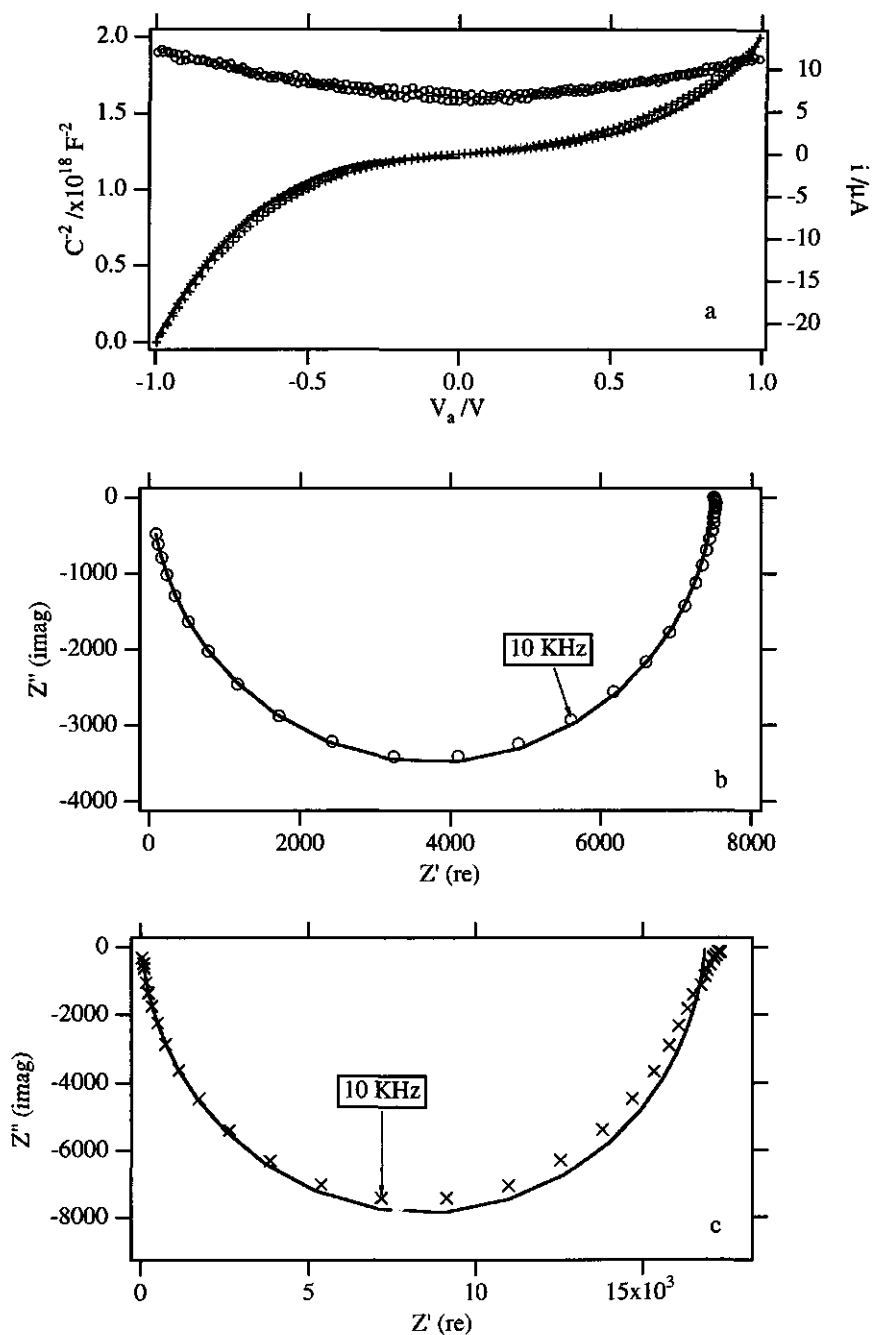


Figure 3. Electrical characteristics of ITO/ZnTHOPP (18 nm)/Hg cell; (a) current (++) and $1/C^2$ (oo) at 10 KHz vs. V_a ; impedance spectra at (b) $V_a = -1 \text{ V}$ and (c) $V_a = 1 \text{ V}$ including fit to model described in text.

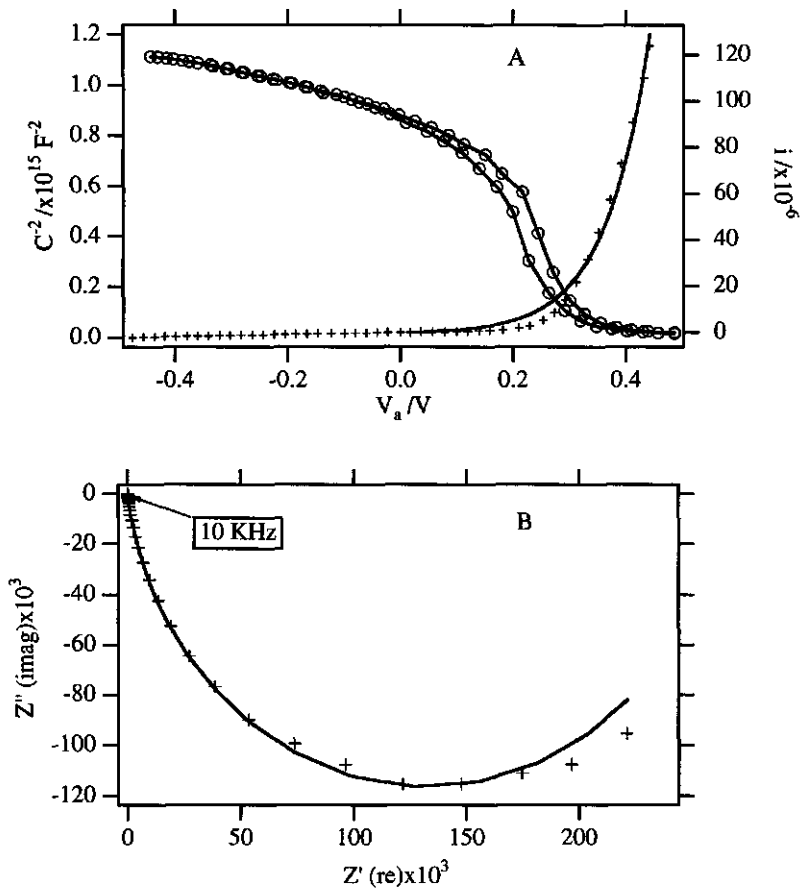


Figure 4. Electrical characteristics of an ITO/H₂TMPyP (25 nm)/Hg cell; (a): current (++) and $1/C^2$ (oo) at 10 KHz vs. V_a ; (b) impedance spectra at $V_a = 0$ V including fit to model described in text.

For an ITO/H₂TMPyP ($d = 25$ nm)/Hg cell the i/V plot and the Mott-Schottky plot are shown in Figure 4a. Although the i/V curves are strongly asymmetric, no short circuit current (i_{sc}) or V_{oc} is observed upon illumination. Figure 4B shows the complex impedance spectrum at $V_a = 0$ V, including a fit. In Figure 4A the intercept of the tangent to the steep part with the x-axis yields $V_{bi} = 0.35$ V for this cell. For $V_a > V_{bi}$ (0.35 V) the impedance plot deviates from a semicircle and for fitting the data points a diffusion limiting element has to be introduced in the equivalent circuit (data not shown).

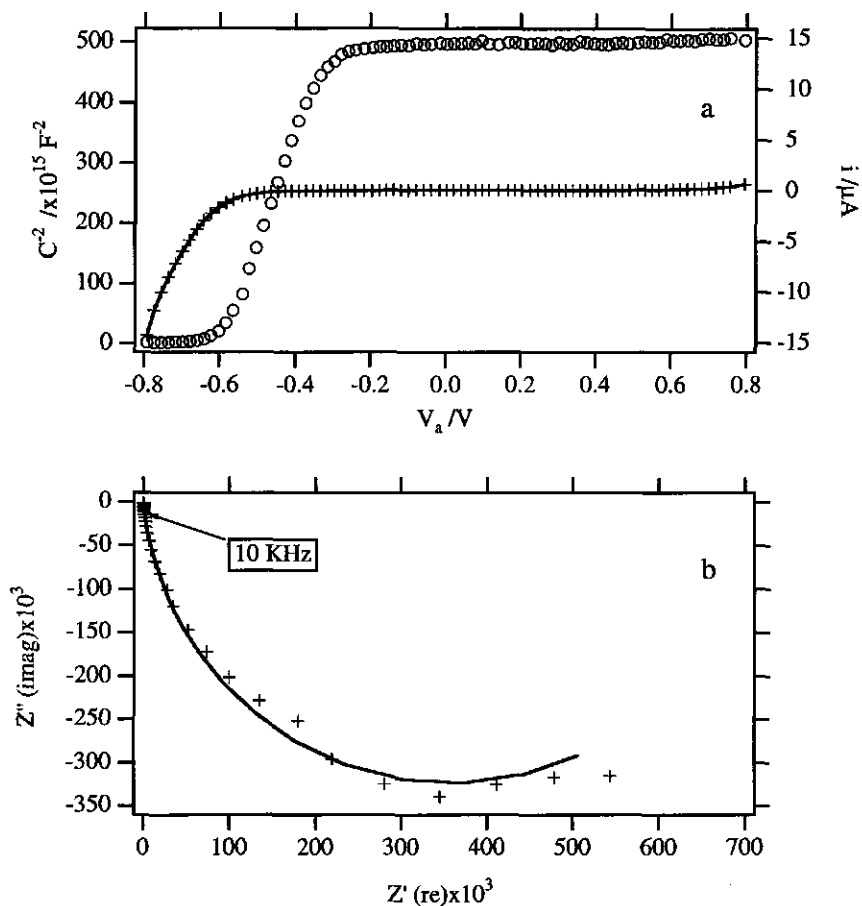


Figure 5. Electrical characteristics of an ITO/ZnTHOPP (18 nm)/ H₂TMPyP /Hg cell; (a) current (++) and $1/C^2$ (oo) at 10 KHz vs. V_a ; (b) impedance spectra at $V_a = 0.7$ V including fit to model described in text.

A cell containing a heterojunction double layer in the configuration ITO/ZnTHOPP (18 nm)/ H₂TMPyP/Hg, shows a clearly asymmetric i/V plot (Figure 5a). Note that contrary to an ITO/H₂TMPyP/Hg cell, where a forward bias is applied, when the Hg electrode is positive w.r.t. ITO, now a forward bias applies to the Hg electrode negative w.r.t. ITO. This implies that under forward conditions electrons flow from the Hg electrode to the ITO, i.e. from the H₂TMPyP to the ZnTHOPP. The Mott-Schottky plot at 10 KHz shows a voltage dependent capacity (Figure 5a) and the complex impedance plot (Figure 5b) at $V_a = 0$ V represents again a partial semicircle.

Figure 6 shows the i/V curves under illumination and in the dark for an ITO/ZnTHOPP/ H₂TMPyP/Hg cell. The photocurrent is anodic at $V_a = 0$ V indicating that the direction of electron transport is from ZnTHOPP to H₂TMPyP. The generated photocurrent (i_{ph}) at $V_a = 0$ V depends on the light intensity I_0 as $i_{ph} \propto I_0^m$, with $m = 0.7 - 0.85$. In figure 5a the intercept of the tangent to the steep part with the x-axis yields $V_{bi} = -0.58$ V for this porphyrin heterojunction. The maximum recorded V_{oc} , however, is smaller i.e. -0.42 V (Figure 6).

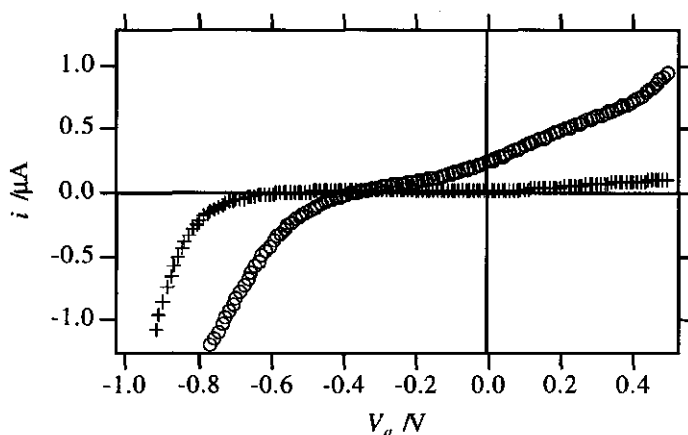


Figure 6 i/V plots of an ITO/ZnTHOPP (15 nm)/ H₂TMPyP/Hg cell with an effective area of 0.78 mm^2 under illumination with 13 mWatt.cm^{-2} at 440 nm (ooo) and in the dark (+++).

Table 2. Results from fitting the dispersion spectra ^a

Cell	V_a	d ^b	R_s	R_p	C
ITO/org/Hg	(V)	(nm)	(K Ω)	(Ω)	(nF)
ZnTHOPP	-1.0	18	0.02	8K	1.6 (0.96)
ZnTHOPP	1.0	18	0.04	17K	1.5 (0.96)
H ₂ TMPyP	0.0	25	0.1	0.3 M	63 (0.92)
ZnTHOPP/ H ₂ TMPyP ^c	0.7	18	0.1	0.7 M	2.8 (0.94)

^a $\chi^2 < 2.8 \times 10^{-3}$ for all fits. ^b Thickness of p-type layer. ^c Approximate thickness 5 nm.

Figures 7a and c show the absorption spectra of ITO/ZnTHOPP/ H₂TMPyP/Hg cells in the region between 500 and 700 nm with different thicknesses of both individual layers. Figures 7b and 7d present the corresponding photocurrent action spectra at $V_a = 0$ V. The photocurrent response is expressed as the incident photon to current conversion efficiency (IPCE) by:

$$IPCE = \frac{i_{ph}}{eI_0} 100\% \quad (5)$$

where e is the electronic charge and I_0 the number of incident photons $s^{-1}cm^{-2}$. Due to considerable overlap between the absorption spectra of ZnTHOPP and H₂TMPyP, the porphyrin layers cannot be excited separately. However, comparing the absorption spectra with the photocurrent action spectra it can be seen that both layers give rise to a photo-current, considering the presence of pronounced ZnTHOPP and H₂TMPyP Q bands at 565 nm and 520 nm, respectively, in the action spectrum. Increasing the thickness of either the ZnTHOPP layer or the H₂TMPyP layer or both results in a decrease of the photocurrent.

The Fermi energy (E_f) levels of ZnTHOPP and H₂TMPyP are collected in Table 1. For ZnTHOPP $E_f \approx 5.3$ eV, close to the value predicted by the oxidation potential of the porphyrin monomer in solution [8]. The Fermi level of the H₂TMPyP layer at 4.7 eV indicates that it is positioned halfway the energy band gap.

6.1.4 Discussion

Illumination of cells consisting of two porphyrin layers with appropriate redoxpotentials on top of each other, results in a photo-induced unidirectional charge separation. By contrast, separate layers do not show a photovoltaic response [8]. As already mentioned two different models i.e. the formation of a space charge region as in a conventional p/n-junction and the interfacial model have been proposed to describe the cell characteristics. First we discuss the presence of possible barriers between both organic layers and/or between one of the organic layers and the electrodes using impedance spectroscopy.

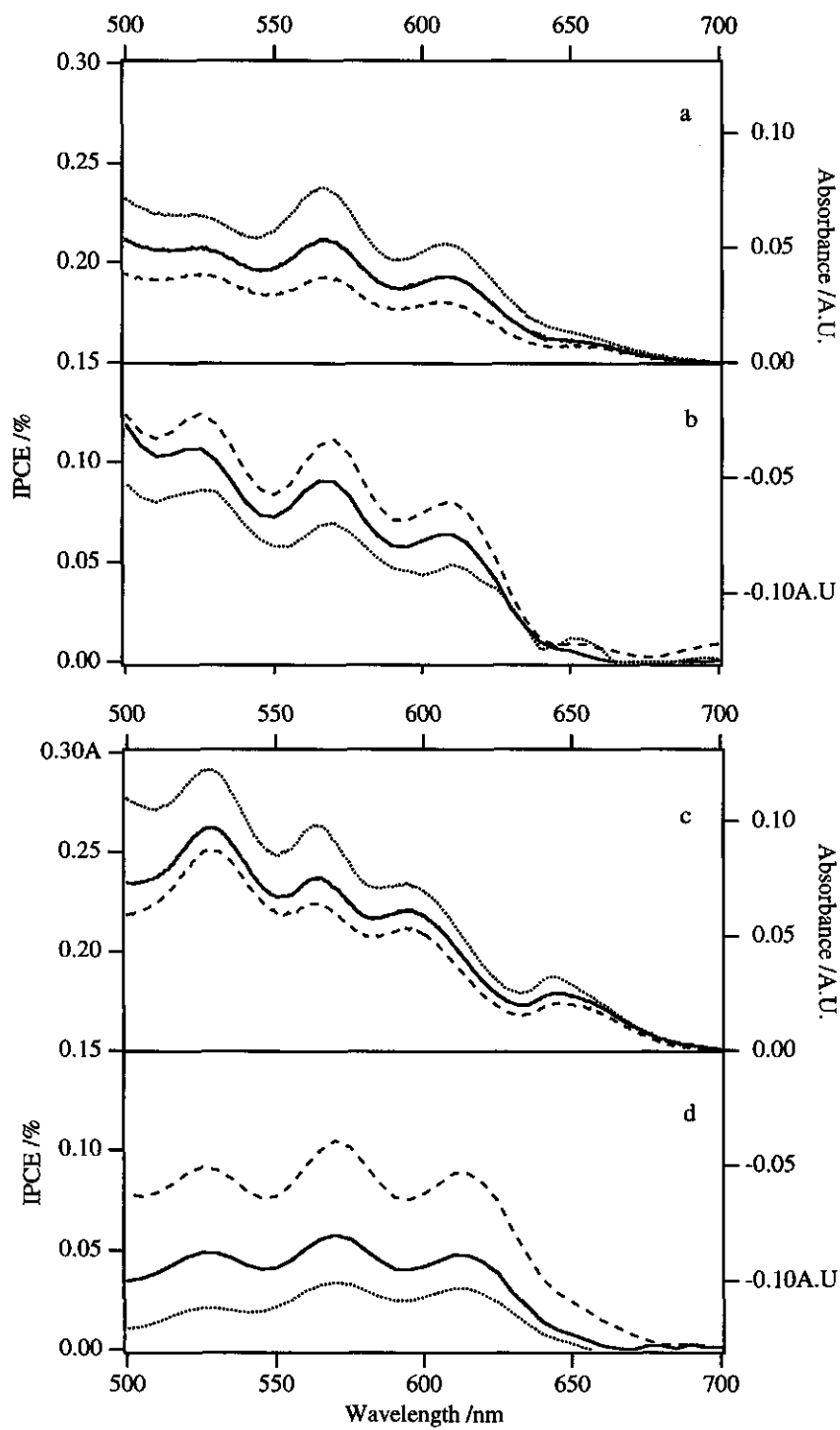


Figure 7. Absorption spectra (a,c) and short circuit action spectra expressed as *IPCE* (b,d) of various ITO/ ZnTHOPP/ H₂TMPyP/ Hg cells with different thickness of the organic layers. Thickness of ZnTHOPP layer: 6.4 nm (---), 11 nm (—), 18 nm (···); thickness of H₂TMPyP layer: (a,b): 5 nm, (c,d): 19 nm.

Impedance measurements

For an ITO/ZnTHOPP/Hg cell the current depends non-linearly on the applied potential, indicating a space charge limited current [22]. The capacitance at 10 KHz is found to be almost voltage independent. This observation and the almost symmetrical *i/V* curves are strongly indicate that no barriers are present at either interface. The capacitance is thus geometrically determined. Using

$$C = \frac{\epsilon_o \epsilon_r A}{d} \quad (6)$$

the relative dielectric constant ϵ_r of the porphyrin layer can be determined, where A is cell area and d the layer thickness. For a ZnTHOPP layer we find $\epsilon_r \approx 4.2$ similar to ϵ_r values reported for thin films of phthalocyanines [20].

In contrast with the above findings, an ITO/H₂TMPyP/Hg cell exhibits a potential-dependent capacitance and an asymmetric *i/V* curve (Figure 4). Upon application of a positive bias at the Hg electrode the current shows conventional thermionic emission behaviour [22]. This indicates the existence of an n-type band bending for electrons in the porphyrin layer at the H₂TMPyP/Hg interface or a p-type band bending at the ITO/H₂TMPyP interface. The Kelvin probe measurements indicate, however, that a p-type contact at the ITO ($E_f = 5.2$ eV), H₂TMPyP ($E_f = 4.7$ eV) interface is energetically not feasible.

Using equation (1) the product $\epsilon_r N_d$ was determined from the $1/C^2$ vs. V_a plot (Figure 4). For an ITO/H₂TMPyP/Hg cell this plot exhibits two regions with different slopes. Since ϵ_r (ITO) = 8.9 and $N_d > 10^{20} \text{ cm}^{-3}$ for this kind of ITO [28], $\epsilon_r N_d > 8.9 \times 10^{20} \text{ cm}^{-3}$. The value of $\epsilon_r N_d = 4.5 \times 10^{21} \text{ cm}^{-3}$ determined from the slope of $1/C^2$ in the potential region 0.0 to -0.4 V thus indicates a band bending in the ITO substrate. The slope in the potential range between 0.3 and 0.2 V yields $\epsilon_r N_d = 4.0 \times 10^{20} \text{ cm}^{-3}$, which applies to the porphyrin layer. We conclude that there are two barriers in a ITO/H₂TMPyP/Hg cell, the band bending in the porphyrin film at the H₂TMPyP/Hg

interface being the dominant one. Since the spin-coating method does not produce homogeneously thick layers, calculation of ϵ_r for this kind of layers is not expected to give reliable results.

An ITO/ZnTHOPP/H₂TMPyP/Hg cell exhibits also a potential dependent capacitance and an asymmetric i/V plot, but now the currents at forward bias appear at negative applied potentials, in contrast to an ITO/H₂TMPyP/Hg cell. Again, the $1/C^2$ vs. V_a plot shows two different slopes, yielding $\epsilon_r N_d = 1.2 \times 10^{18} \text{cm}^{-3}$ and $\epsilon_r N_d \approx 1 \times 10^{20} \text{cm}^{-3}$, respectively. Since we expect an n-type barrier at the H₂TMPyP/Hg interface and an Ohmic contact at the ITO/ZnTHOPP interface, the only possibility to explain these characteristics is the formation of a barrier between both porphyrin layers. Based on the forward bias < 0 V we conclude that the ZnTHOPP /H₂TMPyP binary layer acts as a p/n heterojunction. This is consistent with the Fermi energy levels of 5.3 and 4.7 for the ZnTHOPP and H₂TMPyP layers, respectively.

Since both porphyrin layers are chemically different and have been deposited by different methods, N_d and to a smaller extent ϵ_r must be expected to be different for both layers. From the measurements on ITO/H₂TMPyP/Hg cells N_d is estimated to be $\approx 10^{19} \text{cm}^{-3}$. Therefore, we ascribe the capacity change in the potential range -0.58 to -0.23 V (Figure 5) to the increasing depletion of the ZnTHOPP layer. Above -0.23 V the complete ZnTHOPP layer is depleted. At $V_a = -0.23$ V the capacity of the ITO/ZnTHOPP/ H₂TMPyP/Hg cell is found to be 1.4 nF (Figure 5) and using eqn. (6), ϵ_r is calculated to be 3.8, close to its independently determined value for an ITO/ZnTHOPP/Hg cell. Using eqn. (1) we find $N_d = 3.1 \times 10^{17} \text{cm}^{-3}$ for the ZnTHOPP layer.

Upon formation of a ZnTHOPP/ H₂TMPyP heterojunction the ZnTHOPP layer is fully depleted at $V_a = 0$ V, even for a ZnTHOPP layer with the largest thickness (18 nm). So far there have been several reports of relatively large depletion regions for organic systems (> 40 nm) [23-25, 29, 30] but these barriers were formed upon contacting an organic material with a metal with a low work function, i.e. aluminium. By contrast, we assign the formation of the observed space charge region to the contact of a p and n-type porphyrin layer.

Several authors [31, 32] correlated the ionisation potentials of phthalocyanine-like thin films, determined with He I photoelectron spectra (UPS), to their redoxpotentials. From these studies it turned out that molecular materials with the highest occupied molecular orbitals (HOMO) at ≤ 6.3 eV vs. vac. behave as p-type materials, whereas materials with HOMO energies ≥ 6.5 eV vs. vac. behave as n-type. Upon comparison of

the redoxpotentials of these films with those of the porphyrin films in this work, we conclude that our results are consistent with p type character of the ZnTHOPP and n-type character of a H₂TMPyP layer (Table I).

N-type behaviour of porphyrins with pyridyl substituents similar to H₂TMPyP has been proposed previously [33, 34] based on *i/V* curves and electrochemical measurements. Naturally occurring defects in layers consisting of porphyrins equipped with pyridyl groups, have been suggested as the source of an excess electrons [32]. By contrast, the interaction of oxygen with porphyrins having a low oxidation potential, such as ZnTHOPP is expected to produce an excess of holes [20], resulting in p-type behaviour.

Note that all Mott-Schottky plots have been recorded at 10 kHz , five orders of magnitude higher than used by a number of other reports [23-25]. In these works low analysing frequencies had to be applied, since the mobility of the charge carriers in those materials was presumably extremely low.

Upon illumination of the cell the values of for the components of the equivalent circuits C , R_s and R_p do not change significantly. This indicates that the rate constant for recombination of photo-generated electron hole-pairs is fast compared to the analysing frequency of 10 kHz .

Photoelectric measurements

To obtain more evidence for an adequate model, applying to the porphyrin heterojunctions we also measured their photoelectric properties. By changing the individual thicknesses, the extent and nature of the photo-active region of the junction can be determined [11]. For this purpose absorption spectra and photocurrent action spectra of the junctions are compared.

All action spectra of ITO/ZnTHOPP/ H₂TMPyP/Hg cells at $V_a = 0$ V contain contributions of both the ZnTHOPP and the H₂TMPyP layer (see Results). A stepwise increase of the ZnTHOPP layer thickness up to a factor three, decreases the photocurrent, but leaves the shape of the photocurrent action spectrum unaffected (Figures 7B and 7D). Increasing the H₂TMPyP layer by more than threefold also results in a lowering of the photocurrent, in addition to a slight change in the photocurrent action spectrum at short wavelengths. Since the mercury back contact is

expected to reflect the transmitted light efficiently the H₂TMPyP layer acts as a filter resulting in the observed small change in the photo current action spectrum.

Sofar, we have assumed that the investigated photo-diode is ideal, i.e. $R_{sh} \rightarrow \infty$ and $R_s \rightarrow 0$. It is known, however, that electro-polymerised porphyrin films have low conductivities [26,35,36]. In addition, there may be photo-conduction, contributing to the photocurrent action spectrum [20,27]. From the different slopes of the i/V curve at different light intensities it can be concluded [22] that photo-conduction indeed occurs. Comparing the different action spectra (Figures 7b and 7d) the contribution of the photo-conduction to the action spectra can only be relatively small, however, since the action spectra do not show significant changes, if the thickness of the individual layers is varied.

The above mentioned results can be interpreted as follows:

The finding that an increase of the layer thickness (and thus of the depletion thickness) produces a lower photocurrent, could be caused by the high resistivity of the organic material, overshadowing the increase of the photocurrent. However, the photocurrent action spectra (Figure 7) demonstrate that the relative contributions of both layers do not change upon increasing of the layer thickness of either one or of both layers. This implies that the photo-active part of the cell must be relatively narrow and independent of the layer thickness. Therefore, we conclude that charge separation occurs entirely at the interface of both porphyrin layers. At increasing thickness the photocurrent is lowered as a result of the filter effect of the non-photo-active bulk material and by the increasing Ohmic resistance.

This implies that in the organic bulk layer possible production of electron and holes by optical excitation of the material is expected to be followed by fast recombination. On the other hand, optical excitation of the interface, may lead to effective photo-induced charge separation and eventually to a photocurrent.

These conclusions are confirmed by calculations based on the Onsager theory [38-40] predicting that in a homogeneous organic layer with a low value of ϵ_r photo-induced charge separation into free electrons and holes does not occur due to strong Coulombic interaction. This is in contrast with inorganic semiconductors, where electrons in the conduction band can have diffusion lengths of several micrometers or more [22].

If we take into account results from independent optical studies on porphyrin heterodimers with similar redox potentials in a medium with low dielectric constant [41], efficient photo-induced charge separation can also be expected at the interface between

both porphyrin layers in the heterojunction. Since at the interface of the heterojunction both types of porphyrins are in close contact with each other, structures similar to hetero-dimers as in solution can be formed. The presence of these interfacial species is confirmed by the resemblance of the heterojunction photo-current action spectrum and the absorption spectrum of ZnTHOPP/ H₂TMPyP hetero-dimers [8].

Following charge separation the photo-generated electron/hole pair at the interface can recombine to the ground state or by consecutive dissociation separate into free charge carriers, eventually leading to charge collection by the electrodes. In an organic film with $\epsilon_f \approx 4.5$ and thus a relatively large Coulombic attraction between electrons and holes ⁴², consecutive dissociation of the electron/ hole pair competes with recombination to the ground state. However, the internal electric field present in the depletion layer causes the photo-induced charge carriers generated at the interface to drift to the electrodes, resulting in charge collection.

The resulting energy diagram for the investigated heterojunctions is shown in Figure 8. The energy gaps of 2.0 and 1.8 eV for ZnTHOPP and H₂TMPyP, respectively, correspond to the lowest S₀-S₁ excitation energy. The valence band energies at 5.4 and 6.0 eV for ZnTHOPP and H₂TMPyP are related to their respective oxidation potentials [20]. From the impedance measurements we conclude that the p-type layer and to a smaller extent the n-type layer are in depletion. At the interface different energy steps in the valence and conduction band are present. Whereas the H₂TMPyP/Hg interface shows an n-type bandbending, the ZnTHOPP/ITO interface forms an Ohmic contact.

Summarising the discussion, we suggest that a combination of the p/n - and the interface models as described in the Introduction and Figure 8 adequately explains of porphyrin heterojunctions.

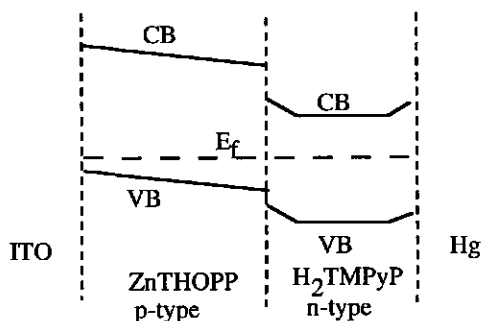


Figure 8. Energy band diagram for a ITO/ZnTHOPP/H₂TMPyP/Hg cell in the dark.

Regarding the heterojunction interface as being built from ZnTHOPP/H₂TMPyP heterodimers with similar geometry as in solution [41] photo-induced charge separation in these dimers results in the creation of a dipole with $\mu = 17$ D, if both molecules are considered as point charges. Upon applying an electric field of 1.5×10^5 V.cm⁻¹, along the axis of the dipole, typical for our junction, the ion pair energy is lowered by at most 5.2 meV. Since the energy step in the conduction band is almost one order of magnitude higher, the presence of an electric field of the above mentioned size does not noticeably affect the efficiency for charge separation at the interface. In addition, biasing the cell as for the *i/V* plot of figure 6 is thus not expected to influence the efficiency for charge separation. However, the net electric field over the cell increases the drift of the charge carriers, thus controlling the ratio between the rates of charge transport through the bulk layers of both types of porphyrins and electron/hole recombination.

Improvement of this kind of heterojunction cells can be achieved by reducing the cell thickness, thereby diminishing the optical filter effect and the resistance of the bulk material. The efficiency, however, remains limited by the optical absorption of the interface of both organic layers. So far exciton diffusion within the bulk layers has not been taken into account. Although the exciton diffusion length can not easily be obtained experimentally, its increase may greatly enhance the photo-current [13, 43].

Conclusions

A heterojunction of a porphyrin donor/acceptor pair forms a depletion layer upon contact and can be described as a p/n junction, analogously to that for inorganic semiconductors. From Mott-Schottky plots the doping concentration is of the order of $\approx 10^{17}$ cm⁻³ for ZnTHOPP layers and $\approx 10^{19}$ cm⁻³ for H₂TMPyP layers. Since the photocurrent action spectra are independent on individual layer thickness we conclude that photo-induced charge separation is confined to the interface of both porphyrin layers.

The internal electric field in the depleted bulk layers causes the photo-induced charge carriers at the interface to drift to their electrodes, leading to charge collection. The photovoltaic characteristics of the junction can be adequately described by combining a p/n- and an interface model.

Acknowledgements

This investigation was supported by the Netherlands Foundation for Chemical Research (SON) with financial aid of the Netherlands Organisation for Scientific Research (NWO). The authors wish to thank C.H.M. Marée for RBS measurements and Dr. B.A. Boukamp for providing impedance spectroscopy software.

References

1. A. Kay, R. Humphrybaker and M. Grätzel, *J. Phys. Chem.* **1994**, *98*, 952.
2. B. A. Gregg and Y. I. Kim, *J. Phys. Chem.* **1994**, *98*, 2412.
3. K. Kalyanasundaram, N. Vlachopoulos, V. Krishan, A. Monnier and M. Grätzel, *J. Phys. Chem.* **1987**, *91*, 2342.
4. A. Kay and M. Grätzel, *J. Phys. Chem.* **1993**, *97*, 6272.
5. B. O'Regan and M. Grätzel, *Nature* **1991**, *334*, 737.
6. B. A. Gregg, M. A. Fox and A. J. Bard, *J. Phys. Chem.* **1990**, *94*, 1586.
7. B. A. Gregg, *Mol. Cryst. & Liq. Cryst. A* **1994**, *257*, 219.
8. T. J. Savenije, R. B. M. Koehorst and T. J. Schaafsma, *Chem. Phys. Lett.* **1995**, *244*, 363.
9. D. Wöhrle, L. Kreienhoop, G. Schnurpfeil, J. Elbe, B. Tennigkeit, S. Hiller and D. Schlottwein, *J. Mat. Chem.* **1995**, *5*, 1819.
10. D. Wöhrle, B. Tennigkeit, J. Elbe, L. Kreienhoop and G. Schnurpfeil, *Mol. Cryst. & Liq. Cryst. A* **1993**, *228*, 221.
11. S. Günster, S. Siebentritt and D. Meissner, *Mol. Cryst. & Liq. Cryst. A* **1993**, *230*, 351.
12. S. Günster, S. Siebentritt, J. Elbe, L. Kreienhoop, B. Tennigkeit, D. Wöhrle, R. Memming and D. Meissner, *Mol. Cryst. & Liq. Cryst. A* **1992**, *216*, 641.
13. N. Karl, A. Bauer, J. Holzapfel, J. Marktanner, M. Mobus and F. Stolzle, *Mol. Cryst. & Liq. Cryst. A* **1994**, *252*, 243.
14. S. Morita, S. B. Lee, A. A. Zakhidov and K. Yoshino, *Mol. Cryst. & Liq. Cryst. A* **1994**, *256*, 839.
15. T. Shimidzu, H. Segawa, Wu F. and N. Nakayama, *J. Photo. Chem. & Photo. Bio. A* **1995**, *92*, 121.
16. J. P. Gong, S. Ohnishi and Y. Osada, *Polymer J.* **1994**, *26*, 754.
17. A. D. Xia, S. J. Fu, H. B. Pan, X. Y. Zhang, Z. Xu, Q. Liu and R. K. Yuan, *Solid. Stat. Comm.* **1995**, *95*, 713.
18. M. Hiramoto, H. Fujiwara and M. Yokoyama, *J. Appl. Phys.* **1992**, *72*, 3781.
19. C. W. Tang, *Appl. Phys. Lett* **1986**, *48*, 183.

20. J. Simon and J. Andre, *Molecular semiconductors* ; Springer-Verlag, Berlin, 1985.
21. K. Yamashita, Y. Harima and H. Iwashima, *J. Phys. Chem.* **1987**, *91*, 3055.
22. S.M. Sze, *Physics of semiconductors devices* ;Wiley, New York, 1981.
23. Y. Harima, T. Kodaka, H. Okazaki, Y. Kunugi, K. Yamashita, H. Ishii and K. Seki, *Chem. Phys. Lett.* **1995**, *240*, 345.
24. Y. Harima, K. Takeda and K. Yamashita, *J. Phys. Chem. Solids* **1995**, *56*, 1223.
25. C. Nasr, S. Hotchandani, H. Kassi, S. Nsengiyumva and R. M. Leblanc, *Sol. Energ. Mat. & Sol. Cells* **1995**, *36*, 261.
26. E. Moons, T.J. Savenije, A. Goossens, T. J. Schaafsma, J. Schoonman, submitted to *J. Phys. Chem.*
27. C. H. M. Marée, S. J. Roosendaal, T. J. Savenije, R. E. I. Schropp, T. J. Schaafsma and F. Habraken, *J. Appl. Phys.*, *in press*
28. G. Frank and H. Koestlin, *Appl. Phys.* **1982**, *197*, A 27.
29. E. J. Lous, P. W. M. Blom, L. W. Molenkamp and D. M. Deleeuw, *Phys. Rev. B* **1995**, *51*, 17251.
30. I. H. Campbell, D. L. Smith and J. P. Ferraris, *Appl. Phys. Lett.* **1995**, *66*, 3030.
31. J. Bufler, C. Ziegler and W. Gopel, *Synth. Met.* **1993**, *61*, 127.
32. D. Schlettwein and N. R. Armstrong, *J. Phys. Chem.* **1994**, *98*, 11771.
33. K. Yamashita, Y. Harima and T. Matsubayashi, *J. Phys. Chem.* **1989**, *93*, 5311.
34. S. Antohe, *Phys. Stat. Solid. (a)* **1993**, *136*, 401.
35. B. A. White and R. W. Murray, *J. Am. Chem. Soc.* **1987**, *109*, 2576.
36. F. Bedioui, J. Devynck and C. Biedcharreton, *Acc. Chem. Res.* **1995**, *28*, 30.
37. T. J. Savenije, R. B. M. Koehorst and T. J. Schaafsma, submitted to *J. Phys. Chem.*
38. Z. D. Popovic, *J. Chem. Phys.* **1982**, *77*, 498.
39. Z. D. Popovic and A. M. Hor, *Mol. Cryst. & Liq. Cryst. A* **1993**, *230*, 75.
40. H. Antoniadis, M. A. Abkowitz, J. A. Osaheni, S. A. Jenekhe and M. Stolka, *Chem. Mat.* **1994**, *6*, 63.
41. U. Hofstra, R. B. M. Koehorst and T. J. Schaafsma, *Chem. Phys. Lett.* **1986**, *130*, 555.
42. G. L. Gaines, Michael P. O'Neil, Walter A. Svec, Mark P. Niemczyk and Michael R. Wasielewski, *J. Am. Chem. Soc.* **1991**, *113*, 719.
43. B. A. Gregg, *Appl. Phys. Lett.* **1995**, *67*, 1271-1273.
44. K. Kalyanasundaram and M. Neumann-Spallart, *J. Phys. Chem.* **1982**, *86*, 5163.

Transient photo-current measurements

6.2.1 Introduction

Until now, there have been numerous publications reporting the utilisation of organic dye molecules as active components in photovoltaic cells [1-5]. The photovoltaic effect in these cells can be explained as a photo-induced electron transfer at the interface between two different type of layers, one consisting of molecules acting as an electron donor and one acting as an electron acceptor. Recent studies have shown that the exothermicity of the electron transfer reaction is related to the presence of the photovoltaic effect [1, 2]. Varying the exothermicity of the photo-induced electron transfer reaction, by changing the redox potentials of the used donor - and acceptor molecules, the relative positions of different energy levels and thus the change in free energy associated with the electron transfer reaction could be revealed. By reducing the exothermicity of the photo-induced electron transfer reaction between both cell components the observed photo-current dramatically decreases. Both studies concluded that the change in free energy is smaller than the reorganisation energy and thus in the terminology of the Marcus theory the reactions take place in the normal region [6].

The kinetics of the photo-induced electron transfer reaction in organic heterojunctions may yield additional information about the basic mechanism for the photovoltaic effect in cells based on various molecular materials. Until now there have been numerous studies focused on the description of different kinetic parameters involved with the photo-induced electron transfer in synthetic donor/acceptor systems in liquid solution. See for reviews [7,8]. Different techniques, e.g. transient optical measurements and transient electron spin resonance have successfully been applied [9-11]. Until now however, these techniques have been scarcely applied to donor/acceptor model systems in condensed media [12], due to the limited volume in which the reaction occurs (mostly restricted to an interface) and the large spread in the results due to inhomogeniouties in the solid material, e.g. lattice imperfections and impurities.

A straightforward technique to determine the rate constants of the electron transfer processes in solid state cells is provided by transient photo-current measurements. In this technique the cell is exposed to an ultrashort laser pulse, while recording the voltage or current output of the cell. A unidirectional electron transfer at the interface of

both layers in the cell induced by the laser pulse can be recorded as a potential across an external resistance. Care, however, must be taken when interpreting the results of transient current measurements, since these may also be generated by charge transport due to internal barriers in the cell at an interface with e.g. one of the electrode. Also, changes in dielectric constants in the material upon excitation may lead to a photo-current. Furthermore, the product of the sum of the external resistors and the cell capacity yields a characteristic response time of the external sensing circuit which may affect or even dominate the observed transient response. A detailed description of the photo-physical behaviour of semiconductor devices upon excitation by ultra short laser pulses is given by Willig [13, 14]. Until now, this technique has only been applied on a few cells based on molecular semiconductors [15, 16]. Extraction of the rate constants for the molecular processes from the transient has not yet been feasible.

To elucidate the photo-physical processes in cells consisting of two thin porphyrin layers as described in Paragraph 6.1, transient photo-current measurements can yield valuable information. In this Paragraph preliminary results of transient photo-current experiments are presented.

6.2.2 Experimental

Palladium tetra (hydroxyphenyl) porphyrin (PdTHOPP) (Midcentury Chemicals) polymer films on ITO substrates were made by electro-polymerisation [2]. The free base tetra (methyl-pyridinium) porphyrin (H₂TMPyP) layer was applied by spin coating a 10⁻³M solution in methanol onto the PdTHOPP/ITO substrate at 3000 RPM. The samples were dried at 100°C for 30 min., stored in sealed vessels and kept in the dark.

The electrical top contact of the cell consists of a mercury drop, connected to the sensing electrode, with an effective area of 0.78 mm² integrated in a metal housing. For (photo) current measurements we used a potentiostat Autolab PGstat10 (Ecochemie) controlled by GPES3 software (Ecochemie) in combination with a chopped 150 Watt Xenon light source (Spectral Energy) and a monochromator GM 252 (Spectral Energy). For the time resolved photocurrent measurements we made use of a mode locked argon-ion laser (System 2000, JK laser) as a light source ($\lambda = 532$ nm, FWHM of the laser pulse 14 ns). Both the photocurrent and a reference signal, detected by an ultra fast photodiode (BPW 28) negatively biased at 160 V, are simultaneously recorded over a

50 Ohm resistance by a digital oscilloscope (Tektronix, TDS 620A) remotely controlled by a PC. Currents are not corrected for the illuminated area.

6.2.3 Results

Figure 1 shows the i/V curves of an ITO/ PdTHOPP/H₂TMPyP/ Hg cells under chopped illumination at $\lambda = 532$ nm. Open circuit voltage and short circuit currents are similar as those measured for ITO/ ZnTHOPP/H₂TMPyP/ Hg cells. This indicates that the electro-polymerised PdTHOPP layer is also acting as the electron donor layer in a similar way as an electro-polymerised layer of ZnTHOPP [2].

Figure 2 shows the transient photo-current response of an ITO/ PdTHOPP/ H₂TMPyP/ Hg cell and of the reference photo-diode to the laserpulse. The direction of the photo-current response is similar to that using a continuous light source. Investigating the separate layers we observe for an ITO/PdTHOPP/Hg cell a similar transient with a peak current one order of magnitude smaller and with a reverse sign. For an ITO/ H₂TMPyP/ Hg cell we could not detect any transient photocurrent. By plotting the photocurrent decay in a semilog plot we obtain an approximately straight line and a long weak tail. The dominant first part can be fitted with a single exponent: $i = A * e^{-t/\tau}$; $A \approx 4 \cdot 10^{-3}$ A, $\tau \approx 1.10^{-7}$ s.

6.2.4 Discussion

Cells consisting of two different porphyrin layers exhibit photocurrents which are approximately one order of magnitude larger than cells with a single type of layer. The decay of the current is determined by a single response time. To explain this decay one approach is compare the observed response time with that of the circuit. If the organic material is assumed to act as an insulator, the cell can be seen as a geometric capacitor with an area $A = 0.78 \text{ mm}^2$, a relative dielectric constant of 4.5 (see Paragraph 6.1.4) and a thickness in the order of several tens of nm., yielding a capacity of 0.5 - 1 nF. The sum of the resistors in the external circuit is $> 100 \Omega$, formed by the square resistance of ITO $30 \Omega/\square$, and the external resistance of 50Ω . Using these numbers the response time of the circuit is close to that found by fitting the current transient decay. A way to interpret the current transient decay is thus formed by the discharging of the geometric cell capacitance over the external circuit. Decreasing the ITO resistance and using

thicker layers in the cells resulted in smaller response times (data not shown). Since with these cells both the rise time as well as the decay time are determined by the width of the laser pulse, we can conclude that the kinetics responsible for the photocurrent results in a response time which is obviously equal or shorter than the width of the laser pulse, i.e. $k < 10$ ns. The origin of the process of charging of the capacitor is not yet clarified, but photo-induced electron transfer at the interface is a logical explanation processes. Trivial processes e.g. the change of the dielectric constant of the organic material upon excitation can not yet been eliminated, however.

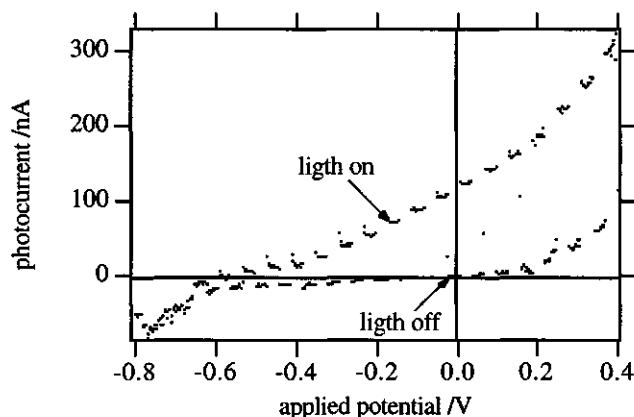


Figure 1 i/V curves for an ITO/ H_2TMPyP / Hg cell under chopped illumination at $\lambda = 532$ nm and area 0.78 mm^2

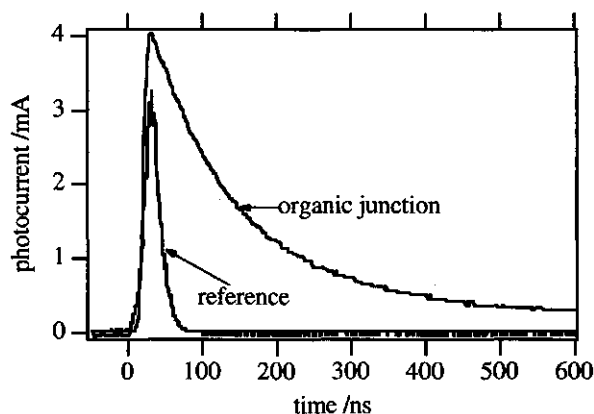


Figure 2 Transient photo-current response of the same cell using a laser pulse and a reference signal.

The long tail can be explained by the presence of deep traps in the bulk of the organic layers. Upon excitation the traps are filled and recombine only with a very small rate constant. These effects have also been observed previously for similar layers as in this work [17] and for phthalocyanine layers [15].

References

1. Umeda, M.; Shimada, T.; Aruga, T.; Niimi, T. and Sasaki, M. *J. Phys. Chem.* **1993**, 97, 8531.
2. Savenije T.J.; Koehorst R.B.M. and Schaafsma T.J. *Chem. Phys. Lett.* **1995**, 244, 363.
3. Tang, C. W. *Appl. Phys. Lett.* **1986**, 48, 183.
4. Wöhrle, D.; Kreienhoop, L.; Schnurpfeil, G.; Elbe J.; Tennigkeit, B.; Hiller, S. and Schlettwein, D. *J. Mat. Chem.* **1995**, 5, 1819.
5. Morita, S.; Lee, S. B.; Zakhidov, A. A. and Yoshino, K. *Mol. Cryst. & Liq. Cryst. A* **1994**, 256, 839.
6. Marcus, R.A. *Rev.Mod. Phys.* **1993**, 65, 599.
7. Wasielewski, M. R. *Chem. Rev.* **1992**, 92, 435.
8. Chanon, M.; Hawley, M.D. and Fox, M. A. *Photoinduced Electron Transfer A, Chapter 1* Elsevier: Amsterdam, 1988.
9. Vergeldt, F. J.; Koehorst, R. B. M.; Schaafsma, T. J.; Lambry, J. C.; Martin, J. L.; Johnson, D. G. and Wasielewski, M. R. *Chem. Phys. Lett.* **1991**, 182, 107.
10. Tran-Thi, T. H.; Dormond, A. and Guillard, R. *J. Phys. Chem.* **1992**, 96, 3139.
11. Segawa, H.; Takehara, C.; Honda, K.; Shimidzu, T.; Asahi, T. and Mataga, N. *J. Phys. Chem.* **1992**, 96, 503.
12. Tran-Thi, T. H.; Lipskier, J. F.; Houde, D.; Pepin, C.; Langlois, R. and Palacin, S. *J. Chem. Soc. Far.Trans.* **1992**, 88, 2529.
13. Willig, F. *Ber. Bunsenges. Phys. Chem.* **1988**, 92, 1312.
14. Willig, F.; Bitterling, K.; Charlé, K. P. and Decker F. *Ber. Bunsenges. Phys. Chem.* **1984**, 88, 374.
15. Fox, M. A.; Pan, H. L.; Jones, W. E. and Melamed, D. *J. Phys. Chem.* **1995**, 99, 11523.
16. Isoda, S.; Nishikawa, S.; Ueyama, S.; Hanazato, Y.; Kawakubo, H. and Maeda, M. *Thin Solid Films* **1992**, 210, 290.
17. Marée C.H.M.; Roosendaal S.J.; Savenije T.J.; Schropp R.E.I. and Schaafsma T.J. *J. Appl. Phys. in press*.

Summary

Since quite some time similarities have been noted between the photo-generation of charge carriers (electrons and holes) in a molecular semiconductor and the photosynthetic reaction centre of bacteria. For example, the mechanism for charge carrier generation by light in phthalocyanine films is largely dependent on the presence of ionised impurities. These impurities have been proposed to play a role similar to that of the special pair in bacterial reaction centra. In addition, the redox chain cascade in the reaction centra has a comparable function for charge transport as the internal field of a Schottky barrier. Although the present work applies to entirely different molecular system, this analogy is confirmed by the results of our experiments.

Chapter 1 contains a general introduction and the theoretical framework to understand the basics of charge separation processes in organic donor/acceptor combinations and in p/n heterojunctions. In this study the expertise at the Department of Molecular Physics with water-soluble porphyrin heterodimers has been used as a starting point to examine the photophysical and charge-transfer properties of molecular assemblies upon organising them as two thin layers on top of each other. A complication arises from the requirement to produce pinhole-free films for (photo) electrical measurements.

Experimental procedures to perform photo-electric measurements, optical characterisation and other techniques are described in Chapter 2.

In Chapter 3 we describe the adsorption of a fourfold positively charged tetrakis(4-methyl pyridinium) porphyrin and its metal derivatives on glass surfaces from basic aqueous solutions. The thickness and the depth profile of the chemical composition of these films has been determined using optical and ion beam techniques. Upon exposure to a buffered porphyrin solution, the glass surface is initially almost completely coated with a monomolecular porphyrin layer ($5 \cdot 10^{13}$ molecules \cdot cm $^{-2}$). Subsequently, the area of the glass surface available for deposition increases due to leaching of the glass by the buffer solution, resulting in an almost linear increase of the amount of adsorbed organic material with the period of exposure.

In Chapter 4 a different technique to produce thin films on transparent, electrically conducting substrates (ITO) is introduced, i.e. the electro-polymerisation of hydroxy-

phenyl substituted metallo-porphyrins. During electro-polymerisation an ether bond is formed between the phenyl rings of two porphyrin units, leaving the porphyrin macrocycles undisturbed. Using this deposition technique the thickness as well as the redoxpotentials of the layer can be accurately controlled. Using spectro-electrochemical techniques we can conclude that the oxidised film effectively consists of dimeric porphyrin mono-cations as the building blocks. To characterise charge carrier conduction in the polymerised films, diffusion coefficients were determined and found to be $(1-2) \cdot 10^{-10} \text{ cm}^2 \text{ s}^{-1}$ for films of porphyrins with varying number of hydroxyphenyl substituents, indicating that no correlation exists between the value of the diffusion coefficient and the number of cross links per porphyrin unit. This suggests that charge transport is mainly from ring to ring.

Chapter 5 demonstrates a photovoltaic effect in organic heterojunctions, made by the consecutive deposition of two different types of porphyrins onto an ITO substrate equipped with a mercury top contact, using a home-built measuring cell. From photo-electric measurements of the separate and composite electron donor- and acceptor porphyrin layers with varying order of the layers it can be concluded that the photo-active region is located at or near the interface of both porphyrin layers. Changing the redoxpotentials for the porphyrin donor/ acceptor combinations results in different values of the observed short circuit current, demonstrating the dependence of the photo-induced electron transfer on the exothermicity of the electron transfer. Depending on the layer thickness and type of porphyrins, the open circuit voltage is typically $\leq -0.4 \text{ Volt}$ and the short circuit current $\leq 130 \mu\text{A} \cdot \text{cm}^{-2}$ using illumination of $13 \text{ mWatt} \cdot \text{cm}^{-2}$ at 440 nm .

To clarify the photovoltaic mechanism of these porphyrin heterojunctions cells in greater detail Chapter 6 reports the results of impedance spectroscopy providing evidence for the formation of a depletion layer upon contacting the two porphyrin films. This depletion layer can be described in the same way as in a conventional p/n heterojunction of inorganic semiconductors. From Mott-Schottky plots the doping concentration is found to be $\approx 10^{17} \text{ cm}^{-3}$ for electro-polymerised zinc tetra-(hydroxy phenyl) porphyrin films and two orders of magnitude higher for spin-coated films of free base tetra (methyl pyridinium) porphyrin. Excitation of these cells with a nanosecond laser pulse reveals a lower limit for the photocurrent response time of $\leq 10 \text{ ns}$.

From the results of Chapters 5 and 6 we conclude that charge separation and thus the photo-active part of the cell is confined to the interface of both layers. For charge collection, consecutive dissociation of the electron/hole pair competes with charge recombination, in particular in organic heterojunctions with presumably low values of the dielectric constant. The internal field over the heterojunction space charge layer causes the photo-induced charge carriers which are generated at the interface to drift through the bulk layer to the electrodes. This explanation for the photovoltaic effect in organic heterojunctions implies that for a device to be efficient, the rate for electron transfer at the interface must be optimised, next to the presence of an internal field. This also implies that for a sandwich-type cell, such as described in this work (but also many other cells reported in literature) the efficiency ($\eta \leq 2\%$) is restricted by the absorbance of only a few dye monolayers. For application of this kind of charge generation layers in organic solar cells an antenna layer must be added to the cell.

Samenvatting

In wetenschappelijke publicaties is regelmatig melding gemaakt van de overeenkomsten tussen het ontstaan van ladingdragers bij belichting in zogenaamde moleculaire halfgeleiders en in het fotosynthetische reactiecentrum van sommige bacteriën. Het mechanisme van de licht-geïnduceerde generatie van ladingdragers in een ftalocyanine film is bijvoorbeeld sterk afhankelijk van de aanwezigheid van geïoniseerde onzuiverheden. In organisch materiaal worden deze verondersteld dezelfde rol te vervullen als het "special pair" in het bacterieel reactiecentrum. De redoxketen van opeenvolgende acceptors in dat reactiecentrum heeft een vergelijkbare functie als het interne elektrische veld in een Schottky barrière. Hoewel dit werk zich richt op een totaal ander moleculair systeem, bevestigen de interpretatie van de resultaten in dit onderzoek de bovenstaande analogie. Hoofdstuk 1 bevat naast een algemene introductie een uiteenzetting van de basisprincipes over electronoverdracht in organische donor/acceptor systemen en in zogenaamde p/n- heterojuncties van halfgeleiders.

In dit onderzoek is de expertise binnen de Vakgroep Moleculaire Fysica op het gebied van wateroplosbare porfyrine systemen als uitgangspunt gebruikt om de fotofysische en electronenoverdrachts-processen te bestuderen, die in en tussen verschillende moleculaire materialen optreden, als zij als twee op elkaar gestapelde ultradunne lagen zijn georganiseerd. Het maken van deze ultradunne homogene gaten-vrije lagen van enkele nanometers dik voor foto-electrische metingen vormt daarbij een uitdaging op zichzelf.

De experimentele procedure voor foto-electrische- en optische metingen en andere gebruikte technieken zijn beschreven in hoofdstuk 2.

In hoofdstuk 3 wordt de adsorptie van porfyrines voorzien van vier positieve ladingen, namelijk vrije base tetrakis(4 - methyl pyridinium) porfyrine en verschillende metaal derivaten hiervan, vanuit een basische oplossing op glas beschreven. De dikte en de chemische samenstelling van deze geadsorbeerde lagen is bepaald met behulp van optische methoden en hoog-energetische ionenbundeltechnieken. Het glasoppervlak blijkt na blootstellen aan een gebufferde, basische porfyrine oplossing bijna volledig bedekt te zijn met een monolaag van porfyrine moleculen ($5 \cdot 10^{13}$ moleculen \cdot cm $^{-2}$).

Vervolgens wordt door het uitloggen van het glas door de bufferoplossing het beschikbare oppervlak voor adsorptie steeds groter, wat resulteert in een bijna lineaire toename van de geadsorbeerde hoeveelheid organisch materiaal met de tijd van blootstelling aan de bufferoplossing.

In hoofdstuk 4 wordt een andere techniek besproken om ultradunne lagen op transparante, geleidende substraten (ITO) aan te brengen, namelijk electropolymerisatie van porfyrynes, die zijn uitgerust met hydroxyfenyl groepen. De polymerisatie resulteert in een etherbrug tussen de fenytringen van twee verschillende porfyrynes, m.a.w. het geconjugeerd ringsysteem van de afzonderlijke porfyrynes blijft intact. Met deze techniek is het mogelijk om zowel de dikte als de redoxpotentiaal van de film gecontroleerd te variëren. Spectro-electrochemische metingen wijzen uit dat een electrochemisch geoxideerde film beschouwd mag worden als een laag opgebouwd uit eenheden van kationen van porfyryne dimeren. De diffusieconstanten van ladingdragers in dit soort films, die zijn geproduceerd door electropolymerisatie van porfyryne monomeren met een verschillend aantal hydroxyfenyl groepen zijn alle in de orde van $10^{-10} \text{ cm}^2\text{s}^{-1}$. Dit betekent dat de diffusiecoëfficiënten voor ladingdragers in deze films onafhankelijk is van het aantal vertakkingen in de polymere film. Ladingstransport door de films lijkt dus plaats te vinden door sprongsgewijze verplaatsing van lading tussen de porfyryne-ringen, zonder tussenkomst van de verbindende ketens.

Hoofdstuk 5 laat zien dat er inderdaad een foto-voltaïsch effect optreedt in een organische heterojunctie. De complete cel bestaat uit twee ultradunne lagen met een dikte variërend tussen enkele tientallen en honderden nanometers, van verschillende type porfyrynes op een ITO substraat en aan de andere kant voorzien van een kwik-contact dat m.b.v. een metalen celhouder wordt aangebracht. De foto-voltaïsche metingen aan dergelijke cellen bestaande uit één of twee typen lagen (waarbij ook de volgorde van beide types verwisseld kan worden) tonen aan dat de foto-actieve laag zich bevindt aan het grensvlak tussen beide organische lagen. Het veranderen van de redoxpotentialen van beide type lagen leidt tot een verandering in de foto-stroom. Dit toont aan dat de snelheidsconstante van de licht-geïnduceerde electronoverdracht afhankelijk is van de exothermiciteit van de reactie. Afhankelijk van de laagdikte en het gebruikte type porfyrynes wordt een open klemspanning van ≤ -0.4 Volt en een kortsluitstroom van $\leq 130 \mu\text{A.cm}^{-2}$ gevonden bij bestraling met 440 nm licht met een intensiteit van 13 mWatt.cm^{-2} .

Om het mechanisme dat ten grondslag ligt aan het foto-voltaïsch effect van deze porfyriene heterojunctie cellen beter te begrijpen is in hoofdstuk 6 impedantie spectroscopie op de heterojuncties toegepast. Met deze techniek kon worden aangetoond dat er een depletielaag aanwezig is, zoals ook optreedt bij een conventionele anorganische p/n heterojunctie. Met behulp van Mott-Schottky plots kon de concentratie ladingdragers worden vastgesteld voor beide afzonderlijke lagen: voor geëlectropolymeriseerde zink tetra-(hydroxy fenyl) porfyriene films is de donordichtheid $N_d \approx 10^{17} \text{ cm}^{-3}$ en twee ordes hoger voor de vrije base tetra (methyl pyridinium) porfyriene films, die d.m.v. spin-coating op ITO zijn aangebracht. De foto-stroom die ontstaat door belichting van deze cellen met een lichtpuls van enkele tientallen nanoseconden geeft aan dat de foto-fysische processen in de films sneller verlopen dan 10 ns.

De resultaten van de hoofdstukken 5 en 6 kunnen worden verklaard met een model, waarbij het foto-actieve gedeelte van de cel zich bevindt aan het grensvlak van beide organische lagen. De dissociatie van een licht-geïnduceerd electron/gat paar aan het grensvlak naar de afzonderlijke elektrodes concurreert daarbij met de recombinatie naar de grondtoestand, juist in media met een lage dieëlectrische constante, zoals in organische films. Het interne elektrische veld over de organische lagen zorgt echter voor een efficiënte dissociatie van het electron/gat paar, dat gegenereerd is aan het grensvlak en zorgt bovendien voor het ladingstransport door het organische materiaal naar de afzonderlijke elektrodes. Deze verklaring voor het foto-voltaïsch gedrag van een organische heterojunctie impliceert echter wel, dat voor het maken van een efficiënte cel zowel de reactie constante voor electronoverdracht tussen beide lagen als de grootte van het intern elektrisch veld moeten worden geoptimaliseerd. Bovendien is de maximale efficiëntie van een uit dunne vlakke lagen bestaande cel (tot nu toe $\leq 2\%$), zoals beschreven in dit werk (maar ook van veel andere in de literatuur beschreven cellen) beperkt door de geringe optische absorptie van enkele monolagen. Toepassing van foto-actieve lagen zoals in dit proefschrift beschreven in zonnecellen moet daarom worden gecombineerd met een antenneachtige structuur, die het opvallende licht zoveel mogelijk absorbeert en d.m.v. energieoverdracht de excitatie-energie doorgeeft aan de foto-actieve laag.

Curriculum vitae

De schrijver van dit proefschrift, Tom Savenije, werd geboren op 26 april 1967 te Eindhoven. In 1985 behaalde hij het Gymnasium B diploma aan het "Van Maerlantlyceum" te Eindhoven. Na één jaar studie fotografie aan de kunstacademie te Breda werd van koers veranderd en gekozen voor de studie Moleculaire Wetenschappen aan de Landbouwniversiteit te Wageningen.

Tijdens de studie werd een afstudeervak bij de vakgroep Organische Chemie gedaan, gevolgd door een stage van zes maanden bij het Unilever Research laboratorium te Vlaardingen. Bij beide onderdelen stond synthese en karakterisatie van (enantiomeer zuivere) organische verbindingen centraal.

Een tweede afstudeervak werd uitgevoerd bij de vakgroep Moleculaire Fysica, waarbij onderzoek werd verricht naar de delocalisatie van een radicaal in een porfyrine dimeer met behulp van ESR.

Na het behalen van het doctoraal examen in januari 1992 koos de schrijver voor een functie als Onderzoeker In Opleiding, mogelijk gemaakt door de stichting SON en gefinancierd door NWO bij de vakgroep Moleculaire Fysica onder leiding van Prof. Schaafsma, wat heeft geresulteerd in dit proefschrift. Gedurende deze tijd is intensief samengewerkt met de vakgroep Organische Chemie van de Landbouwniversiteit te Wageningen, de vakgroep Atoom- en Interface Fysica van de Universiteit van Utrecht en de vakgroep Anorganische Chemie van de Technische Universiteit te Delft.

Vanaf 1 februari 1996 is de schrijver werkzaam als Toegevoegd Onderzoeker in het kader van een onderzoeksproject naar de haalbaarheid van organische zonnecellen, gefinancierd door de Nederlandse Organisatie voor Energie en Milieu.

Nawoord

Graag wil ik hierbij een aantal personen bedanken die een bijdrage hebben geleverd bij het tot stand komen van dit proefschrift. Allereerst wil ik mijn promotor Tjeerd Schaafsma bedanken voor zijn duizend en één ideeën, zijn objectieve wetenschappelijke visie, en het uitbundig corrigeren van de diverse manuscripten. "Tjeerd, jouw persoonlijke interesse voor dit onderzoek was duidelijk merkbaar in je enthousiaste begeleiding". Verder mijn kamergenoot Rob Koehorst, die mij altijd met raad en daad terzijde stond. De studenten Marcel, Niels, Jan-Willem, Ed en Ad die allen een afstudeervak in het kader van dit onderzoek hebben verricht, wil ik gaarne bedanken voor hun getoonde inzet. "Hoewel jullie bijdragen niet direct verzilverd zijn in publicaties, hebben jullie wel een belangrijke invloed gehad op de loop van dit project". Natuurlijk ook het technische wetenschappelijk personeel van onze vakgroep; "Arie, Adri en Frank, jullie hulp bij allerlei technische problemen heeft mij veel tijd en moeite bespaard". Verder wil ik iedereen van de vakgroep, inclusief de tijdelijke medewerkers en studenten hartelijk bedanken voor de gezellige en sportieve tijd van de afgelopen jaren.

De wetenschappelijke inbreng in dit project van de deelnemers van onder andere het NOVEM project was onontbeerlijk; "Gerrit, Ellen, Albert, Jan, Peter, Ernst, Tom, Ruud en Jeannette alsmede hun studenten, bedankt voor de discussies, samples, metingen en de gezellige tijd".

Tot slot wil ik mijn familie, vrienden, mijn zonen Arnold en Victor en in het bijzonder Margriet bedanken voor al die dingen van minder wetenschappelijke aard.